

# **GEOLOGICAL CHARACTERISATION OF THE LAI PING ROAD LANDSLIDE**

**GEO REPORT No. 166**

**N.P. Koor & S.D.G. Campbell**

**GEOTECHNICAL ENGINEERING OFFICE  
CIVIL ENGINEERING AND DEVELOPMENT DEPARTMENT  
THE GOVERNMENT OF THE HONG KONG  
SPECIAL ADMINISTRATIVE REGION**

# **GEOLOGICAL CHARACTERISATION OF THE LAI PING ROAD LANDSLIDE**

**GEO REPORT No. 166**

**N.P. Koor & S.D.G. Campbell**

**This report was originally produced in December 1998  
as GEO Geological Report No. GR 3/98**

© The Government of the Hong Kong Special Administrative Region

First published, May 2005

Prepared by:

Geotechnical Engineering Office,  
Civil Engineering and Development Department,  
Civil Engineering and Development Building,  
101 Princess Margaret Road,  
Homantin, Kowloon,  
Hong Kong.

## PREFACE

In keeping with our policy of releasing information which may be of general interest to the geotechnical profession and the public, we make available selected internal reports in a series of publications termed the GEO Report series. The GEO Reports can be downloaded from the website of the Civil Engineering and Development Department (<http://www.cedd.gov.hk>) on the Internet. Printed copies are also available for some GEO Reports. For printed copies, a charge is made to cover the cost of printing.

The Geotechnical Engineering Office also produces documents specifically for publication. These include guidance documents and results of comprehensive reviews. These publications and the printed GEO Reports may be obtained from the Government's Information Services Department. Information on how to purchase these documents is given on the last page of this report.



R.K.S. Chan

Head, Geotechnical Engineering Office  
May 2005



## FRONTISPIECE



Frontispiece: The Main Scarp of the Composite Landslide with Two Generations of Slickensides and a Distinct Vegetation Line of Ferns and Moss Indicating at Least Two Phases of Landslide Development

EG 97/117/22

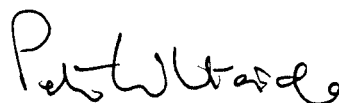
## FOREWORD

This report describes the geological and engineering geological features of the Lai Ping Road Landslide which occurred on the evening of the 2nd of July 1997 during an exceptionally heavy rain storm. There were no injuries or major damage to property. The landslide affected a cut slope and adjoining quasi-natural terrain up-slope. The cut slope has had a long history of failure, and although the subject of earlier phases of ground investigation, no remedial work was carried out. The report was produced by the Planning Division as part of a wider technical investigation by GEO (Sun and Campbell, 1998), and in parallel with consultants working on behalf of the Territory Development Department.

The landslide comprises a series of failures at five locations within the original cut slope. All but one of these represent the reactivation of an existing failure scar. Extensive deformation was also identified in the quasi-natural terrain above the cut slope indicating a larger composite (Cruden and Varnes, 1997) landslide. Subsequent ground investigation has demonstrated that the composite landslide affects a thick saprolite mass (c. 20 m) and has an estimated volume in the order of 100,000 m<sup>3</sup>.

The report, prepared by N.P.Koor and S.D.G.Campbell, summarises the results of aerial photograph interpretation in which M.J.Shaw provided additional assistance, a desk study, detailed geological and engineering geological mapping, and a comprehensive ground investigation. Helpful comments were given by many GEO colleagues, most notably Mr K.K.S.Ho, Dr H.W.Sun, Dr C.A.M.Franks and Dr C.J.N.Fletcher.

Technical assistance was provided by Mr George Cheng, Mr Dicky Chan, Mr K.C.Yip and Mr W.H.Ho. Ms K.K.Siu, Ms Loretta Pau and Mr Andrew Wu assisted on site during the ground investigation. Digital compilation of the maps and figures was undertaken by staff of the Cartographic Unit of Planning Division, including Ms P.L.Chan (who directed the work), Mr Samson Lee, Mr Y.M.Tam and Ms Elsa Lam.



P.G.D. Whiteside  
Chief Geotechnical Engineer/Planning

## EXECUTIVE SUMMARY

On 2 July 1997, a series of landslides occurred on cut slope No. 7NE-C/C95, located on the northern side of Lai Ping Road, in Kau To Shan, Sha Tin. The landslides occurred after several days of intense rainfall concentrated mainly within the Sha Tin valley. The incident reported to the Geotechnical Engineering Office (GEO) consisted of five individual landslides (landslide scars 1-5) and affected a 135 m section of the cut slope and the quasi-natural slope above. The combined volume of these failures is approximately 4000 m<sup>3</sup>. The debris from landslide scars 1 and 4 flowed over Lai Ping Road. The debris from landslide scar 4 also collided with a covered service reservoir on the opposite side of Lai Ping Road. This debris also over-topped the bounding upstand to the reservoir compound and moved down the quasi-natural (cf. King, 1996) slope below, where it flowed onto hardstanding surrounding a church. A zone of major surface deformation was identified, extending up to 50 m above the crest of the cut slope. The deformation is bounded by a main scarp, up to 4 m high, that shows evidence of fresh vertical and horizontal displacement. The main scarp defines the limit of a large, *slow moving, composite, retrogressive landslide* (terminology after Cruden and Varnes, 1996). This has an estimated total volume of approximately 100,000 m<sup>3</sup> and a maximum horizontal displacement of c. 8 m.

In order to advance the understanding of large-scale landslides in Hong Kong, a detailed investigation of the landslide was carried out by a team from the Special Projects and Planning divisions of GEO. The main focus of the investigation was to establish the mechanism and cause of the failure, and its debris mobility. The investigation was carried out between July 1997 and June 1998. This report documents the geological investigation carried out by Planning Division as part of the Lai Ping Road landslide investigation. A companion volume, dealing with the broader geotechnical aspects, has also been produced (Sun and Campbell, 1998).

Up to 4 m of colluvium occurs locally above landslide scar 5, but elsewhere it is thin or absent and overlies coarse ash crystal tuff and subordinate quartzphyric rhyolite dykes. The tuff is weathered to a depth of 22 m below ground level within the confines of the main scarp. The limit of deformation is related to the thickness of saprolite, with the 15 m saprolite isopach closely matching the position of the main scarp.

The cut slope, which had a maximum height of c. 40 m and an as-built overall slope angle of 33°, has had a longed history of previous failure. Initial instability occurred in 1978, within one year of the slope being formed. Further significant landslides followed in 1979, 1980, 1983, 1987, 1989 and 1993.

The main discontinuities that affect the stability of the rock mass are joints. These are generally medium to closely-spaced, and are often smooth or slickensided, undulose, and very narrow to tight. They are commonly coated or infilled with manganiferous deposits, limonite and white or buff kaolin. The predominant joint sets have dip and dip directions of 49°/198° and 86°/098° with minor sets at 28°/001° and 75°/207°. A sheeting joint set, dipping at a low angle parallel to the original natural terrain slope surface (c. 26°) has not been identified, which suggests that most of the slope has been comparatively stable (sheeting joints are developed following the removal of overburden (Nichols Jr. 1980) such as a landslide event), and that erosion rates were very slow.

The rock mass weathering has influenced the mode of failure of the cut slope. Composite translational slides and gully erosion have typically occurred in the PW0/30 zones (landslide scars 1, 2, 3 and 4A). Where rock content is higher, and discontinuities affect the mass strength, planar rock and soil slides have occurred (landslide scars 4A and 5).

The main surfaces of rupture of the (*slow moving, composite, retrogressive*) landslide are characterised by crushed zones within the saprolite, dilation of joints, void openings around corestones and *en echelon* sub-vertical shear zones. The surfaces of rupture are deflected around corestones. The following evidence suggests that the basal surface of rupture lies at or close to the base of the saprolite; a steep main scarp, disrupted zones close to rockhead identified in drillholes, a regular 15 m spacing of first order main scarps, evidence from SPT results of a weak zone in the saprolite within a few meters above rockhead, and the 15 m saprolite isopach coinciding with the position of the main scarp.

Groundwater flow paths are concentrated below the landslide site at the weathering front. They coincide with landslide scars 4 and 5 and a major seepage point in landslide scar 3B. The orientation of the principal transient groundwater flow paths appears to coincide with the overall direction of movement of the (*slow moving, composite, retrogressive*) landslide.

The initial slope instability was not controlled by existing discontinuities within the saprolite mass, but subsequent failures may have been, at least in part, due to the oversteepening of the slope as a result of failure. Initial failure of the cut slope is considered to have been through intact saprolite and triggered by elevated pore pressures following heavy rainfall. Development of the (*slow moving, composite, retrogressive*) landslide was triggered by cutting of the slope, combined with intense rainfall. Further reactivation was in response to heavy rainfall, rather than by small scale failures at the toe of the mass. The cut slope and quasi-natural slope above are prone to large volume, deep seated failure because of the thick sequence of saprolite at the site combined with a concentration of groundwater flow within a V-shaped depression above rockhead.

## CONTENTS

	Page No.
Title Page	1
PREFACE	3
FRONTISPIECE	4
FOREWORD	5
EXECUTIVE SUMMARY	6
CONTENTS	8
1. INTRODUCTION	11
2. DESK STUDY	12
2.1 Topography	12
2.2 Existing Geological Information	12
2.3 Previous Ground Investigations	13
2.4 Aerial Photograph Interpretation	13
3. FIELD MAPPING	14
3.1 Introduction	14
3.2 Geology	14
3.2.1 Introduction	14
3.2.2 Superficial Deposits	14
3.2.3 Solid Geology	15
3.2.4 Faults	16
3.3 Landslide Morphology	16
3.3.1 General Description	16
3.3.2 Main and Minor Scarps	17
3.3.3 Landslide Scars 1 to 5	18
3.3.4 Seepage Observations	22
4. GROUND INVESTIGATION	22
4.1 Introduction	22
4.2 Drillholes	23

	Page No.
4.3 Trial Pits and Trenches	23
4.4 Block Samples	24
4.5 Geophysics	24
5. ENGINEERING GEOLOGY	24
5.1 Debris Characterisation	24
5.2 Ground Conditions	25
5.3 Rock Material and Mass Weathering	26
5.3.1 Material Weathering	26
5.3.2 Mass Weathering	27
5.4 Discontinuities and Surfaces of Rupture	28
5.4.1 Introduction	28
5.4.2 Discontinuities	28
5.4.3 Surfaces of Rupture	29
5.5 Hydrogeology	31
5.6 Kinematic Stability Analysis	32
6. LANDSLIDE DEVELOPMENT	33
6.1 Main and Minor Scarp Development	33
6.1.1 Displacement	33
6.1.2 Time Constraints	33
6.1.3 Displacement Model	34
6.2 Mode of Failure	35
7. CONCLUSIONS	36
8. REFERENCES	37
LIST OF TABLES	39
LIST OF FIGURES	44
LIST OF PLATES	64
APPENDIX A: AERIAL PHOTO INTERPRETATION	103

	Page No.
APPENDIX B: DETAILED CORE DESCRIPTIONS AND PHOTOGRAPHS	109
APPENDIX C: TRIAL PIT LOGS	114
APPENDIX D: BLOCK SAMPLE DESCRIPTIONS AND PHOTOGRAPHS	123
APPENDIX E: DISCONTINUITY DATA OBTAINED WITH BOTH IMPRESSION PACKER AND ACOUSTIC TELEVIEWER	148
APPENDIX F: MINERALOGICAL AND MICROTTEXTURAL REPORT	153
LIST OF DRAWINGS	



## 1. INTRODUCTION

On 2 July 1997, a series of landslides occurred on cut slope No. 7NE-C/C95, located on the northern side of Lai Ping Road, in Kau To Shan, Sha Tin (Figure 1 & Plate 1). The landslides occurred after several days of intense rainfall concentrated mainly within the Sha Tin valley. The cut slope failures consisted of five individual landslides (landslide scars 1 to 5 in the report; Plate 2) and affected a 135 m section of the cut and quasi-natural slope above. The combined volume of the most recent failures of landslide scars 1 to 5 is approximately 4000 m<sup>3</sup>. The debris from landslide scars 1 and 4 flowed over Lai Ping Road. The debris from landslide scar 4 also collided with a covered service reservoir (Plates 2 and 3). This debris over-topped the bounding upstand to the reservoir compound, moved down the quasi-natural slope below and flowed onto the hardstanding surrounding a church (Plate 1 & Figure 1).

A preliminary investigation of the landslide area was carried out by the Special Project and Planning divisions of the Geotechnical Engineering Office (GEO) between 3 and 20 July 1997. During this investigation, a zone of major surface deformation was identified extending up to 50 m above the crest of the cut slope (Figure 1). The deformation is bounded by a main scarp, up to 4 m high, that shows evidence of fresh vertical and horizontal displacement. The main scarp defines the limit of a large, possibly deep-seated *composite* (terminology after Cruden and Varnes, 1996) landslide with an estimated total volume of approximately 100,000 m<sup>3</sup>. There was concern soon after the slope failure that if the large, deep-seated landslide started to move rapidly down-slope, the integrity of the service reservoir could be affected, together with the residential blocks on the south-west side of Kau To Hang (Plate 3 & Figure 1).

In order to advance the understanding of large-scale landslides in Hong Kong, a detailed investigation of the landslide was carried out by a team (comprising geotechnical engineers, an engineering geologist and a geologist) drawn from Special Projects and Planning divisions. The main focus of the detailed investigation was to establish the mechanism and cause of the failure, and its debris mobility. The investigation was carried out between July 1997 and June 1998. Maunsell Geotechnical Services (MGS), working on behalf of the Territory Development Department, are responsible for the design and implementation of the remedial works to the slope. Therefore much of the ground investigation (GI) and laboratory testing was carried out in conjunction with MGS.

This report documents the principal geological contribution made by Planning Division to the Lai Ping Road landslide investigation. In Section 2, desk study information is presented. The results of the field mapping of the landslides and descriptions of the geology are presented in Section 3. The GI is briefly described in Section 4. Engineering geological characterisation of the landslide site is presented in Section 5. In Section 6, the development of the landslide is discussed and includes evidence for the magnitude of displacements, time constraints for earlier landslide movements and a proposed mode of failure. The conclusions are presented in Section 7. A companion volume (Sun and Campbell, 1998), which deals with broader geotechnical aspects of the landslide, including detailed modelling of the failure mechanism and investigations of the debris mobility, should be read in conjunction with this report.



Two phases of GI were conducted between October 1997 and June 1998 by Enpack (Hong Kong) Ltd. The results of the GI are contained in two field work reports (Enpack, 1998<sup>a</sup> & Enpack, 1998<sup>b</sup>) and these should also be read in conjunction with this report.

## 2. DESK STUDY

### 2.1 Topography

The landslides occurred predominantly in a south-west-facing soil and rock cut slope along the north-east side of Lai Ping Road (Figure 1). The road provides access to Kau To Village and Kau To Shan borrow area north-west of the landslide site, and runs across a south- and south-west-facing slope that rises to an easterly-trending ridge at up to +230 mPD. The average natural slope angle above the landslide site is 26°. On the south-west side of the road, below the landslide, there is a covered service reservoir and further down-slope, a small complex of buildings includes hardstanding, a church and a stand (Figure 1).

Prior to the 1997 series of landslides, the slope comprised a series of cut slopes, platforms and sloping ramps with scars related to previous failures of the original cut slope (Figure 2). Alongside the slope, Lai Ping Road falls from about +100 mPD in the north-west to about +85 mPD in the south-east. The cut slope had a maximum elevation of about +134 mPD in its central part and was up to about 40 m high in places. In front of the cut slope, there was a platform, varying in height from about +105 mPD in the north-west to about +86 mPD in the south-east. A 50 mm water pipe and an overhead power-line ran across the platform from south-east to north-west. A grave site was located to the east of the cut slope.

The area above landslide scars 1 to 5 includes the uppermost part of the original cut slope with the broken remnants of a concrete drain marking its furthest limit. The slope above the drain is predominantly natural, but there are some man-made influences including paths, grave sites, open trial pits, remnants of drilling platforms, drillhole sites, and locally some made ground (mainly comprising boulders). Consequently, this slope is interpreted as quasi-natural (cf. King, 1996) rather than natural. Vegetation on both the cut and quasi-natural portions of the slope includes locally dense trees and shrubs, but low vegetation is generally sparse.

Natural drainage around the site includes prominent drainage lines located north-west and south-east of the slope, fed by a catchment area of approximately 31,000 m<sup>2</sup>. Where the slope was cut, however, the only pre-existing stream courses were shallow and ephemeral. These were intercepted by a surface U-channel, constructed around the crest of the cut slope. This had become largely ineffective, due to fracturing and blockages, long before the recent phase of slope instability.

### 2.2 Existing Geological Information

The 1:20 000-scale geological map of the area (GCO, 1986) shows that the landslide site lies in an area of undifferentiated tuff and tuffite, with a north-trending quartzphyric dyke just to the north-west (Figure 3). Notes on the related manuscript map (1983-84) record mainly coarse ash and coarse ash-lapilli tuff with corestones around the site, and at the site

itself, a landslide in residual soil and tuff with a few corestones. A north-east-striking contact separating the undifferentiated tuffs of the landslide from crystal tuffs of the Yim Tin Tsai Formation is shown just to the north-west of the cut slope involved in the failures. Two east-south-east-striking faults are also shown just to the north of the cut slope. No superficial deposits were mapped on or close to the site, with the exception of some alluvial deposits in the valley below the site.

### 2.3 Previous Ground Investigations

Prior to the 1997 failures, five ground investigations had been made, between 1973 and 1995, on or close to the slope. The locations of each of the drillholes and trial pits associated with these investigations are shown on Figure 1. A summary of the ground conditions encountered in each of the GI is contained in Table 1.

### 2.4 Aerial Photograph Interpretation

A detailed aerial photograph interpretation (API) report can be found in Appendix A. The API report is summarised below and on Figures 4 & 5. Prior to the commencement of the borrow area in 1976, the site was natural terrain (with minor footpaths) comprising a gently sloping concave landform in-between two low ridges (Figure 4). A small cut slope, associated with the haul road to Kau To Shan borrow area, was formed in 1976 and was substantially extended, both laterally and vertically, between 1977 and 1978 (Figure 5). Drainage channels were constructed on the berms, though these are only readily observed on the eastern side. The extended slope appears not to have had any surface protection applied, although some chunam or grass was placed on the lower eastern side after initial formation into batters. Plate 4 is of a view from the south-east of the cut slope in 1978. The haul road alignment, which was further south-west and straighter than Lai Ping Road is today, was moved in 1978 as part of the development of a cut and fill platform on which the salt water service reservoir was ultimately constructed. Two realignments of the road were constructed during 1978. One, which forms the present alignment of Lai Ping Road, was constructed in part on a fill ramp. The earlier realignment had been constructed even closer to the cut slope, but by the end of 1978, only part of the road, below the south-east part of the slope, remained intact. It is inferred that the continuation of the haul road to the north-west was probably damaged by a failure of the adjacent cut slope and had been removed by late 1978.

The earliest observed slope instability, a minor failure, took place in 1977 on the western, uppermost part of the cut slope. The first substantial failure occurred in 1978 and affected the central part of the slope, but the extent of this failure is poorly constrained by available photographs. By the end of 1979, failures had occurred at the base of the eastern end of the cut slope, and larger landslides, or erosional features, are evident in its western and central areas. Instability recurred on a number of occasions (associated with extensive erosion), mainly on the central western side of the slope (Figure 5) with significant events noted in 1980, 1983, 1987, 1989 and 1993. Two major tension cracks on the upper eastern side of the cut slope, and subsidiary minor cracks on its lower eastern side, have been clearly visible on aerial photographs taken since 1983 (Figure 5). From 1979 onwards, the possible locations of scarps on the quasi-natural slope above the cut slope can be inferred on the basis of disturbances of the vegetation. No remedial works appear to have been carried out, or

surface protection applied, following the various failures. Secondary vegetation has only ever grown over part of the slope, and the upper central and eastern sides of the slope have almost always been bare.

### 3. FIELD MAPPING

#### 3.1 Introduction

Preliminary geological and landslide morphology mapping of the slope was carried out between 8 July 1997 and 14 July 1997. Detailed mapping of the geology at 1:200-scale was carried out during August and September 1997.

Surveying and mapping of the main and minor scarps above the cut slope was carried out between July and September 1997. The scarps were mapped (prior to comprehensive topographic survey of the entire landslide site by Survey Division of CED) with reference to a series of base stations established using a Global Positioning Satellite (GPS) system. Further known points were added using tape and compass surveying between GPS base stations. Boulder mapping was finally carried out with reference to the established locations of the scarps.

General mapping of landslide scars 1 to 5 took place between July and November 1997. Landslide scars 1 to 5 were surveyed in detail using a total station survey on the 26 and 27 August 1997. All the mapping data have been transferred to Microstation DGN files and three maps of the landslide have been produced (Drawing Nos. EG 499, EG 502 & EG 503).

#### 3.2 Geology

##### 3.2.1 Introduction

Detailed geological surveying (1:200 scale) included the following:

- a) surface geological observations within landslide scars 1 to 5, and
- b) mapping of the slope above the cut slope, including the rare surface outcrop, the morphology of scarps and tension cracks and their exposed geology, and the nature and distribution of boulders.

##### 3.2.2 Superficial Deposits

Significant thicknesses of colluvial deposits (c. > 1 m) are largely restricted to landslide scar 5 and to the area above it, extending up to and beyond the main scarp (Drawing No. EG 504). Elsewhere on the site, colluvium occurs locally but is generally less than 1 m thick.

The colluvium is up to 4 m thick and there appear to be two units within landslide scar 5. The upper unit, up to 2.3 m thick, comprises brown to reddish-brown sandy, clayey silt with gravel, cobbles and occasional boulders of coarse ash tuff and occasional rhyolite, varying from moderately to completely decomposed. Towards the base of the upper unit, clasts typically have a coating of very dark brown manganiferous silt. The lower unit of colluvium, which is up to 1.7 m thick, comprises yellowish-brown to slightly reddish-brown, mottled buff and white, sandy, clayey silt, with some angular gravel and cobbles of coarse ash tuff and occasional rhyolite, varying from moderately to mainly highly and completely decomposed. Soil pipes (0.02 to 1.5 m wide and up to 0.5 m high) are developed at several locations towards the base of both units of colluvium. Persistent groundwater flow was noted from several of these pipes after heavy rain. Site photographs indicate that two of the largest pipes have been present, and actively seeping, for at least 18 years (Plate 4).

### 3.2.3 Solid Geology

The dominant rock-type on site is a grey to bluish grey, sparsely lapilli-bearing coarse ash crystal tuff, varying to a lapilli-ash tuff and ash-lapilli tuff (Plate 5). Lapilli, up to 25 mm in size, include quartz and feldspar crystals and sub-angular fine ash tuff and rhyolite. With increasing decomposition, the tuff becomes white to buff and mottled orangish and reddish brown, yellowish and white. The tuff locally exhibits a discontinuous compactional fabric and alignment of lithic clasts and crystals that indicate a weak stratification. This dips typically towards the north-north-east, but also less commonly to the north or north-north-west, at angles generally between 25 and 40°. Locally, the stratification is more strongly developed and the lithology resembles a medium- to coarse-grained volcanoclastic sandstone.

Subordinate rock-types include bluish grey, varying to yellowish and reddish brown and white when more decomposed, aphyric and quartzphyric rhyolite. The rhyolite is often flow-banded (Plate 6), flow-folded and autobrecciated and occurs as dykes, generally 0.5 to 4 m wide, that can be traced laterally for up to 20 m. Just to the north-west of landslide scar 5, one sub-vertical dyke is up to 10 m wide (Drawing No. EG 503). The dykes occupy several orientations including: steeply dipping (74 to 88°) to the south-east or south-south-east; steeply dipping (62°) to the south-south-west; and moderately inclined (30-45°) to the north-north-east.

The tuff also forms as corestones, up to 10 m across within the saprolite. These are widely developed across the site, and especially in landslide scar 4. A particularly large corestone lies between the scarps of landslide scars 4 and 5 (Drawing No. EG 499). Although many of the boulders show evidence of at least some disturbance, the relatively consistent orientation of volcanic fabric seen in some of the boulders, particular north-east of landslide scar 4, suggests they are mostly corestones that have undergone minor disturbance at most, rather than transported colluvial boulders. This accords with observations made in the main scarps of landslide scars 1 to 4. Areas of particularly abundant boulders occur immediately up-slope from landslide scars 1 and 2, north-east of landslide scar 4, and about 45 m up-slope from landslide scar 5 (Drawing No. EG 502). The area north of landslide scar 4 has relatively few boulders protruding from the surface, as is the case for much of the slope above landslide scar 5. In these areas, a layer of colluvium, up to 4 m thick is present. Other zones where boulders are rare or absent, on the north-east part of the slope, are

interpreted to be underlain by rhyolitic dykes, which do not typically generate large corestones when weathered (Drawing No. EG 502).

A zone of intense alteration within the saprolite can be traced from north-west to south-east across landslide scars 4, 3 and 2. The zone is characterised by a deep red to reddish pink coloration (iron and manganese staining), and the common development of white to buff, kaolin-infilled relict joints, with some dark brown manganiferous deposits (Plate 7a & 7b). The kaolin infills are up to 30 mm thick. The altered zone appears to dip into the hillside, towards the north-north-east at c. 25-40°, and in the same general direction as the fabric and stratification within the tuff. A discontinuous rhyolite intrusion (sill?) is also emplaced along the zone of alteration in landslide scar 4 (Drawing No. EG 499). Although many of the alteration features of the zone are consistent with weathering of the tuff and rhyolite, the zone may be one of pre-existing hydrothermal alteration. The altered tuff is extremely weak, and when broken down by finger pressure its constituents initially feel silt sized. However, with further pressure the altered tuff quickly becomes very clayey and greasy and appears to release some water.

#### 3.2.4 Faults

Faults have been inferred to strike west-north-west across the area of quasi-natural slope above the landslide scars, but they are poorly constrained (Drawing No. EG 502). They are associated with quartz veins and more general silicification. In the north-west part of the landslide site, sub-vertical, milky quartz veins (up to 0.8 m wide) are seen in bouldery exposures. Elsewhere, quartz breccias and silicified tuffs occur locally. This fault set also appears to truncate the rhyolitic dykes in the north-east of the landslide site. A northerly-trending fault may be inferred on the right hand flank of landslide scar 4A, mainly on the basis of an abrupt increase to the east in the thickness of saprolite identified from drillhole data (Drawing No. EG 503). However, there is no further confirmation of the existence of such a structure.

### 3.3 Landslide Morphology

#### 3.3.1 General Description

As described in Section 2.4, the cut slope has had a history of instability since its initial formation in 1978. The present landslide morphology (Drawing No. EG 503) has therefore developed over a period of about nineteen years. It includes an area of minor scarps, tension cracks and erosional features above the original cut slope, bounded by a main scarp. At the toe of the highly deformed landslide mass are five individual landslide scars (landslide scars 1 to 5), each with a different morphology. The Lai Ping Road landslide is therefore composed of a large deformed mass which extends into quasi-natural terrain with smaller landslides occurring at the toe. Since different types of movement occur in different areas of the displaced mass, the Lai Ping Road landslide can be described as *composite* (Cruden and Varnes 1996).

All but one of the landslide scars 1 to 5 are located within the original cut slope profile (Figure 1). The exception, landslide scar 1, an entirely new scar developed in 1997, occurred largely on quasi-natural terrain, although the toe of the failure was within the cut

slope. Landslide scars 2 to 5 were re-activations, or extensions, of existing failures of the original cut slope face.

For simplicity, the description of the landslide morphology has been split into two sections, namely, the area of main and minor scarps and tension cracks and, landslide scars 1 to 5. Each landslide is described individually, but an overall description for the Lai Ping Road landslide will be developed throughout the report. The terminology used here to describe the landslides is based on Cruden and Varnes (1996) and, where applicable, Hutchinson (1988).

### 3.3.2 Main and Minor Scarps

A series of scarps and cracks are developed on the quasi-natural slope above the cut slope and in landslide scars 1 to 5 (Drawing No. EG 502). They are interpreted as surfaces of rupture and tension cracks associated both with the recent development of the landslide and with the earlier failure history of the cut slope.

The main scarp of the system, marking the apparent up-slope limit of the deformation, extends to a maximum elevation of +156.6 mPD, some 24.8 m above and 56 m beyond (in plan view) the highest point of any of landslide scars 1 to 5. The scarps are typically steep. They have differential vertical offsets of up to 3.8 m (Plate 8) and horizontal extensions of up to 4.2 m. Most scarps dip directly or obliquely down-slope, consistent with the down-slope mass movement. However, a few scarps dip up-slope. Some reflect locally generated compression, i.e. heave (Plate 9), within the moving mass, while others are the down-slope margins of extensional grabens. Individual scarps extend laterally for up to 100 m. In plan (Drawing No. EG 502), the array of scarps displays a wide range of forms varying from curvilinear to rectilinear segments, and includes bifurcations, conjugate shear sets, left- and right-stepping *en echelon* sets, S- and Z-shaped inflections, duplexes, and other complex movement transfer zones. Segments nearer the cut slope are generally shorter (typically < 8 m long) than those further up-slope, close to and including parts of the main scarp. Only one linear segment, forming part of the main scarp on the north-east side of the landslide, is greater than 15 m in length. The scarps nearer the cut slope are generally considered to be older features than those further up-slope, and many were not activated during the recent slope movements. Their comparatively short lengths reflect truncations caused by the progressive development of younger scarps.

Locally, the scarps follow relict joint surfaces (Plate 10) but generally, no such structural control can be observed at ground level. However, deeper-seated structural control of the orientation of the scarps is apparent from the similar dip directions of linear segments of the scarps and the dominant joint sets (see Section 3.3.4). There is also a relatively regular spacing of the scarps. First order scarps, traceable laterally for distances of several tens of metres, being typically about 15 m apart, whereas second order features, traceable laterally for up to about 20, are approximately 7 to 8 m apart. The regular spacing of the first and second order scarps suggests that they are geologically controlled.

The morphology of the main and minor scarps, particularly the presence of the steep main scarp, grabens and compressional features, suggests that the large area of deformation can be classified as a *compound slide*. *Compound slides* are characterised (Hutchinson,

1988) by markedly non-circular slip surfaces formed by a combination of a steep, curved or planar rearward part and a flatter sole. They generally reflect the presence of a heterogeneity beneath a slope, often a weak layer or a boundary between weathered and unweathered material.

### 3.3.3 Landslide Scars 1 to 5

Landslide scars 1 to 5 are shown in detail on Drawing No. EG 499 and their dimensions are contained in Table 2, together with the landslide volumes and travel angles (Cruden and Varnes 1996) of the debris.

(a) Landslide scar 1 (Plate 11) has its toe within the original cut slope and its crown within quasi-natural terrain, 20 m to the east of the cut slope (Figure 1). The main scarp is generally trapezoidal in plan, being 13 m wide at the crown, 25 m wide at the toe and 52 m long. At the crown, the main scarp is sub-vertical and about 1.5 m high and is intersected by tension cracks that continue up-slope. The left hand flank of the main scarp is up to 5 m high and inclined at 45°. The right hand flank is up to 4 m high and ranges from sub-vertical to inclined at 45°. The landslide occurred in mainly residual soil grading to completely decomposed tuff in places. Pods of rhyolite dyke are also present (Drawing No. EG 499). Planar slickensided surfaces of rupture are present within the gully eroded surface below the crown of the slide (Plate 12 & Drawing No. EG 499). The slickensides indicate a direction of landslide movement towards 190° at an inclination of between 32° and 45°.

There are three distinct forms of debris associated with landslide scar 1. A relatively intact raft of vegetated soil and rock (35 m by 22 m), up to about 2 m thick (volume of 900 m<sup>3</sup>), lobes of disrupted soil and rock, and reworked debris (i.e. debris that has been eroded by surface water and redeposited further downslope) (Drawing No. EG 499). From the distribution of the landslide debris, three phases of movement may be postulated.

1. Initially, a relatively intact raft of soil and rock moved down-slope blocking Lai Ping Road.
2. As the landslide scarp regressed up-slope, debris flowed into the rear of the raft producing a mound of debris at its trailing edge and a depression behind (Plate 13).
3. Finally, further lobes of debris formed, but stopped short of the raft. Surface and groundwater flow redeposited mainly sand and silt, infilling the small depression behind the raft and forming a flat area (Plate 13).

Approximately two weeks after the main landslide movement, renewed retrogression of the main scarp occurred forming the youngest debris lobe shown (lightest shade of pink) on Drawing No. EG 499. The slickensides were measured either on the left hand flank (c. 45°) or close to the crown (c. 32°) of the landslide scar. They relate to movement phases 2 and 3 and have a higher inclination than the quasi-natural slope (c. 26°).

Persistent ground water seepage was seen close to the right hand flank at +109 mPD. Impersistent seepage was also noted elsewhere within the scar and emerging from the toe of some of the debris lobes (Drawing No. EG 499).

The morphology indicates that the initial phase of movement of landslide scar 1 can be classified as a translational slab slide (Hutchinson, 1988). The planar form of the rupture surfaces noted below the crown of the landslide suggests that the progressive retrogression of the back scarp up-slope was associated with small translational slides. These did not remain intact and probably turned into small earthflows (> 80 % of the debris < 2 mm in size) due to the large amounts of water available at the time of failure. Other evidence for flow includes the smooth lobate form of the debris fans, the remoulded structure of the debris and the debris accumulation against the rear of the intact raft. Landslide scar 1 is therefore classified as a *composite retrogressive, multiple translational slab slide - earth flow*.

(b) Landslide scar 2 (Plate 14) is located within the original cut slope, apart from its extreme north-east corner, and is a re-activation of instability initiated in 1979 (Figure 5). The main scarp is irregular in plan, being about 12 m wide and 35 m long. The crest drainage U-channel of the original cut slope feeds directly into the failure scar. The main scarp is sub-vertical to vertical along the crown and right hand flank and between 0.5 m and 4 m high. The left hand flank is up to 3 m high and inclined at 45° and forms part of the steep ridge separating landslide scars 1 and 2 (Drawing No. EG 499). The landslide occurred in residual soil and completely decomposed tuff with large corestones, some of which have been rotated in the down slope direction (Plate 15). A zone of intensely altered tuff outcrops in both flanks. Locally, made ground, up to 1 m thick, is present in the main scarp (Plate 16). Below the main scarp, steep gullies have been eroded into the saprolite forming prominent ridges, up to 1 m high. No distinct surfaces of rupture were observed.

Two debris lobes of disrupted saprolite were identified, one over-riding the other. This indicates two phases of landsliding. It is possible that the lower lobe is a remnant of landsliding that occurred before 2 July 1997 (see Section 5.1).

Both persistent and impersistent seepage flow were noted below the main scarp between +109 mPD and +110.5 mPD.

The irregular shape of the failure scar and the deep erosion gullies below the main scarp suggest that the recent extension of the scar and transportation of the eroded saprolite were principally caused by gully erosion and flow. For gully erosion to have occurred, there would have to have been a concentrated flow of surface water. This may have been derived from the surface water drainage U-channel which leads directly into the landslide scar. The smooth lobate morphology of the debris and its remoulded nature suggest that it flowed. Landslide 2 is therefore classified as *composite gully erosion - earthflow/debrisflow*.

(c) Landslide scar 3 is located within the original cut slope about 18 m from its toe (Plate 17). The landslide is a reactivation of a 1978 or 1979 landslide (Figure 5) and can be clearly seen in the photograph of the site taken in October 1979 (Plate 18). The scarp, which resembles an inverted L in plan, is sub-vertical and up to 2 m high. At the crown, the main scarp is about 10 m long. The left hand flank is linear and 17 m long. There is no well defined right hand flank, and the landslide debris extends north-west of a prominent north-south ridge within the failure scar (Drawing No. EG 499). A north-west trending tension



crack intersects the main scarp at the crown and extends into the remains of the cut slope to the north-west. The landslide occurred in completely decomposed tuff with zones of intense alteration (Drawing No. EG 499). Planar slickensided surfaces of rupture are present below the crown of the slide and in the scarp along the left flank (Drawing No. EG 499). The main surface of rupture has a dip/dip direction of 40°/222° and locally dips 63°/175°. On the left flank is a lateral release surface which dips at 55°/280°.

Two debris lobes of disrupted saprolite are easily identified, one over-riding the other. These indicate two phases of landsliding. The lower lobe is probably a remnant of an earlier phase of landsliding, and can be clearly seen in Plate 18. A thin veneer of debris, comprising disrupted saprolite with fragments of a concrete surface water U-channels, occurs north-west of the prominent ridge within the scar.

Persistent groundwater seepage occurs at +109 mPD below the scar crown and has extensively eroded the debris and *in situ* saprolite. There is also persistent groundwater seepage from below a large corestone at +101.5 mPD (Drawing No. EG 499).

The planar surfaces of rupture and lateral release surface observed within the landslide scar indicate that the landslide was partly translational. It is likely that there was some concentrated surface water flow from the remnants of the surface water drainage system which empties onto the landslide scar. Landslide debris did not remain intact and probably generated small earthflows (80 % debris < 2 mm in size) due to the large amounts of water available at the time of failure. These formed smooth depositional lobes of remoulded debris. The landslide can therefore be classified as a *composite translational - earthflow*.

Two smaller landslide scars, 3A and 3B, occur close to the right hand flank of landslide scar 3, within an area largely retaining the form of the original cut slope. Landslide scar 3A (Plate 19) appears to be an extension of a small erosion gully formed before October 1978 (Plate 18). The scarp is 5 m wide at the crown and both left and right flanks are 4 m long. The scarp is vertical along the crown and both flanks, and is up to 2.5 m high. The landslide debris forms an irregular mass of disrupted saprolite, giving the appearance of having been deposited without much water being present. The cut slope above the failure has numerous tension cracks sub-parallel to the main scarp, some of which show evidence of forward rotation in the form of a counter-scarp (Plate 20). It is therefore possible that landslide 3A was a *toppling failure* due to loading from up-slope. This would explain the apparent dry nature of the failure debris.

Landslide scar 3B was not reactivated during the 1997 rain storm. It is small, with a scar measuring about 2 m by 3 m. Persistent seepage was noted from the debris at about +102 mPD.

(d) Landslide scars 4 and 4A (Plate 21) are adjoining features located within the original cut slope and are reactivations of 1978 and 1980 landslides (Figure 5 & Plate 18). The main scarp is highly irregular in plan and has a maximum width of 35 m. At the crown, the scarp is sub-vertical and ranges between 0.5 m and 4 m high. The left hand flank, which is 44 m long and has a maximum height of 7 m, is vertical close to the crown and becomes inclined at 30° further down slope. The right hand flank includes a large corestone of moderately to slightly decomposed coarse ash tuff which separates landslide scar 4A from landslide scar 5 (Drawing No. EG 499). The rock mass exposed within the left hand flank is

highly disrupted and sheared, with corestones having rotated and translated down slope (Plate 22). The landslide occurred in moderately to completely decomposed coarse ash tuff which also contains pods of moderately to completely decomposed rhyolite (Drawing No. EG 499). The crown of scar 4 is formed predominantly within rock mass weathering grade PW50/90. A zone of extensively altered tuff runs obliquely north-west to south-east across the scar (see Section 3.2.3). A thin layer of colluvium (c. 1 m thick) is exposed in the scarp of scar 4A.

Planar surfaces of rupture, either along existing joint surfaces or sheared through intact saprolite, were observed at several locations within the scars (Drawing No. EG 499). Joint-controlled surfaces of rupture are concentrated within landslide scar 4 and have a dip and dip direction in the range of 47-58°/210°. The joints are generally smooth, sometimes polished, and undulose with coatings of manganiferous deposits and white kaolin (Plate 23). Slickensides, with trend and plunge of 190°/56°, occur on some of the joint surfaces. Within landslide scar 4A, the surface of rupture appears to occur through intact saprolite. The surfaces have a 15 mm thick coating of stiff medium brown silty occasionally sandy clay with angular clasts of completely decomposed tuff, and are often polished and/or slickensided (Plate 24).

All the debris fans from scars 4 and 4A are composed of remoulded saprolite and are smooth and lobate in form. The debris from landslide scar 4 spread over a large area, crossed Lai Ping Road, and collided with the salt water covered reservoir (Drawing No. EG 499). The debris built up to about 2 m thick against the reservoir wall (Plate 3). The debris also overtopped a low upstand along the south-east boundary of the reservoir compound and flowed down slope, flooding the church courtyard and continued to Lung Ping Path and beyond (Plate 1 & Figure 1). Debris from landslide scar 4A was deposited in distinct smooth lobes (Drawing No. EG 499). These lie on top of the debris from scar 4, apart from its western lobe (Plate 25). The deposition of the youngest lobe (coloured light green on Drawing No. EG 499) was observed by a consultant of the Landslide Investigation Division (GEO) on 3rd July 1998 at around 13:45 hrs. The debris was described as being in "slurry form" which flowed down the slope (Plate 25). Further smaller reactivations of this part of scarp 4A continued up to the middle of July 1997.

A major persistent seepage point is located within the central portion of landslide scar 4 at an elevation of +118 mPD (Drawing No. EG 499). Less persistent seepages are present, principally within landslide scar 4A, at an elevation of +108 mPD.

From the morphology of the landslide scars, debris lobes and the nature of the surfaces of rupture, the type of movement can be separated into two distinct parts. The surface of rupture of landslide scar 4 was predominantly controlled by planar discontinuities within the PW50/90 rock mass. During failure, the partly weathered rock mass broke up and flowed down slope, and can therefore be classified as a *composite planar rock slide-debris flow*.

The surface of rupture of landslide scar 4A was through intact saprolite, predominantly within the PW0/30 rock mass. During failure, the weathered rock mass broke up and flowed down slope in at least two distinct phases. Landslide scar 4A is therefore classified as a *composite translational slide-debris flow/earth flow*.

(e) Landslide scar 5 (Plate 26) is located within the original cut slope and is a reactivation of instability in 1979 and 1987 (Figure 5). It is bounded to the west by a rock cut slope, and to the east by a large, moderately to slightly decomposed tuff corestone. The main scarp is broadly arcuate in plan, with a linear crown 26 m long, and is composed of up to 2.3 m of colluvium overlying up to 1.7 m of older mottled colluvium (Plate 27a). The main scarp is vertical and up to 4 m high. Vertical tension cracks run sub-parallel to, and intersect, the main scarp. They show signs of staining, indicating that they are older than the most recent phase of instability (Plate 27b). The right hand flank is also vertical and up to 3 m high. Planar surfaces of rupture are exposed as a series of steps below the main scarp. They generally occur at, or close to, the interface between the older colluvium and moderately to completely decomposed tuff. The surfaces of rupture have a dip and dip direction of 45-65°/215°, and are generally slickensided and stepped, with a coating, up to 20 mm thick, of kaolin and manganiferous deposits. The surfaces are either joint-controlled, or are the planar interface between old colluvium and saprolite. Slickensides indicate that the main vector of movement of the slide was between 170° to 195°.

Extensive seepage was noted within the main scarp issuing from soil pipes between 1.5 m and 40 mm in diameter (Plates 28 & 29). The smaller pipes increased in size and number over the first few months after the landslide occurred, suggesting that active eluviation was taking place within the saprolite mass.

The landslide debris lobe has an irregular, rough form, and is composed of angular boulders of saprolite and colluvium with some sand and gravel. The form suggests that the debris did not flow down slope.

From the morphology of the landslide scar, the landslide is classified as a *planar soil slide*.

### 3.3.4 Seepage Observations

Observations of seepage, made at regular intervals since the landslide event, are summarised in Table 3. Although the quantities of flow were not measured, a qualitative system, defined in Table 3, was used to describe the flow.

Although variations in seepage intensity were related to rainfall, there appeared to be a time lag of about 2 days between the rainfall event and the peak intensity of flow, especially from seepage points in landslide scars 4 and 5. After each phase of heavy rain following the failures in July 1997, surface water was seen to flow over the crest of the main scarp of landslide scar 5.

## 4. GROUND INVESTIGATION

### 4.1 Introduction

Two phases of GI were carried out at the landslide site, between 30 October 1997 and 30 May 1998, by Enpack (HK) Ltd. under the two year Term Contract GE/95/10. Drillhole and trial pit logs, together with the results of *in situ* testing and ground water monitoring, are contained in the Contractors Final Fieldwork Reports (Enpack, 1998<sup>a</sup> & Enpack 1998<sup>b</sup>).

Inclinometers were installed as part of the Phase 1 GI to measure slope movements. The locations of all the investigation points are shown on Figure 1 and Drawing No. EG 504.

Full time supervision of the GI was carried out by Maunsell Geotechnical Services, with representatives from the Special Projects and Planning divisions of GEO also in attendance on a full time basis.

Prior to the recent ground investigation, some sampling and *in situ* testing were carried out within landslide scars 1 to 5. Block samples were taken by Enpack (HK) Ltd from exposed saprolite within scars 1-4. *In situ* sand replacement tests were made in the landslide debris by the Public Works Central Laboratory. Bulk samples were also taken at these locations for subsequent index testing. The sample and test locations are shown on Drawing No. EG 499. The results of the index testing are summarised on Figures 6 to 8.

#### 4.2 Drillholes

A total of 21 vertical rotary drillholes (Figure 1 & Drawing No. EG 504) were excavated to between 30.1 m and 60.2 m below existing ground levels, using either 4CMLC, HMLC, T2-116 or T2-101 core barrels and air-foam flush.

Five drillholes (TT1, TT2, TT2A, DH97/6 and DH97/8) were excavated using continuous 4CMLC (101 mm diameter) triple tube core barrel, principally for logging purposes. However, some lengths of core were taken for laboratory testing. The cores from drillholes TT1, TT2 and TT2A were taken to the Public Works Central Laboratory (PWCL) where they were split, logged in detail and photographed. Detailed descriptions of selected core are presented together with the core photograph in Appendix B. Maizier samples from drillholes DH97/9, 97/13, 97/10, 97/9 and 97/20 were also taken to the PWCL where they were split, logged in detail and photographed (see Appendix B). Two drillholes (DH97/01 and TT2A) were excavated to 60 m below ground level to investigate the possibility of deep instability in the partially weathered rock mass. In drillhole DH97/01, a 5 m zone of fractured slightly decomposed tuff was encountered at 44 m below ground level. No slickensides or other signs of displacement were observed on any of the fracture planes. It is therefore considered that this zone could be related to the emplacement of the granite pluton which was encountered in the drillhole 4.5 m below the fracture zone.

Both impression packer and acoustic televiwer tests were carried out in selected drillholes.

#### 4.3 Trial Pits and Trenches

Eleven hand excavated trial pits and one hand excavated trial trench (Figure 1 & Drawing No. EG 503) were made at the site, to depths of between 1 and 6 m. The majority of the pits were excavated within the limits of the main scarp and were dug principally to characterise the shallow surfaces of rupture and zones of deformation. Two pits (HE14 and HE15) were excavated south of the landslide, adjacent to the stream below Lung Ping Path (Figure 1). One trial pit (HE6) was excavated to a depth of 6 m, within a geomorphological depression east of the landslide. The trial trench was also excavated outside the main scarp

to a depth of 1 m, and deepened locally to 2 m. The trench was excavated to determine if there are any relic tension cracks or eroded scarps outside the present zone of instability but none were found. Block and bulk samples were taken from trial pits HE3, HE5, HE8, HE9 and HE13.

The pits and trench were logged in detail by GEO staff and the logs are presented in Appendix C.

#### 4.4 Block Samples

Twelve block samples (BS1 to BS12) were taken between 9 September to 30 October 1997 from landslide scars 1-4 for both strength and mineralogical testing. The block samples were delivered to the PWCL where they were described, photographed and sub-sampled for testing. Detailed descriptions and photographs of the block samples are found in Appendix D.

#### 4.5 Geophysics

Trial seismic refraction, micro-gravity and resistivity profiling surveys were made at the landslide site by EGS (Asia) Limited between 23 September and 24 October 1997 (EGS, 1998). However, it was considered that the geophysics did not yield accurate enough information on weathering depth to warrant a full scale survey.

### 5. ENGINEERING GEOLOGY

#### 5.1 Debris Characterisation

The debris has been characterised in terms of visual appearance, index testing and density tests. A soil description for seven of the debris lobes is presented on Drawing No. EG 499. The morphology of each of the debris lobes is described in Section 3.3.3. Sampling and testing of the debris was carried out in late August, some eight weeks after the landslide had occurred. Therefore, moisture content and density values determined are not representative of the conditions at the time of failure since some consolidation and drying out would have taken place.

Atterburg Limits and moisture content results are shown graphically on Figure 6. The moisture content of the fine fraction of the failure debris was determined after drying at two temperatures, 45°C and 105°C (Figure 6). There is a 1-2 % difference in moisture content between the two drying temperatures, indicating that some adsorbed water from within the clay mineral lattice was driven off at the higher drying temperature. The moisture content at the time of sampling ranged between 37 % for sample SR4 and 24 % for SR7. All moisture contents fell below the plastic limit by between 3 and 9 %, except for sample SR7 from the lower debris lobe of landslide scar 2, which was 17 % below the liquid limit. The plasticity index generally increases from 23 to 34 % at landslide scar 4, to 35 to 40 % at landslide scar 1, indicating a general increase in clay content of the source rock from north-west to south-east across the site.

A Plasticity chart for the debris is shown on Figure 7. Points lie on or below the “A-line”. The debris can therefore be classified as an inorganic silt of medium to high plasticity. Sample SR3 falls below the main cluster of points. It is notable that this sample was taken from debris that was dark red in colour and derived from the area of intense alteration in landslide scar 4A. Generally, the results fall within the Latosol Zone (Terzaghi *et al*, 1995), normally associated with residual soils derived from volcanic rock in tropical environments, and predominantly containing the clay mineral halloysite.

Particle size distribution for the debris is shown on Figure 8. The clay content increases from north-west to south-east across the site, varying from 15 to 28 % in landslide scar 4, to 37 to 48 % in landslide scar 1. This confirms the trend shown by the plasticity data.

*In situ* bulk densities, determined from the sand replacement tests (GEO, 1996), lie between 1.48 and 1.87 Mg/m<sup>3</sup>. The highest value is from the location of sample SR7. Relative compaction lies between 73 to 90 %, the highest value again being from the location of SR7.

The low moisture content and high relative compaction of the debris at SP7, compared to the sample taken from the overlying lobe, confirms that the lower lobe is a remnant from an earlier phase of landsliding, as suggested in Section 3.3.3.

## 5.2 Ground Conditions

The ground conditions across the landslide site are presented as cross-sections on Drawing Nos. EG 508 and EG 509 and are briefly described below. Detailed soil and rock descriptions are presented in Appendices B, C and D, and on Drawing No. EG 499.

Made ground was encountered along Lai Ping Road, where it is locally up to 6 m thick at drillholes 56A/BH6 and DH97/18 (Figure 1), and in the landslide scars, notably scar 2 (Plate 16). However, it is generally absent over most of the site. The made ground is generally granular, comprising coarse angular gravel to cobble sized moderately strong to strong volcanic rock fragments in a sand matrix. Locally, however, the matrix can be a clayey sandy silt or a silty fine sand. Standard Penetration Test results range between 8 and 58 blows per 300 mm penetration.

Top soil was logged in most of the recent trial pits (Appendix C) and in some of the recent drillholes. It ranges from 0 m to a maximum of 0.6 m thick at trial pit HE3.

Colluvium varies from 0 m and 4.0 m thick across the site but is generally < 1 m thick or absent. Its thickness has been overestimated (up to 13.8 m thick) in some of the previous GI's (Table 1), where it may have been confused with weathered tuff, which has a well developed corestone profile.

Rhyolite dykes were mapped in outcrop (Plate 30) and were also identified in three of the drillholes (DH97/1, DH97/6 and 56A/BH3). They vary from completely to slightly decomposed. The dykes range in thickness from 1.0 m in DH97/1 up to a maximum of 10 m, exposed in the cut slope west of landslide scar 5 (Drawing No. EG 503).

Coarse ash crystal tuff was encountered in all drillholes excavated at the site and varies in degree of decomposition from residual soil to slightly decomposed. The top of the tuff ranges from +157.9 mPD in DH97/13 to +75.1 mPD in DH97/1. The tuff was proven in drillhole DH97/1 to be at least 50.6 m thick. Here it overlies altered rhyolite, which may represent the contact with the roof of the granite which outcrops south of Kau To Hang (Figure 1 & Figure 3). Standard penetration test results (blows/300 mm penetration) range from 6 in the residual soil, to over 300 close to corestones and at the interface between Grade IV-V and III rock.

### 5.3 Rock Material and Mass Weathering

#### 5.3.1 Material Weathering

Detailed rock material descriptions made at exposures within landslide scars 1 to 5 are presented on Drawing No. EG 499. In general, decomposition of the tuff exposed within landslide scars 1 to 5, and in limited out-crop on the cut slope, increases from west to east.

When fresh or slightly decomposed, the tuff is extremely strong to very strong. Joints are discoloured to light brown. Discolouration penetrates up to 5 mm into the rock.

When moderately decomposed, the tuff becomes strong to moderately strong and is increasingly discoloured to light greyish-brown. Joints are often coated with manganiferous and limonitic deposits and sometimes white and buff kaolin, notably in landslide scar 5. Feldspar crystals within the rock mass are commonly bleached. Corestones often have a moderately decomposed rind, up to 100 mm thick, with a slightly decomposed core.

The highly decomposed tuff is weak to very weak and is often discoloured to brownish-grey or orangish-brown throughout. Joints are extensively coated with manganiferous deposits and limonite up to 10 mm thick. Thin infills of white or buff kaolin (1-2 mm thick) are also common at this decomposition grade.

The completely decomposed tuff is extremely weak and easily crumbled with slight hand pressure. Generally, all the feldspars have weathered to clay minerals (probably the kaolin group) and only quartz remains. The rock is often coloured orangish-brown or yellowish-brown and is characteristically mottled red, brown and white. Relict joints are often infilled with manganiferous deposits and white or buff kaolin, up to 20 mm thick (Appendix B). The completely decomposed tuff is a clayey sandy silt. Joint infills of kaolin are composed of between 50 to 82 % halloysite, occurring as fibrous overgrowths on books of kaolinite which make up the remaining clay mineral (Merriman *et al.* 1998, see Appendix F).

Residual soil is exposed mainly in landslide scars 1 and 2 and in the left hand flank of the main scarp of the *composite landslide* (Drawing No. EG 502). The residual soil is generally a soft, or soft to firm, clayey sandy silt, but may grade into a silty clay in places. In the left hand flank of the *composite landslide*, the residual soil is firm, or firm to stiff. The soil is often coloured brown or brownish-yellow and is mottled reddish-brown and pinkish red. Pocket penetrometer tests made in residual soil, exposed below the crown of landslide scar 1, indicate an undrained shear strength in the range of 15 to 30 kN/m<sup>2</sup>. Due to the high silt content of the residual soil, it is susceptible to softening with exposure to water

and to a reduction in total confining stress. Therefore, exposures of this soil are likely to exhibit lower strengths compared to triaxial tests made at realistic confining pressures.

### 5.3.2 Mass Weathering

The distribution of rock mass weathering zone (GCO, 1991) mapped across the landslide scars is shown on Drawing No. EG 499. Landslide scars 1, 2 and 3 are generally formed in PW0/30, with rock occurring as isolated corestones and as pods of less weathered rhyolite dyke in landslide scar 1. Landslide scar 4 grades from PW50/90 below the crown to PW30/50 in the left hand flank, where the rock mass is highly disrupted, and back into PW0/30 in scar 4A. Landslide scar 5 is predominantly formed in PW90/100.

The rock mass weathering has influenced the mode of failure across the site. Composite translational slides and gully erosion have typically occurred in the PW0/30 zones. Where the rock content was higher, and discontinuities affected the mass strength, planar rock slides have occurred.

Isopachs of saprolite thickness (Grade IV & V rock) are shown on Drawing No. EG 503. The 15 m isopach lies close to the limit of landslide movement at surface, as constrained by the main scarp. The most intense area of surface deformation coincides with the area contained within the 20 m isopach. South of Lai Ping Road, the weathering thickness increases to over 30 m (Drawing No. EG 503 and No. EG 508), but no evidence for large scale movement was observed there. Saprolite thickness reduces to about 10 m at the left hand flank of landslide scar 5 (Drawing No. EG 508). This isopach also coincides roughly in plan with the limit of colluvium. Several inferences can be made.

1. The extent of the large *composite landslide* is controlled by the saprolite thickness, and the 15 m isopach appears to limit the approximate extent of the *composite landslide* deformation.
2. The colluvium is probably old landslide debris (rather than being derived from other slope processes). Furthermore, the colluvium is thickest where the saprolite is thinner. This suggests that where it is thinner, the saprolite failed in the past, generating landslide debris. A remnant of this now overlies the remaining thin saprolite.
3. The saprolite is thickest where the slope has not failed in the recent past and therefore is only overlain by isolated deposits of colluvium.
4. The approximately north-south trending zone of saprolite, greater than 20 m thick, may indicate the presence of a north-south trending fault along its western limit.



## 5.4 Discontinuities and Surfaces of Rupture

### 5.4.1 Introduction

Measurements of dip and dip-direction of discontinuity data have been taken from within and outside the landslide main scarp. The following were recorded; joints, planes of rupture, and the trend and plunge (dip-direction and dip of a line) of slickensides observed on the surfaces of rupture. It should be noted that measurements taken from within the landslide boundary (defined here as “within the confines of the main scarp”) can only be used as an indication of orientation, since the residual soil and rock mass within the landslide boundary have moved *en masse*. Comparison with discontinuity data from the nearby Kau To Shan borrow area has not been attempted as the geology there is significantly different (crystal tuffs intruded by granodiorite) from that of the landslide site (Figure 3).

The discontinuity data obtained with impression packer and acoustic televiewer is presented in Appendix E. The results indicate that data obtained from the impression packer tests closely match those from surface mapping (see Figures E1, E2 and Figure 9). The acoustic televiewer results however, show a strong bias towards horizontal features which were not present in the surface mapping or the impression packer results. This may be due to a tendency for the interpretation of horizontal tool marks left by the drilling on the inside of the drillhole to be interpreted as discontinuities.

### 5.4.2 Discontinuities

The main discontinuities that affect the rock mass are joints. These are generally medium to closely-spaced but are locally very closely-spaced. The joints are often smooth or slickensided, undulose, and very narrow to tight. They are commonly coated or infilled with manganiferous deposits, limonite and white or buff kaolin (Plate 23). The coatings and infills are generally less than 2 m thick but locally, manganiferous deposits and kaolin can be up to 30 mm thick. The major joint sets are shown on Figure 9. The predominant joint sets have dip and dip directions of 49°/198° and 86°/098° with minor sets at 28°/001° and 75°/207°.

It is interesting to note the general absence of a sheeting joint set, dipping at a low angle parallel to the original natural terrain slope surface (c. 26°). These sheeting joints, which are common elsewhere in Hong Kong, are thought to develop as a response to unloading of slopes by erosion processes, including landslides (Nichols Jr. 1980). The absence of sheeting joints suggests that most of the slope has been comparatively stable, and that erosion rates were very slow. This is supported by the lack of a substantial thickness of colluvium over most of the quasi-natural slope above landslide scars 1-4.

It should be noted however, that in a report by Binnie and Partners in 1980, they note that a persistent smooth sheeting joint dipping at a slightly higher angle than the cut slope contributed to the failure on 2 June 1978 (GEO, 1998).

### 5.4.3 Surfaces of Rupture

Surfaces of rupture have been mapped in detail within landslide scars 1 to 5 and the main and minor scarp complex. They are characterised by polished or slickensided surfaces (Plate 12). The surfaces are composed of soft to firm light-brown very silty clay, up to 50 mm thick, with much angular coarse quartz sand and fine angular quartz gravel. The orientations of the main and minor scarps are presented on Figure 10 as a contoured plot, on which the main cluster of data is about point B. This represents scarps, associated with predominantly extensional deformation, with a dip and dip direction of  $56^{\circ}/175^{\circ}$ . The cluster at point E, which reflects a dip and dip direction of  $75^{\circ}/246^{\circ}$ , is associated with predominantly strike-slip deformation. Clusters around points A, C and D relate to *en echelon* sets of scarps.

Trend and plunge data for slickensides are shown on Figure 11. These data are concentrated about two centres,  $64^{\circ}/194^{\circ}$  and  $52^{\circ}/189^{\circ}$ . The two points with a plunge of  $67^{\circ}/337^{\circ}$  are slickensides that were measured on down slope scarps of two grabens.

Comparing the main scarp and joint orientation data, it is evident that joint sets 1 and 2 are likely to have exerted some control over the orientation of the scarps (Figures 9 & 10). The landslide mass has moved generally in a north-south direction, but there is a slight divergence, from  $189^{\circ}$  to  $194^{\circ}$ , in the displacement direction. This divergence may be influenced by the large corestone mass located above landslide scar 4 (Drawing No. EG 502).

Shallow surfaces of rupture and zones of deformation were encountered in trial pits HE1, HE2A, HE3, HE5, HE6, HE9 and HE13 and in a temporary excavation made into the left hand flank of landslide scar 4 near the toe of the cut slope. Detailed logs of the trial pits can be found in Appendix C. The surfaces of rupture exposed in the trial pits vary from:

1. a simple, open tension crack, irregular in profile, with little vertical displacement (see HE1, Figure C1) and no slickensides, up to 300 mm wide and infilled with debris composed of loose, brown, clayey, sand with angular gravel and cobbles, twigs and leaves, to
2. a highly complex zone, grading from an infilled tension crack into a disrupted zone composed of a sheared weathered rock mass with many voids (c.  $< 10$  mm wide) (see HE3, Figure C3 and Plate 31).

Characteristic features of the surfaces of rupture include:

- a) a generally complex zone of sheared, weathered rock,
- b) typically deflected around major corestones (see HE3, Figure C3),
- c) often associated with a zone of disruption characterised by opening of relict joints within the rock mass, *en echelon* sets

of minor sub-vertical shear zones and, opening around the margins of corestones (see HE2A, Figure C2), and

- d) where significant vertical displacement has occurred (c. > 2 m), the scarp infill is often very stiff, brown, clayey, sandy, silt with occasional gravel and cobbles, sporadic voids (c. < 5 mm wide) and minor shears. Within 100 mm of the surface of rupture the silt becomes soft (see HE5, Figure C4).

Several features observed in the drillhole cores are considered to indicate movement. However, the evidence is inconclusive and may reflect sample disturbance, at least in part. These features were only identifiable after the samples were split and logged in detail as described below.

- A) Sub-vertical joint sets in completely to highly decomposed tuff with extensive manganiferous deposits on the joint surfaces and within the rock fabric surrounding the joints (Plate 32). This indicates that large volumes of ground water has been flowing through open joints. Their opening could have been caused, at least partly, by landslide displacement.
- B) A disrupted zone, often encountered just above the top of continuous Grade III tuff, that consists of pockets of angular quartz, feldspar and moderately decomposed tuff sand and gravel, stiff brown silty clay and cobbles of sub-rounded highly decomposed tuff (Plate 33). This could be a zone which has been disturbed and disrupted by dilatant mass movement. The resulting increase in permeability could result in a preferential pathway for ground water flow, and so enable the deposition of clay, sand and gravel. However, as the zone was always observed at the end of a core run, it could also be explained by sample disturbance.
- C) In drillhole TT2A, an anomalous zone was encountered between 9.1 and 9.33 m below ground level. It consists of reddish-brown, very silty, well graded angular sand with much sub-angular to sub-rounded, highly to completely decomposed tuff gravel with numerous small pipes (c. <2 mm diameter), and voids which have smooth brown clay coated surfaces (Plate 34). The zone occurs within saprolite and therefore is unlikely to be due to drilling disturbance. It is interpreted either as an infilled pipe, through which much water has flowed, or part of a highly permeable shear zone complex, or both.

From the above, the surface of rupture is likely to be a zone, or zones, of disrupted rock with crushed zones and voids. It will therefore be weaker than the surrounding, less

disturbed saprolite. Standard penetration test profiles should therefore reflect this reduction in strength by a corresponding reduction in SPT N-values (blows/300 mm penetration). However, the N-values are complicated by the presence of corestones within the saprolite, which if encountered over the length of the test, will produce very high N-values. Figure 13 is a plot of SPT N-value versus distance above rockhead (rockhead is defined for this purpose as continuous grade III rock encountered in the drillhole). Only drillholes which lie within the 15 m isopach of saprolite thickness (Drawing No. EG 504) have been plotted.

Within 10 m of rockhead, the SPT N-values generally lie between 20 and 40 blows per 300 mm. Although there is not a consistent decrease in N-value close to rockhead, drillholes BH305, BH97/20 and BH302 all have reduced N-values within about 5 m of rockhead. This suggests the presence of a weaker zone, close to rockhead, that could reflect the sole of the landslide, but the evidence is inconclusive.

Cruden (1991) has proposed a method for determining the depth of the surface of rupture of non-circular, translational landslides in clay, based on the width of grabens at surface. For the landslides he studied, a simple ratio of 1.1 times the graben width correlates well with the known depth to the surface of rupture. The distance between first order scarps (c. 15 m) is also likely to be a function of the depth to the surface of rupture. Using Cruden's multiplier of 1.1, a surface of rupture is predicted at about 16.5 m. Although this can only be a very rough guide, it supports other observations that the surface of rupture is close to the base of the saprolite.

## 5.5 Hydrogeology

A permeability contrast exists between the saprolite ( $k = 5 \times 10^{-5}$  m/s) and the underlying moderately to slightly decomposed tuff ( $k = 6 \times 10^{-6}$  m/s) (GEO, 1998). Therefore, there is the potential for concentrated groundwater flow along the saprolite-moderately to slightly decomposed tuff interface (or rockhead). The topography of this interface, together with the saprolite mass and material properties, phaeitic surface and hydraulic gradient, will determine the flow of groundwater along that surface.

The slope hydrogeology is presented on Figure 14. Subsurface catchment boundaries have been interpreted as sub-surface ridge lines in the saprolite-moderately to slightly decomposed tuff interface. The corresponding depressions are interpreted as pathways for preferential groundwater flow.

There is a more general asymmetric V-shaped depression in the saprolite-moderately to slightly decomposed tuff interface at and above the site, possibly related to a north-south trending fault. This tends to concentrate groundwater flow into the area of the landslide. Within the V-shaped depression, there are three main potential groundwater flow pathways which could further channelise the flow. The three inferred flow pathways coalesce downslope, east of the reservoir, and flow into the deep depression in the saprolite-moderately to slightly decomposed tuff interface down slope from Lai Ping Road. The coalescence coincides with a flattening of the interface. The change in gradient at this point may be inferred to act as a choke to the groundwater flow. As a result, the hydraulic gradient of the phaeitic surface will increase and ground water levels upslope from the feature may be raised to higher levels.

Groundwater flow paths (A, B and C) and catchments are shown (Figure 15) in relation to the main scarp, landslide scars 1 to 5, main seepage points and main corestone masses at surface (Figure 15). Although flow path (A) does not pass through any of the landslide scars, it passes close to the west of the major seepage point in landslide scar 3B. A marked inflection in the catchment boundaries of flow path A also approximately coincides with the location of the main scarp, suggesting a geological control common to both. Furthermore, the main scarp changes orientation from a north-west strike, to a northerly strike, as it crosses the eastern catchment boundary. Flow path (B) intercepts landslide scar 4 and coincides with the major seepage point located below the crown. Flow path (C) intercepts landslide scar 5 at the location of the large soil pipe (Plate 28a). Landslide scars 1 and 2 are located in an area bounded to the north-west and south-east by two sub-surface catchments. The saprolite-moderately to slightly decomposed tuff surface is particularly planar below these two landslide scars (Figure 14) and could possibly explain the planar surface of rupture of landslide scar 1.

Flow path (A) has a southerly direction above the crest of the cut slope. Flow path (B) has a direction slightly west of south. These two orientations agree well with the slight divergence seen in the trend and plunge of slickensides on the right and left hand flanks of the main scarp (Figure 11). It is considered that flow paths (A) and (B) influence the direction of movement of the *composite landslide*. The corestone mass also coincides with the catchment boundary between flow paths (A) and (B). This provides further confirmation of the relationship deduced previously (Section 5.4.4) between landslide movement directions and the location of the corestone mass. The western catchment boundary of flow path B also passes through, or close to, the corestone masses between, and above, landslide scars 4 and 5.

## 5.6 Kinematic Stability Analysis

A simple kinematic stability check has been made for both planar and wedge type failures in the original cut slope profile to determine if the initial failures in the slope were primarily joint controlled, or that failure would have mostly been through intact saprolite (Figure 11). The analysis assumes zero pore pressures in the slope.

By inspection, toppling failure is not possible. The original cut slope, which was cut at an overall angle of about 33°, would have been stable with respect to joint controlled failure, since all potential sliding surfaces dip steeper than the cut slope angle except that reported by Binnie.

From the above, it appears that the original failures in 1978/79 were not controlled by discontinuities within the partially weathered rock mass. Initial failure would have been through intact saprolite, with local oversteepening of the freshly cut slope probably occurring at predominant seepage locations (Plate 4). However, once oversteepening had occurred, to say 55°, there is the potential for both planar failure on joint set 1 and wedge failure on the intersection of joint sets 1 and 4 (Figure 11). Planar rock slides occurred in both landslide scars 4 and 5.

## 6. LANDSLIDE DEVELOPMENT

### 6.1 Main and Minor Scarp Development

#### 6.1.1 Displacement

Observed movement indicators include (Drawing No. EG 502):

1. plunge of slickensides on slip scars,
2. orientations of *en echelon* sets of tension cracks, and
3. orientations of grabens, which mainly strike east-west.

Absolute displacement indicators (Drawing No. EG 502) include:

- a) the width of grabens and tension cracks, which indicate cumulative horizontal displacements of up to 8 m, although some of the wider grabens may also include subsidiary horsts, and
- b) the disparity between the present and former surveyed locations of some known features, most notably boreholes, trial pits, grave sites and drains. These suggest down-slope displacements of 2-3 m (trial pit 56A/TP3 (since 1995) and a grave site above failure scar 1), 3.1-3.3 m (Drillholes BH304 and BH305 (both since 1979) and trial pit 56A/TP4 (since 1995)) and, 10.3 m (Drillhole BH302 since 1979). However, it is likely that the 10.3 m relative displacement for drillhole BH302 is an overestimate resulting from a surveying error.

Up to 8 m of horizontal movement has occurred over a period of about 20 years. This represents an annual rate of movement of 400 mm/year, which falls within velocity class 2 of Cruden and Varnes (1996). The Lai Ping Road landslide can therefore be further classified as a *slow moving composite landslide*.

#### 6.1.2 Time Constraints

With respect to the age of development of the scarps, site observations clearly indicate movement predating the recent phase of failure, on and after, the 2nd July 1997. The scarps formed recently lack vegetation and contrast markedly with older vegetated scarps. In some instances, the uppermost parts of some scarps have a coating of vegetation (moss, ferns etc.), whereas the lower parts, formed during the most recent activity, are bare. This indicates recent reactivation of a pre-existing scarp (Plate 35). Occasionally, it was possible to measure slickensides related to both recent and older phases of movement on the same scarp (Plate 36a & 36b). During the period of surveying, it was noted that the pristine, recently formed scarps began to acquire a thin cover of moss within two months of their development.

Attempts have been made to determine the actual ages of development of the scarps. Two approaches have been used: API and dendrochronology.

(a) *API*. It is very difficult to identify individual scarps on existing aerial photographs of the slope due mainly to the extent of vegetation cover that has been present since the 1970's. However, on the basis of apparent vegetation disturbances, there are suggestions of scarps on aerial photographs taken on 29 November 1979 and on many of the photographs taken subsequently. No scarps have been observed on aerial photographs taken prior to 1979, in the area where the slope was cut. This includes the high quality low level aerial photographs taken on 26 January 1963 at which time the slope was less thickly vegetated.

Some tension cracks can be seen on the unvegetated central part of the cut slope in an oblique site photograph dating from October 1979 (Plate 18), and on aerial photographs taken from 1983 onwards.

(b) *Dendrochronology*. At several locations, trees were noted to have fallen out of, or onto scarps, possibly as a direct result of slope movements, and so causing breakages of trunks and branches, or more general damage. As a consequence, some of the trees changed their directions of growth, either through the growth of new branches or trunks, or by bending of the trunks, often in the up-slope direction, to restore growth to the vertical. In two cases, regrowth of trunks was seen to be directly up existing scarps (Plate 37). Further occurrences of up-slope bending of trunks were noted in areas where more general slope disturbance, rather than discrete scarps, had occurred. At nine locations (Drawing No. EG 502), trees were sampled for dendrochronology to establish the number of years since damage. In the case of trees that had fallen against, or out of the scarps, this would provide a minimum age for the existence of individual scarps. At best, this could provide data on the ages of scarp development, although not necessarily the first phase of movement in the case of reactivated scarps. Preliminary results are contained in Table 4. These data suggest that tree disturbances are not restricted to a single phase of movement. Other than those scarps that were clearly generated during the most recent phase of movement, individual scarps dated using dendrochronology have minimum ages of formation of 3 to 8 years (Table 4). Estimates for previous movement along the main scarp are 3-4 years ago, which accords well with the slope failure in 1993. Estimates for movement on the minor scarps further down-slope appear to be older. They suggest that the minor scarps developed at least c. 8 years ago, which probably relates to slope failure in 1989.

#### 6.1.3 Displacement Model

A synthesis of evidence for the evolution of the scarps is presented in Figures 16, 17 & 18. At least three broad phases of movement are inferred:

1. Prior to October 1979 but after December 1977,
2. 1982-87 and possibly including other phases of movement prior to July 1997, most notably in 1993, and
3. July 1997.

The system of scarps has been interpreted in terms of these three phases which can be related to the known dates of significant failures within the cut slope.

During the period 1978-79, the main failures of the cut slope occurred in the vicinity of the present landslide scars 3, 4 and 5 and to a lesser extent 2. The associated up-slope deformation was concentrated largely above landslide scars 3 and 4 (Figure 16).

Up-slope deformation during 1983-1987 involved a greater area in association with further failures of the cut slope in the vicinity of the present landslide scars 2, 3, 4 and 5. The main scarp migrated further up-slope and to the northeast. Deformation was greatest in the area up-slope from the present landslide scars 2 and 3, where up to 8 m of cumulative horizontal extension has been inferred (Figure 17).

The most recent phase of deformation in July 1997 involved further easterly migration of the system of scarps in association with the development of landslide scar 1. Accordingly, the greatest horizontal extension up-slope from the failure scars (2 to > 2.5 m) appears to have been above failure scars 2 and 1. Up-slope horizontal extension diminished towards the west and was generally < 1 m up-slope from landslide scars 3, 4 and 5, despite the substantial north-westerly migration of the main and minor scarps, particularly above landslide scars 4 and 5 (Figure 18).

Microtextural analysis of kaolin infilled joints indicates three phases of movement (Merriman *et al.* in prep.) (Appendix E). However, the age of the movement is not known and therefore these observations cannot be used to further constrain the development of the landslide.

The retrogressive evolution of the landslide up-slope allows the failure to be further classified as a *slow moving composite retrogressive landslide*.

## 6.2 Mode of Failure

A mode of failure is proposed, based on the following observations.

1. Initial instability occurred within 1 year of the original slope being cut.
2. All of the landslides have toes within the cut slope, but deformation extends well into the quasi-natural hillside above the cut.
3. The *composite landslide* dilates as it moves, as indicated by joints opening and voids forming around corestones.
4. The basal surface of rupture of the *composite landslide* is possibly located close to the Saprolite-moderately to completely decomposed tuff interface (rockhead).



5. The area extent of the *composite landslide* approximately coincides with the 15 m isopach of saprolite thickness.
6. Shallow surfaces of rupture (within 4 m of ground level) are deflected around corestones.
7. No well defined basal surface of rupture has been identified for the *composite landslide*. Zones of crushed saprolite, joint dilation, sub-vertical *en echelon* shear zones, and voids formed around small corestones, are often the only evidence of movement observed in the trial pits.
8. There appears to be a delay in the flow response of the seepage points within landslide scars 1-5 to rain fall events of about two days.
9. The recent phase of movement was triggered by intense rainfall (GEO, 1998)

From the above, the initial cause of the instability was the original cutting of the slope. The cut was made in a quasi-natural slope which had developed a thick, weathered profile (> 20 m in places). It is not known when the *composite landslide* was initiated, but API and other photographic evidence suggests development of scarps above the cut slope in 1979, associated with major failures in the cut slope. It is unclear whether the relatively small instabilities in the cut slope triggered the *composite landslide* due to unloading of the toe, or the main movement was itself related to the original cutting of the slope and to a general, possibly delayed rise in the ground water level after a heavy rain storm event. General unloading at the leading edge of the *composite landslide* contributes to the overall destabilising forces, but it is considered that these events are insignificant when compared to the estimated volume of the *composite landslide* (4000 m<sup>3</sup> of unloading in 1997 compared to 100 000 m<sup>3</sup> of the composite landslide, i.e. 4 %) and are not essential to initiate the large scale failure.

It is postulated, therefore, that the trigger for the *composite landslide* was also the cutting of the slope, in combination with intense rain storm events. The deep weathering profile at the site governs the development of the *composite landslide*. As the saprolite mass moves down-slope, it dilates and the pore pressures reduce. At a critical angle of dilation, the pore pressures will be reduced to a level where movement ceases. The undisturbed slope above the *composite landslide* will be unloaded by the movement and further regression of the main scarp up-slope results. With each slope movement, more sub-vertical tension cracks are created and existing ones extended, thus increasing the vertical permeability of the ground. This in turn allows more infiltration, thus potentially accelerating the groundwater rise during intense rainstorms.

## 7. CONCLUSIONS

- a) Five landslides (landslide scars 1 to 5) occurred on cut slope No. 7NE-C/C95 on 2 July 1997, with a combined volume of debris of 4000 m<sup>3</sup>.

- b) A major zone of deformation, extends up to 50 m beyond the crest of slope No. 7NE-C/C95. The deformation is bounded by a main scarp up to 3.8 m high within which numerous minor scarps are present, and up to about 8 m of horizontal movement has occurred.
- c) The slope has a prolonged history of failure. Initial instability in 1978 occurred within one year of the slope being formed, and was followed by major landslides in 1979, 1980, 1983, 1987, 1989 and 1993.
- d) Up to 4 m of colluvium exists locally. Elsewhere it is thin or absent and overlies coarse ash crystal tuff and subordinate quartzphyric rhyolite dykes.
- e) Landslide scars 1 to 5 include translational slides and gully erosion in PW0/30 and planar rock slides in PW50/90 and PW90/100
- f) The main and minor scarp complex is consistent with the development of a *compound slide*.
- g) The limit of deformation is controlled by the thickness of saprolite, with the 15 m saprolite isopach closely matching the position of the main scarp.
- h) The basal surface of rupture is inferred to lie at, or close to, the base of saprolite
- i) Groundwater flow paths are concentrated beneath the landslide site at the interface between saprolite and moderately to slightly decomposed tuff. Their principal pathways coincide with landslide scars 4 and 5 and a major seepage point in landslide scar 3B.
- j) The groundwater flow paths coincide with the direction of movement of the *slow moving composite retrogressive landslide*.
- k) Discontinuities probably did not control the initial slope instability, but influenced subsequent failures, at least in part. Initial failure was probably through intact saprolite and was triggered by elevated pore pressures following heavy rainfall.
- l) *Slow moving, composite, retrogressive landslide* development resulted from instability caused by heavy rainfall and a transient rise in the ground water table, the cutting of the slope, and was triggered, rather than by small scale failures at the toe of the *composite* landslide.

## 8. REFERENCES

- Cruden, D.N. (1991). Observation of graben geometry in landslides. Slope stability engineering. Thomas Telford, London, pp. 33-35.
- Cruden, D.N. and Varnes, D.J. (1996) Landslide Types and Processes. Landslides: investigation and mitigation (Ed. Turner, A.K. and Schuster, R.L.), Special Report 247 of the Transport Research Board, National Research Council, National Academy Press, Washington D.C. Chapter 3, pp. 36-75.

- EGS (1998). Slope Failure at Lai Ping Road Kau To Borrow Area, Geophysical Survey - Final Report. Contract No. GE/97/12, Works Order No. GE/97/12.2 14p, 3 drawings.
- Enpack (1998)<sup>a</sup> Slope Failure at Lai Ping Road - Ground Investigation - Final Field Work Report. Contract No. GE/95/10, Works Order No. GE/95/10.97, vol. 4.
- Enpack (1998)<sup>b</sup> Slope Failure at Lai Ping Road - Ground Investigation - Final Field Work Report - Phase 2. Contract No. GE/95/10, Works Order No. GE/95/10.97, vol. 4.
- GCO (1991). Guide to Rock and Soil Descriptions-Geoguide 3. Geotechnical Control Office, Hong Kong, Second Edition, 199p.
- GEO (1996). Methods of Test for Soils in Hong Kong for Civil Engineering Purposes (Phase 1 Tests). GEO Report No.36 by P.Y.M.Chen, Geotechnical Engineering Office, Hong Kong, 90p.
- Hutchinson, J.N. (1988). General Report: Morphology and geotechnical parameters of landslides in relation to geology and hydrogeology. Proceedings of the Fifth International Symposium on Landslides, 10-15 July 1998, Lausanne, pp3-35.
- King, J.P. (1996). The Tsing Shan Debris Flow. SPR 6/96, Special Project Report, Geotechnical Engineering Office, Hong Kong, Volume 1, 133p., 7 drawings.
- Merriman, R.J. Kemp, S.J. Hards, V.L. and Murphy, H.A. (1998). A mineralogical and microtextural study of the Lai Ping Road Landslip, Hong Kong. British Geological Survey Technical Report, Mineralogy and Petrology Series. Report No. WG/98/25C. 9 plates, pp 11.
- Nichols Jr., T.C. (1980) Rebound, its nature and effect on engineering works. Quarterly Journal of Engineering Geology, Geological Society of London, Volume 13, pp. 133-152.
- Sun and Campbell (1998). Report on the Lai Ping Road Landslide of 2 July 1997 - Findings of the Landslide Investigation. Landslide Study Report LSR 27/98, Geotechnical Engineering Office, Hong Kong SAR Government.
- Terzaghi, K., Peck R.B. and Mesri G. (1995). Soil Mechanics In Engineering Practice. Third Edition, John Wiley & Sons, Inc., p549.

LIST OF TABLES

Table No.		Page No.
1	Summary of Previous Ground Investigations	40
2	Dimensions of Landslide Scars 1 to 5	41
3	Seepage Observations	42
4	Dendrochronology Dating of Scarp Ages	43

Table 1 - Summary of Previous Ground Investigations

Ground Investigation	Drillhole Depth (m) and Number	Made Ground thickness (m)	Col thickness (m)	Residual Soil thickness (m)	Grade V-IV Tuff thickness (m)	Top grade III-II Tuff (+mPD)	Ground Water Level (+mPD)
Malayan Drillers (HK) Ltd. 1973	19.8 (KT-2A) (1) <sup>dh</sup>	0	1.8	6.7	5.8	62.05	NP
Lam Construction Co., Ltd. 1979	15 - 24.9 (BH302-307) (6) <sup>dh</sup>	0 - 3.7	1.8 - 10.7?	0	8.4 - 12.8	106.2 - 132.2	133.7 - 113.3
Lam Construction Co., Ltd. 1980	11.65 - 15.2 (P1-5) (5) <sup>dh</sup>	0	2.5 - 8.4?	0	3.15 - >10.9	84.3 - 87.5	90.2 - 84.9
Enpack (Hong Kong) Ltd. 1992	12 - 20.2 (BH1-9) <sup>dh</sup>	0 - 2.0	0 - 3.0	0	2.2 - >20	<70.1 - 101.7	102.1 - 76.5
Geotechnics & Concrete Engineering (Hong Kong) Ltd. 1995	5.6 - 29.7 (56A/BH1-8) (8) <sup>dh</sup> (56A/TP1-6) (6) <sup>tp</sup>	0 - 0.6	0 - 13.8?	0	0.3 - 9.2	79.2 - 141.0	<144 <sup>D</sup> - 91.8

Definitions

Col - Colluvium

? - Questionable thickness

NP - Ground water measuring instrument not installed

<144<sup>D</sup> - Ground water measuring instrument installed to +144 mPD and was dry

Ground water level - range of highest recorded levels

(BH302-307) - Drillhole code

(6)<sup>dh</sup> - 6 number drillholes(6)<sup>tp</sup> - 6 number trial pits

Table 2 - Dimensions of Landslide Scars 1 to 5

Scar No.	W <sub>d</sub> (m)	W <sub>r</sub> (m)	L <sub>d</sub> (m)	L <sub>r</sub> (m)	L (m)	H (m)	$\alpha$ (°)	V (m <sup>3</sup> )
1	25	16	60	45	72	29	18	1250
2	11	8	25	27	41	20	26	315
3	9	11	23	19	32	20	22	150
3A	13	5	9	3	11	9	39	35
3B	3	3	8	3	10	6	31	5
4	67	19	90	14	102	39	21	1750
4A	17	17	34	12	43	26	31	500
5	15	25	40	8	43	23	28	100

Definitions after Cruden and Varnes, 1996.

W<sub>d</sub> - Width of Displaced Mass

W<sub>r</sub> - Width of Surface of Rupture

L<sub>d</sub> - Length of Displaced Mass

L<sub>r</sub> - Length of Surface of Rupture

L - Total Length

H - Height of the Landslide

$\alpha$  - Travel Angle

V - Volume of the Landslide

Table 3 - Seepage Observations

Seepage Point	Date of Seepage Observations Made in 1997							
	4/7	14/7	30/7	4/8	12/8	14/8	26/8	29/8
1a	NO	SF	D	SF	SF	NO	NO	NO
2a	O	SF	NO	NO	MF	NO	NO	NO
3a	O	MF	NO	MF	NO	NO	SF	NO
3b	NO	NO	NO	NO	NO	NO	MF	NO
4a	HF	HF	MF	HF	HF	NO	MF	NO
5a	HF	SF	NO	HF	HF	NO	NO	SF
5b	NO	MF	NO	HF	HF	HF	NO	SF
5c	NO	MF	NO	HF	HF	HF	NO	SF
5d	NF	NF	NF	NF	NF	MF	NO	SF
5e	NF	NF	NF	NF	NF	MF	NO	SF
5f	NF	NF	NF	NF	NF	MF	NO	SF
5g	NF	NF	NF	NF	NF	MF	NO	SF

Key - Visual Determination only

HF - Heavy Flow

MF - Moderate Flow

SF - Slight Flow

D - Dry

NF - Soil pipe not formed on that date

NO - No observation made on that date

O - Observed to be flowing by others

Table 4 - Dendrochronology Dating of Scarp Ages\*

Sample number	Tree years since disturbance (minimum age of scarp)
1	8
2	5-6
3	8
4A	3
4B	3
5	4
6	5
7	2-3
8	4
10A	4

Age determinations made by Mr C.C.Lai of the Department of Agriculture and Fisheries.

Ranges in years denotes uncertainty in age dating.

\* Location of tree ring samples taken for dendrochronology dating are shown on Drawing EG502. Data are for trees whose growth has been disrupted by scarp development.



LIST OF FIGURES

Figure No.		Page No.
1	Site Plan	46
2	Site Plan (Prior to 1997 Failure) Based on Topographic Survey by Maunsell in 1995 and the 1:1000 - scale Survey Plan	47
3	Geology of the Landslide Site as Shown on Part of Hong Kong Geological Survey Sheet 7 (Sha Tin, 1:20,000-scale; GEO, 1986)	48
4	Aerial Photograph Interpretation of Area Surrounding Lai Ping Road Landslide Site Prior to Its Development - Aerial Photographs Used 1964	49
5	Aerial Photograph Interpretation of Slope 7NE-C/C95	50
6	Atterberg Limits and Moisture Content of the Debris from Landslide Scars 1 to 4	51
7	Plasticity Chart for Landslide Debris	52
8	Particle Size Distribution of Landslide Debris	53
9	Contour Plot and Pole Plot of Joint Orientations	54
10	Contour Plot and Pole Plot of Orientations of Main and Minor Scarps above Landslide Scars 1 to 5	55
11	Contour Plot of Trend and Plunge of Slickensides Measured on Surfaces of Rupture	56
12	SPT 'N-Value' Versus Distance above Rockhead for Drillholes within the 15 m Saprolite Thickness Isopach	57
13	Hydrogeology	58
14	Hydrogeological Flow Paths in Relation to Landslide Scars, Main Scarp, Seepage Points and Sub-surface Catchments	59
15	Stability Plot for Landslide Scars 1 to 5	60
16	Composite Landslide Displacement Model - Pre-October 1979	61

Figure No.		Page No.
17	Composite Landslide Displacement Model - 1983-1987 Including Further Activity Prior to July 1997	62
18	Composite Landslide Displacement Model - July 1997	63

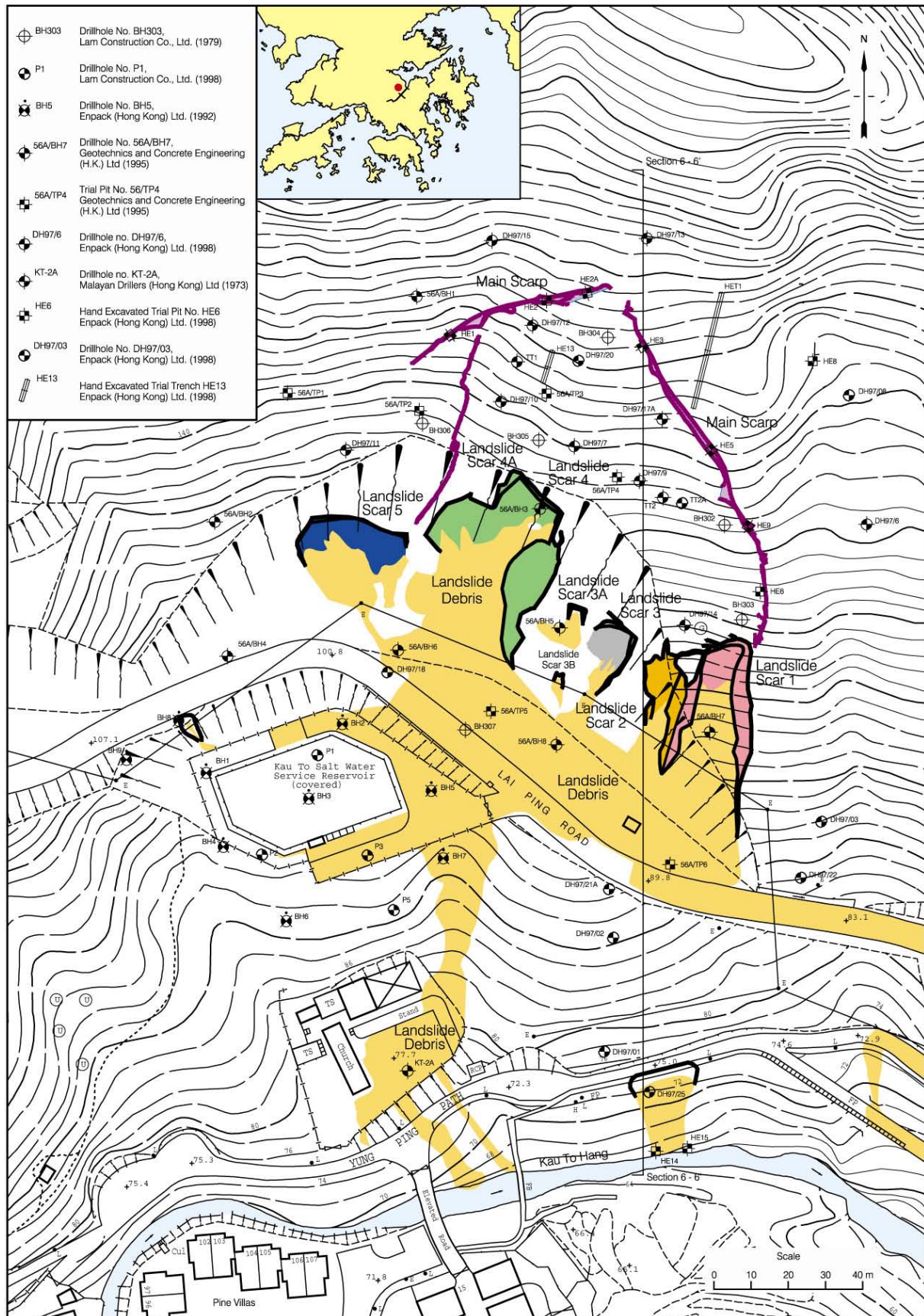


Figure 1 - Site Plan







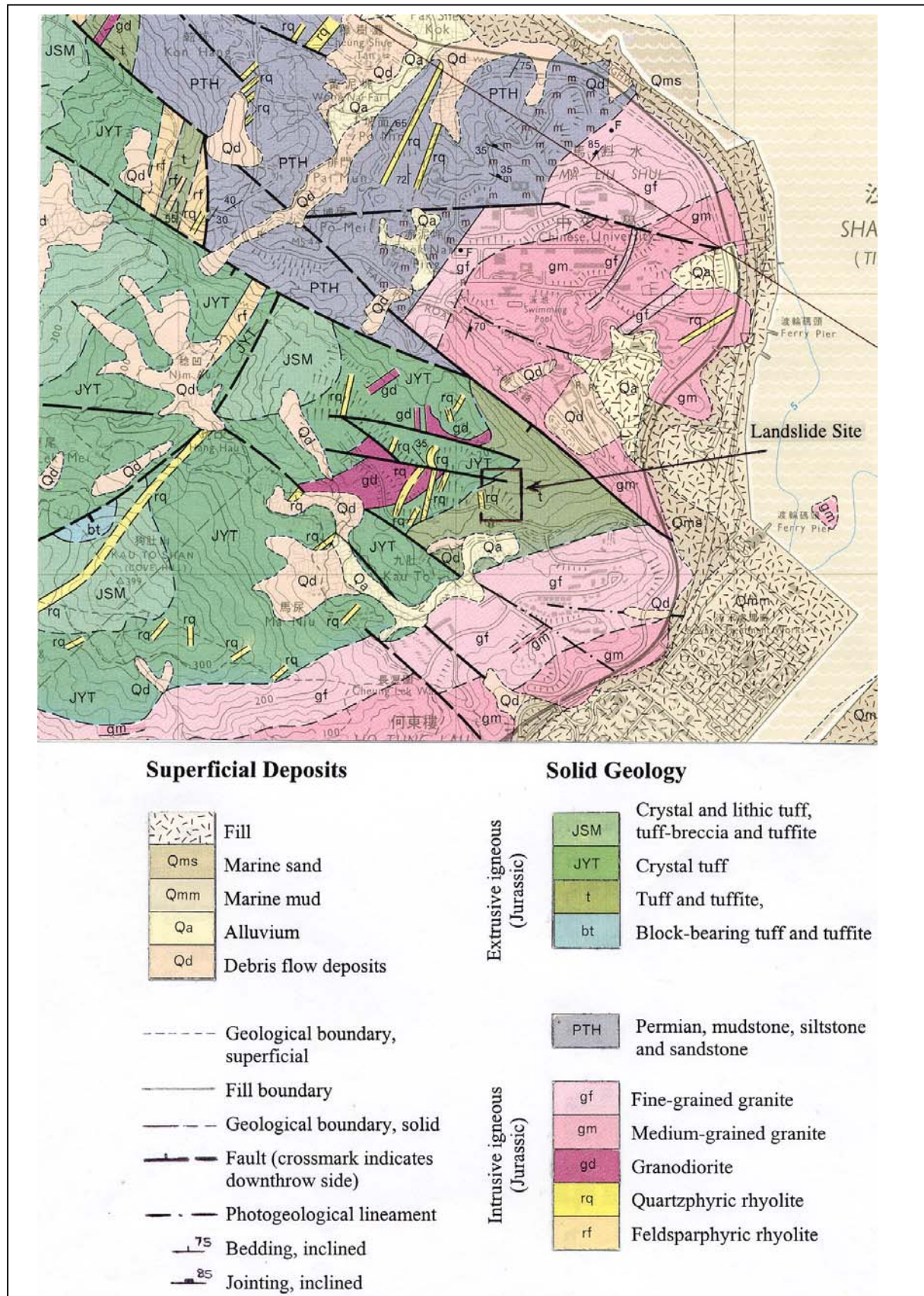


Figure 3 - Geology of the Landslide Site as Shown on Part of Hong Kong Geological Survey Sheet 7 (Sha Tin, 1:20,000-scale; GEO, 1986)

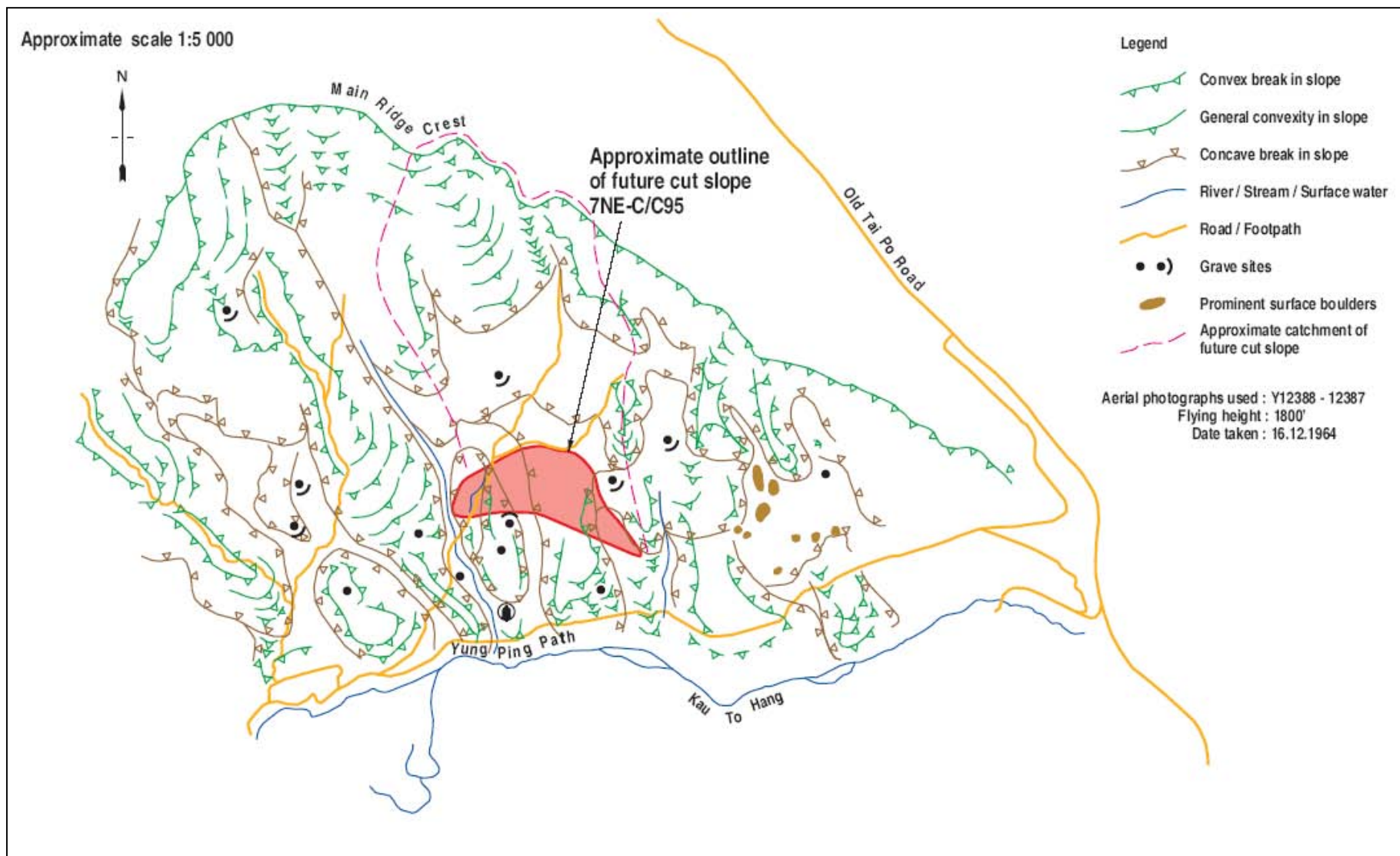


Figure 4 - Aerial Photograph Interpretation of Area Surrounding Lai Ping Road Landslide Site  
Prior to Its Development - Aerial Photographs Used 1964





Figure 5 - Aerial Photograph Interpretation of Slope 7NE-C/C95

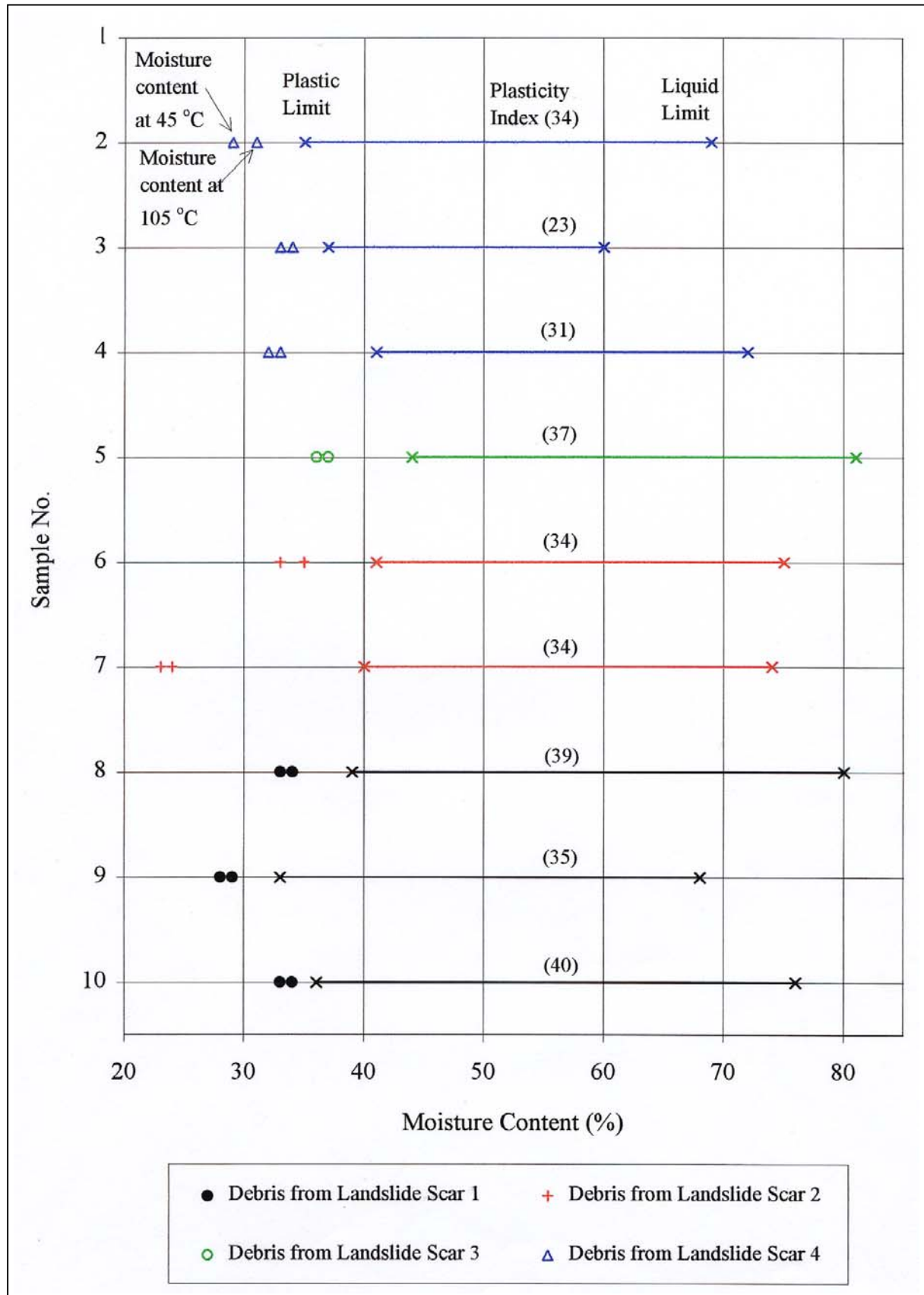


Figure 6 - Atterberg Limits and Moisture Content of the Debris from Landslide Scars 1 to 4



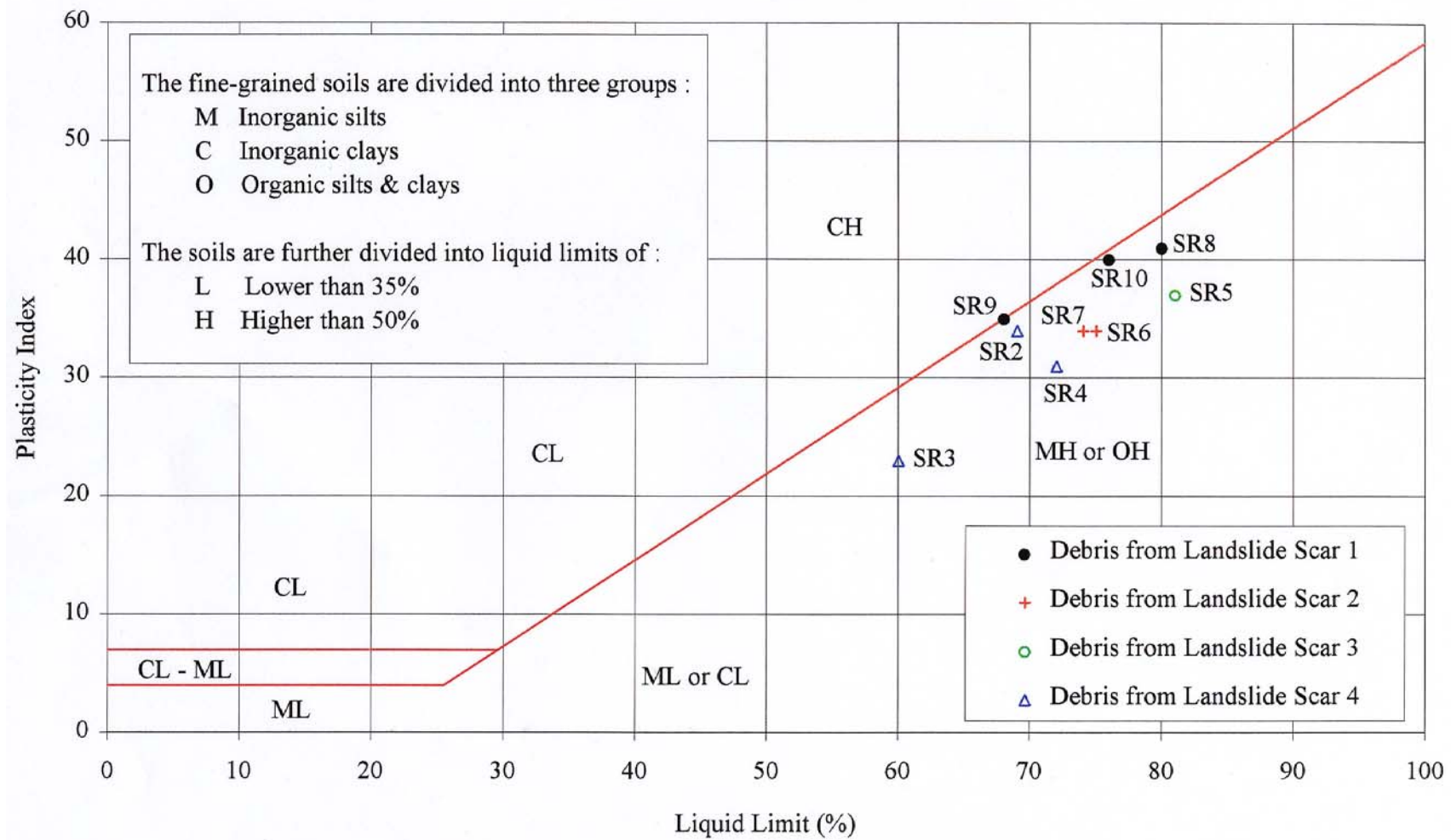


Figure 7 - Plasticity Chart for Landslide Debris

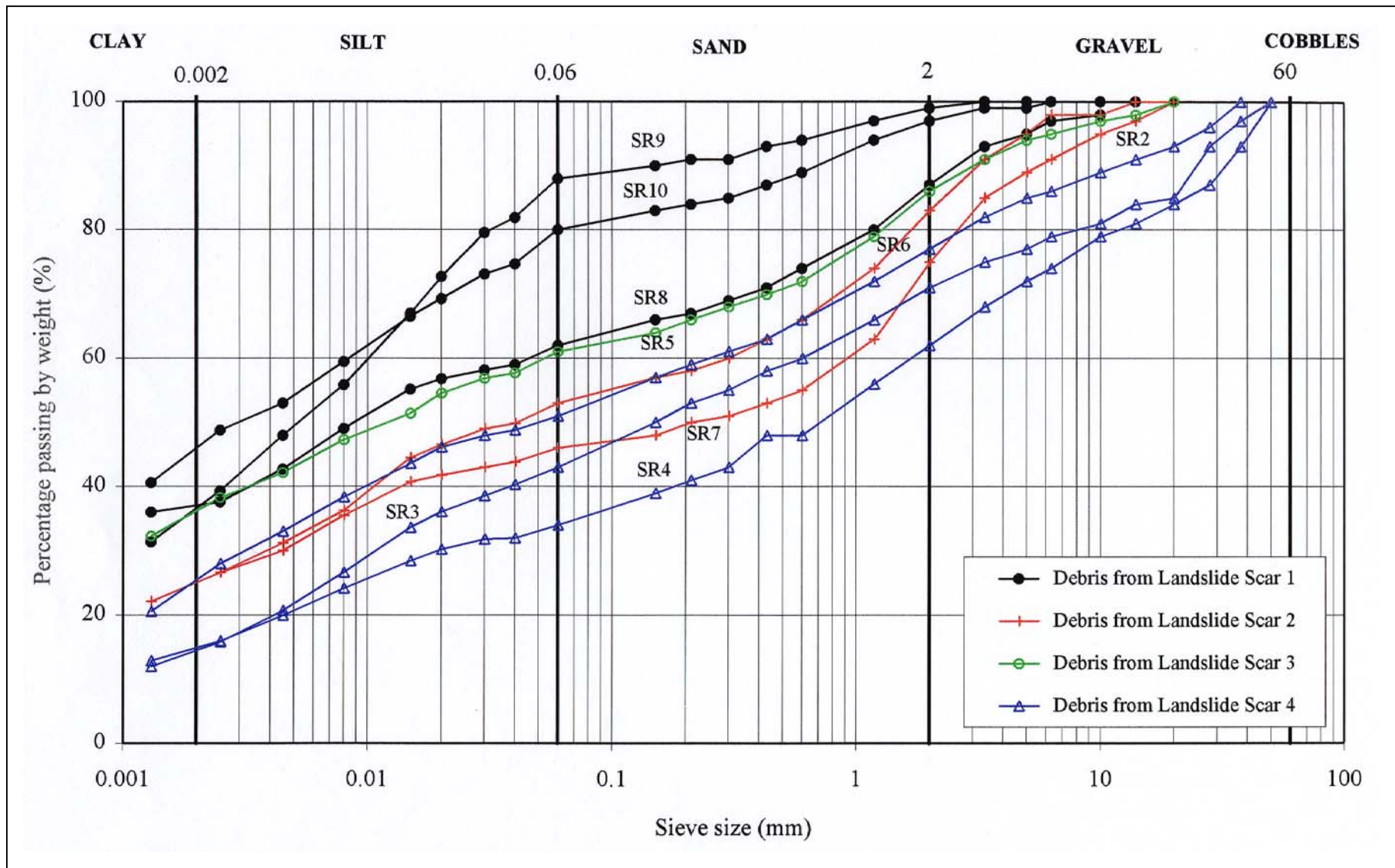


Figure 8 - Particle Size Distribution of Landslide Debris

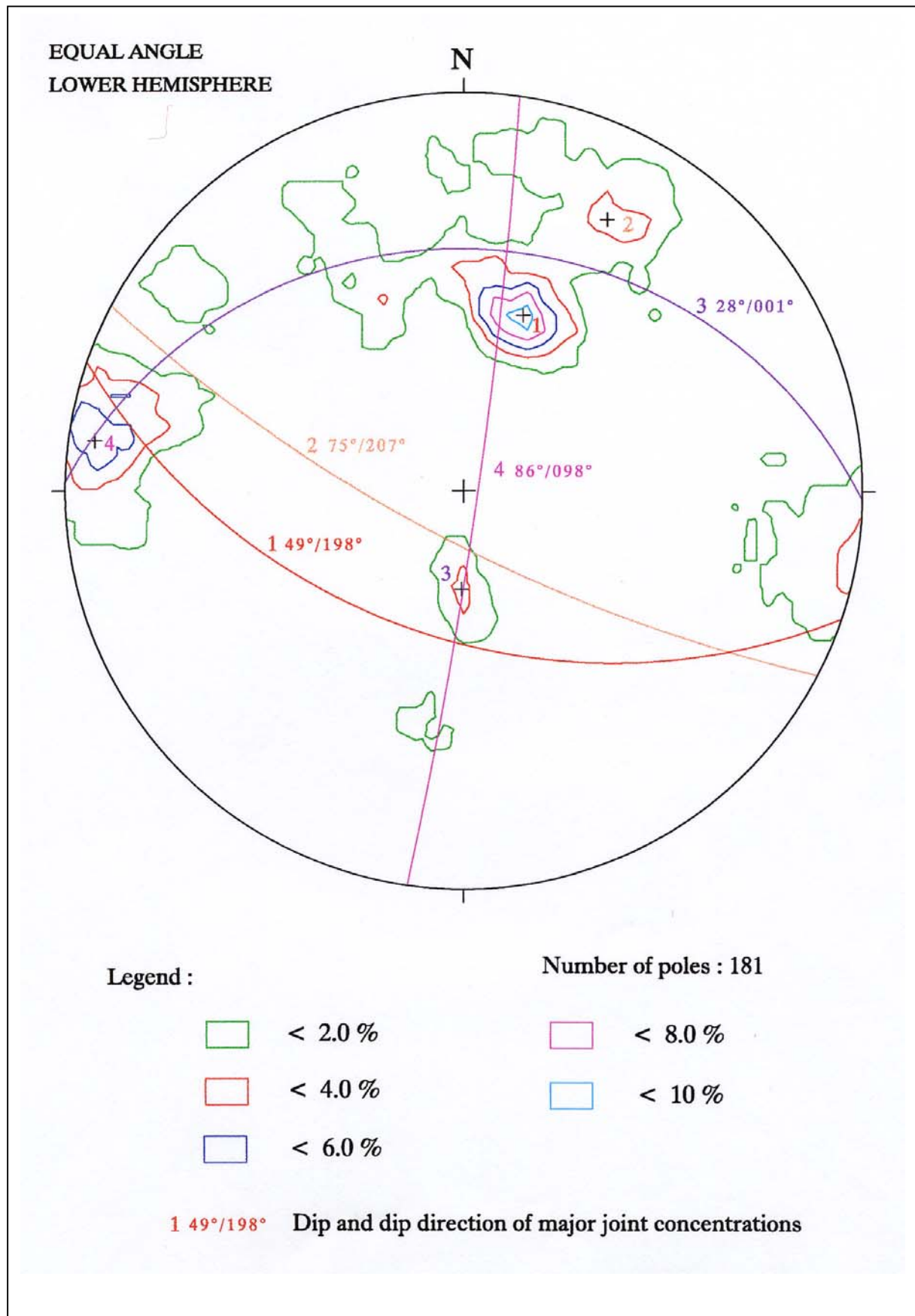


Figure 9 - Contour Plot and Pole Plot of Joint Orientations

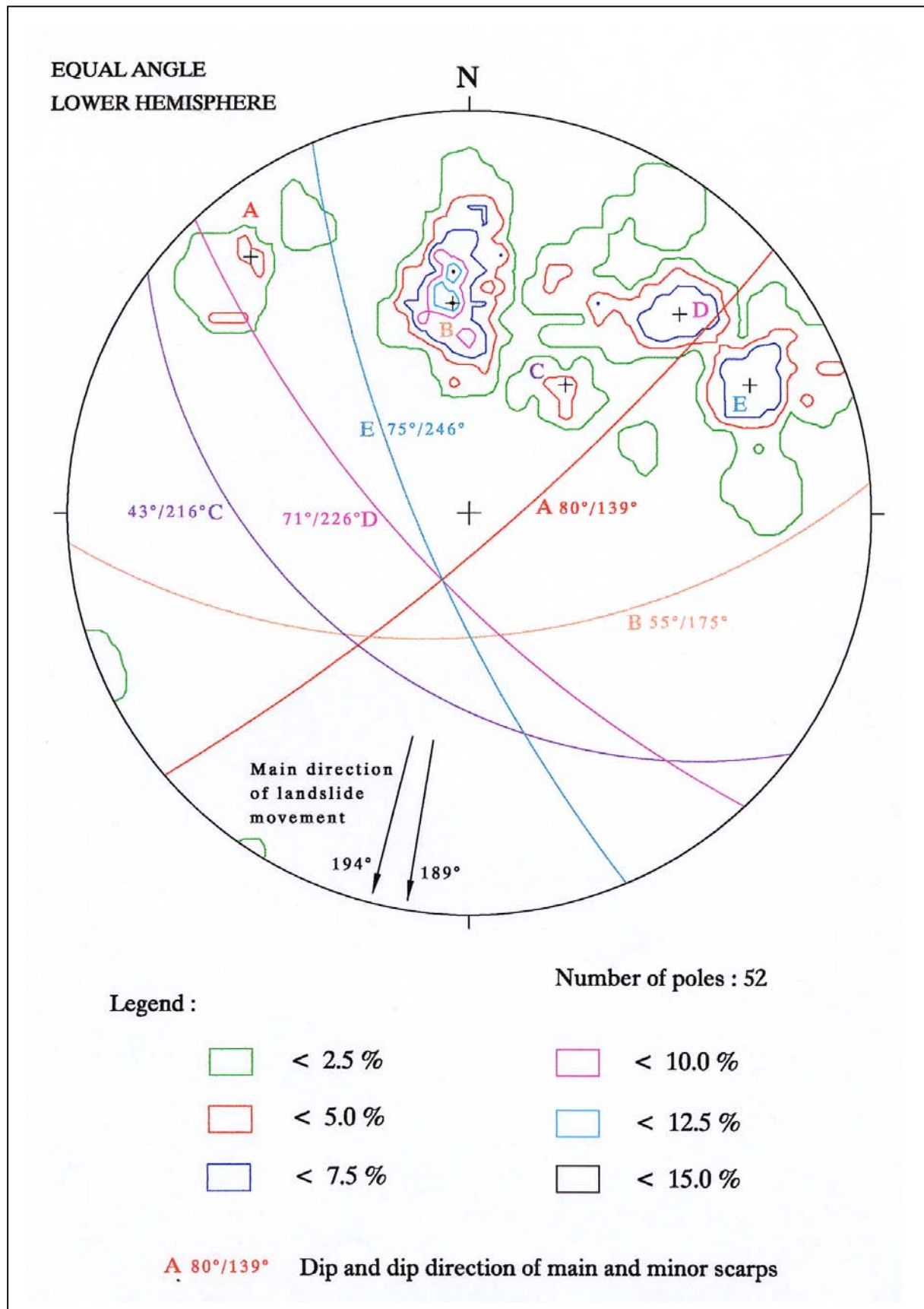


Figure 10 - Contour Plot and Pole Plot of Orientations of Main and Minor Scarps above Landslide Scars 1 to 5



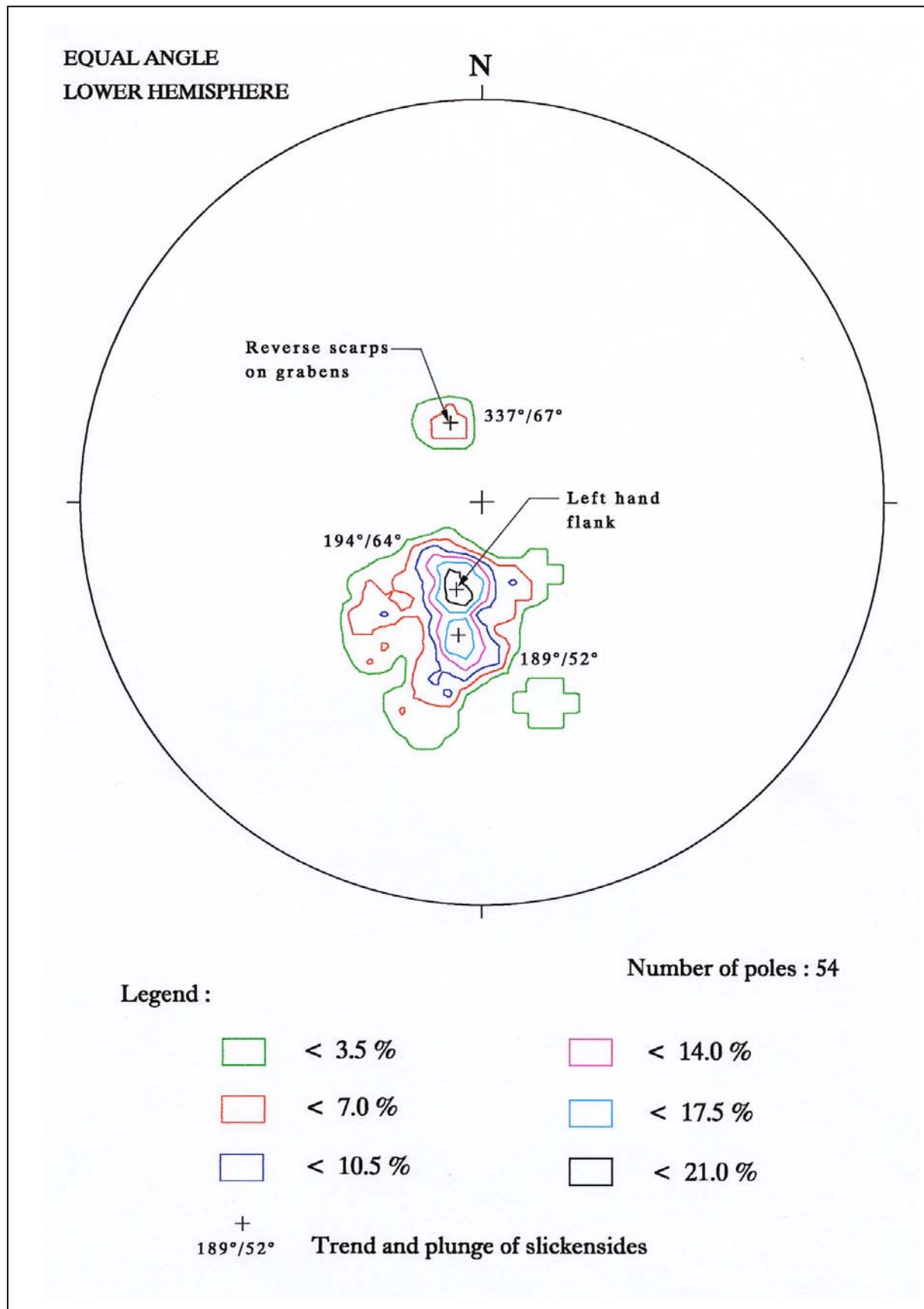
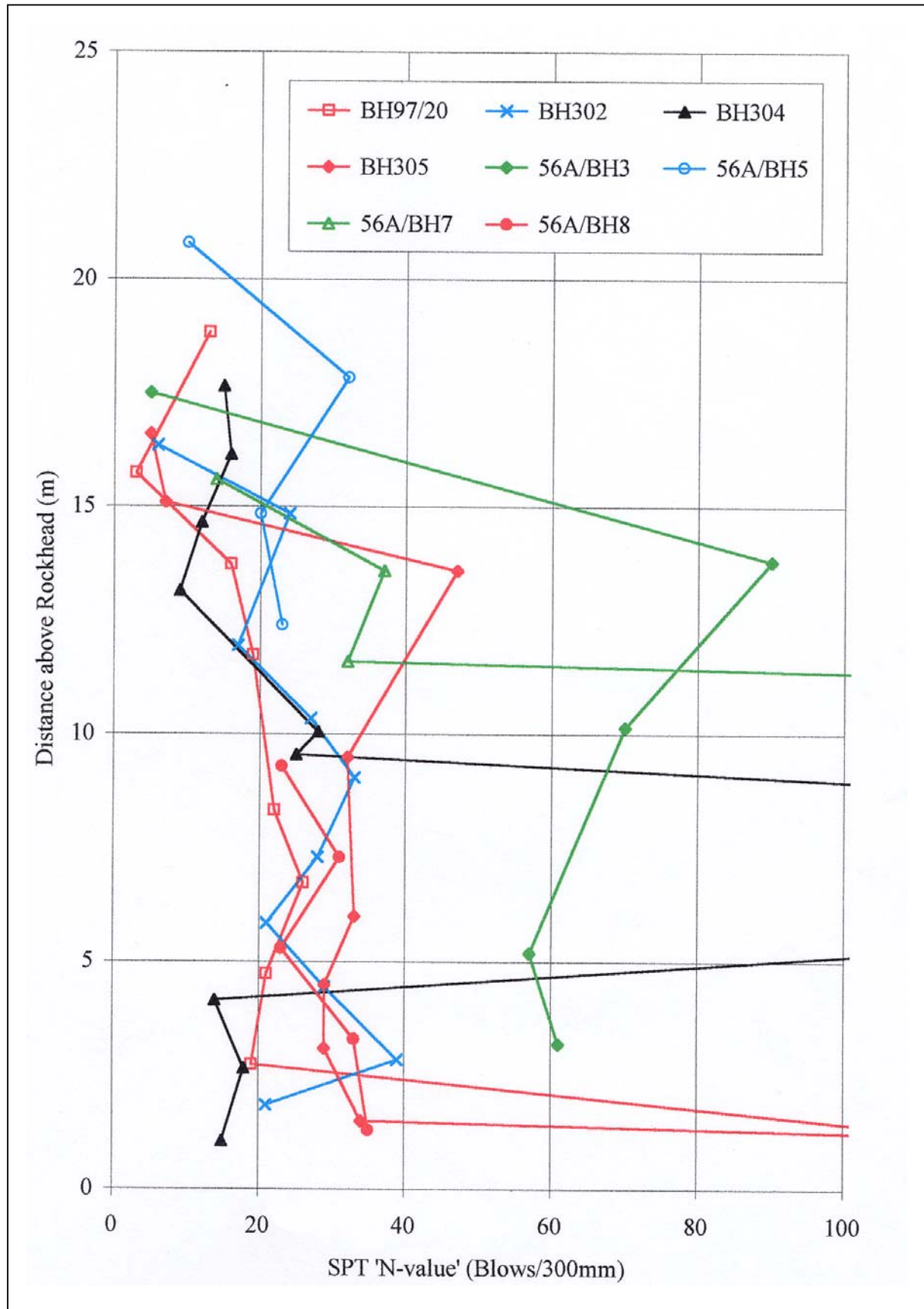


Figure 11 - Contour Plot of Trend and Plunge of Slickensides Measured on Surfaces of Rupture



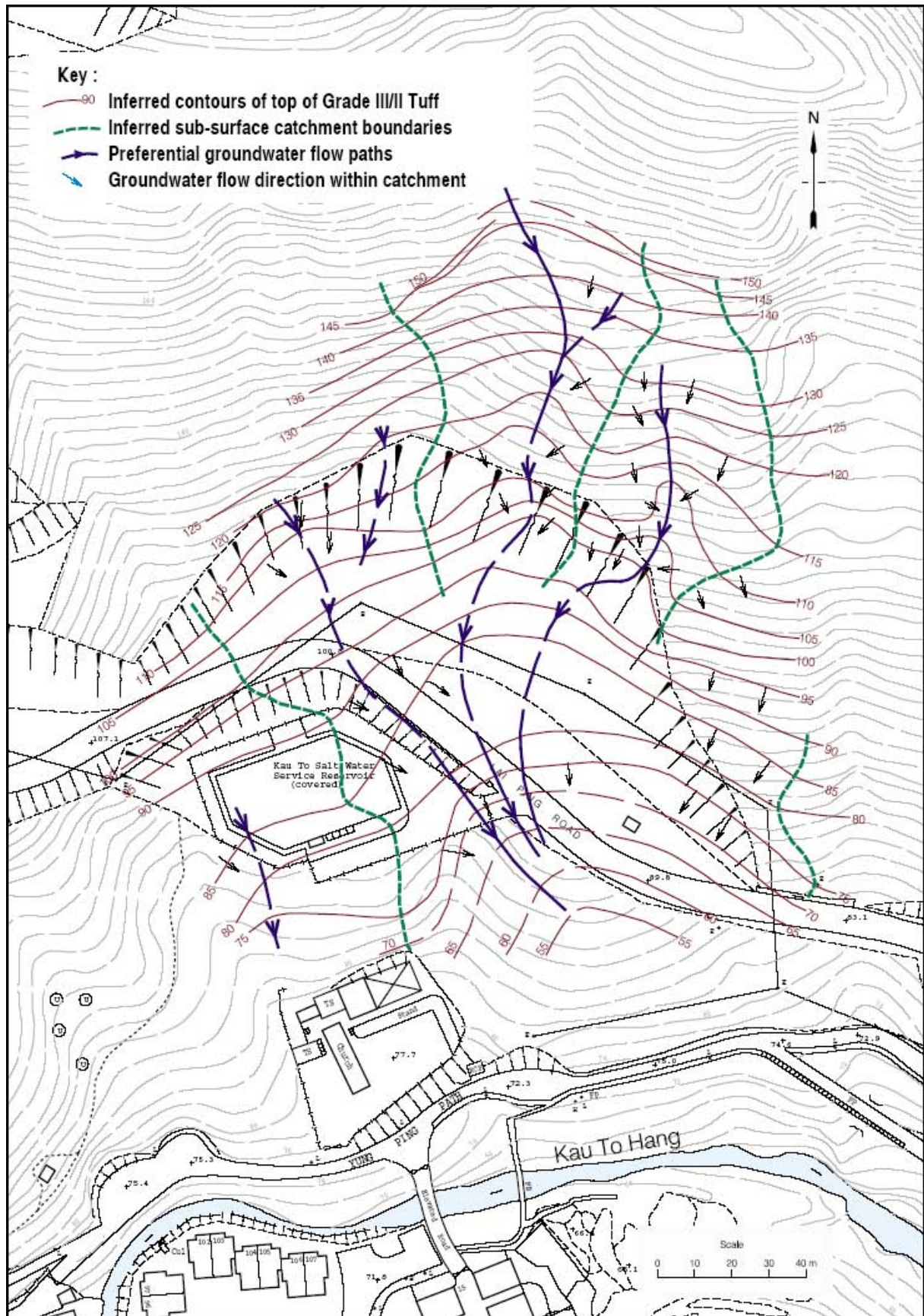


Figure 13 - Hydrogeology



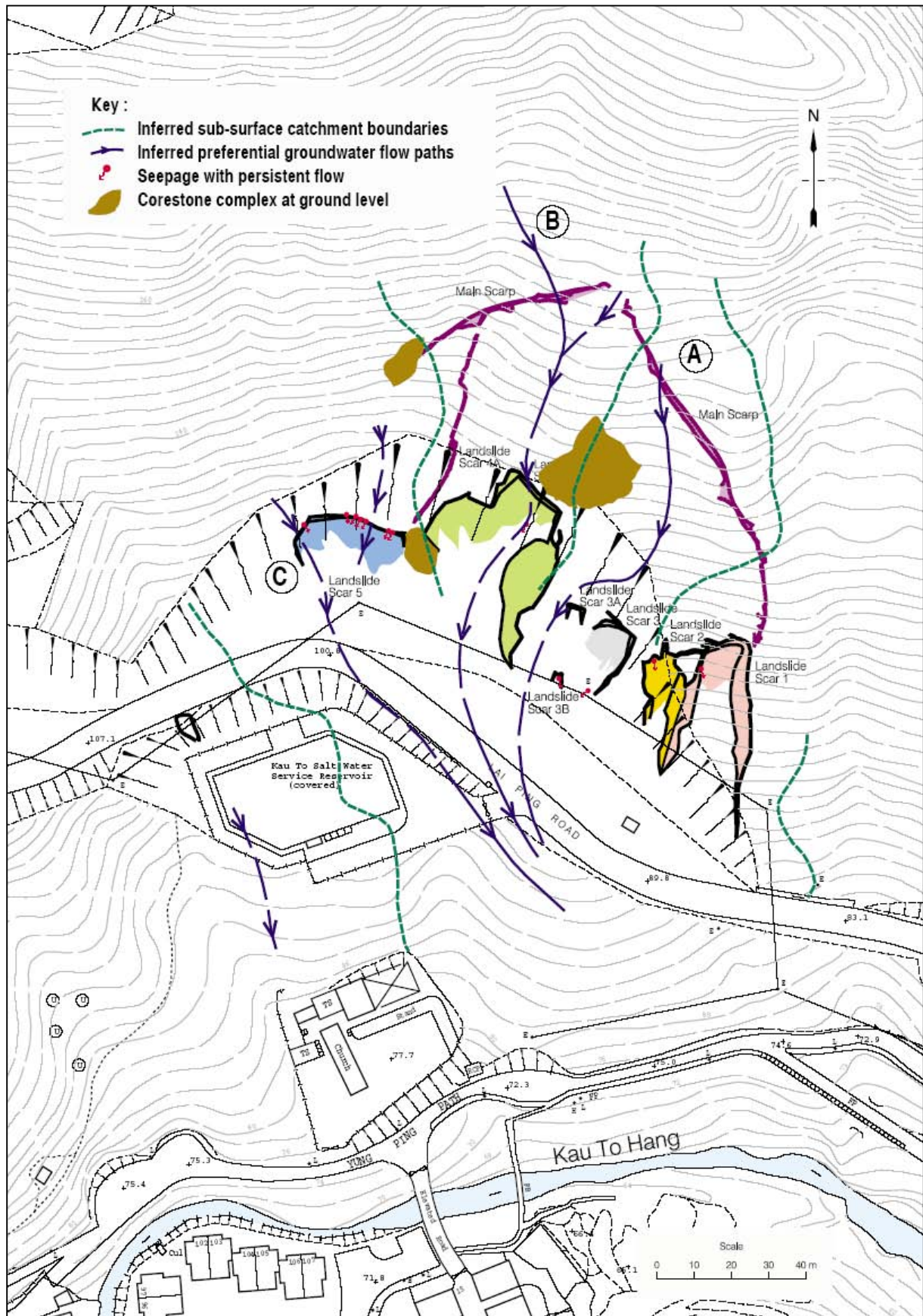


Figure 14 - Hydrogeological Flow Paths in Relation to Landslide Scars, Main Scarp, Seepage Points and Sub-surface Catchments



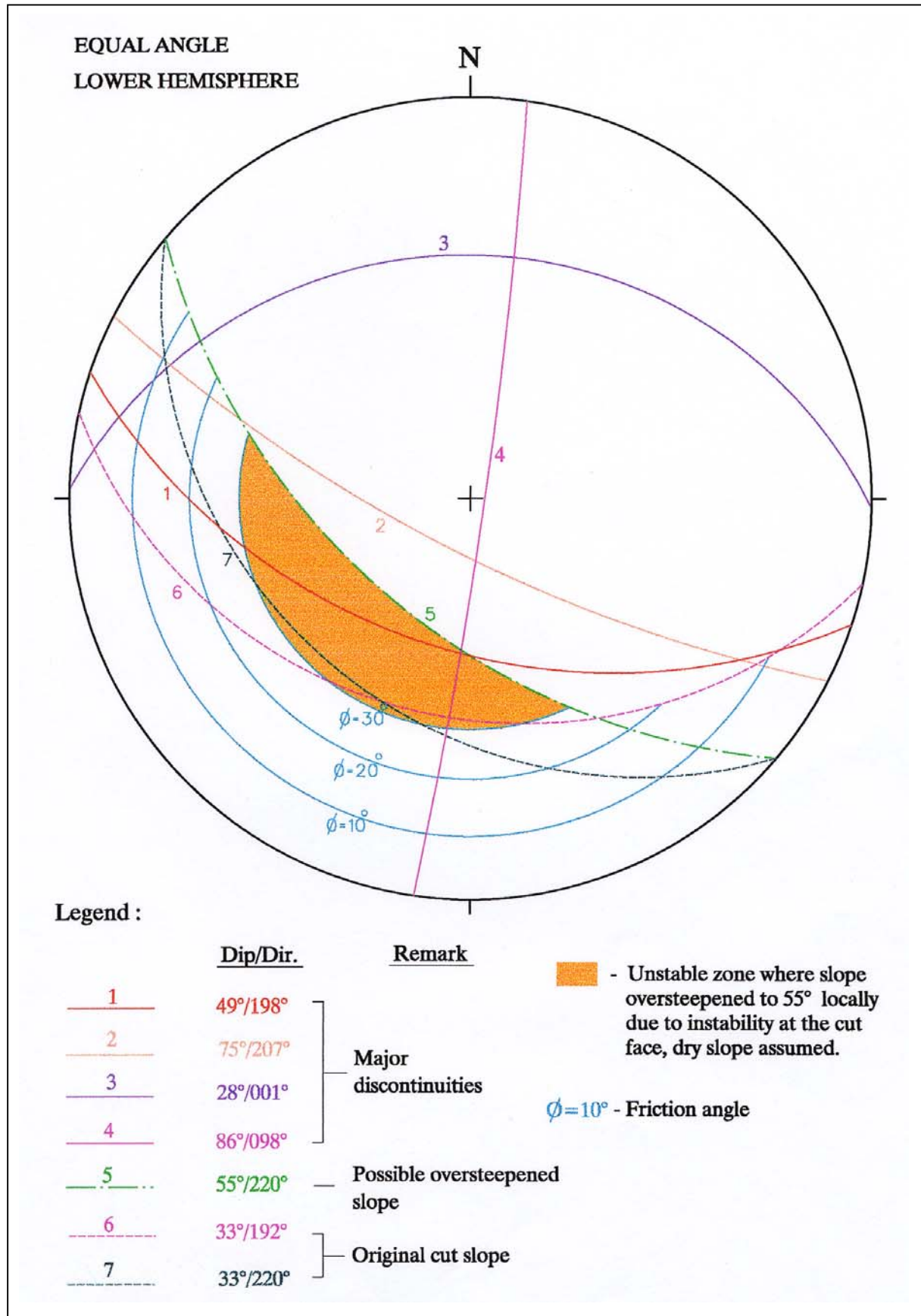


Figure 15 - Stability Plot for Landslide Scars 1 to 5

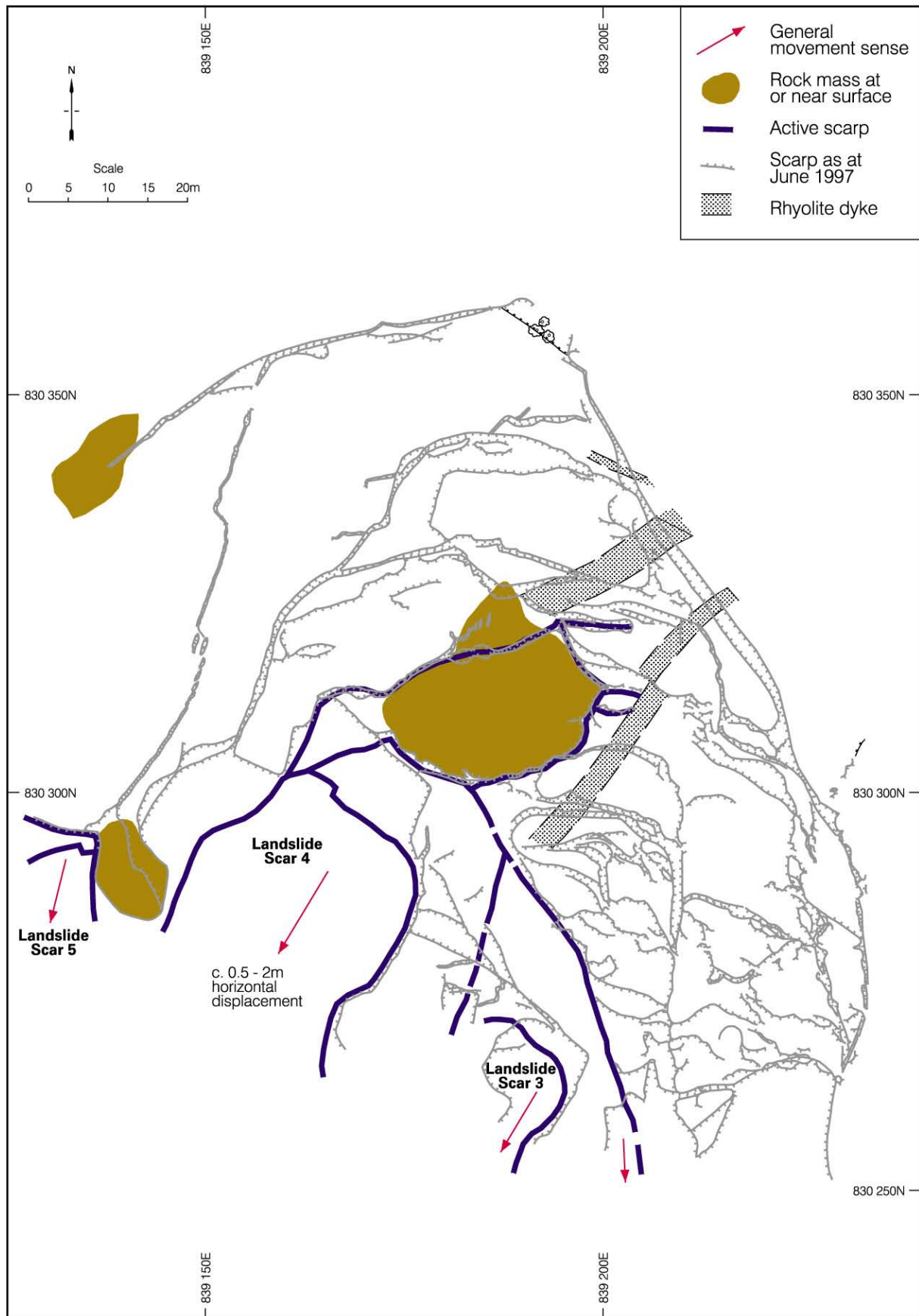


Figure 16 - Composite Landslide Displacement Model - Pre-October 1979

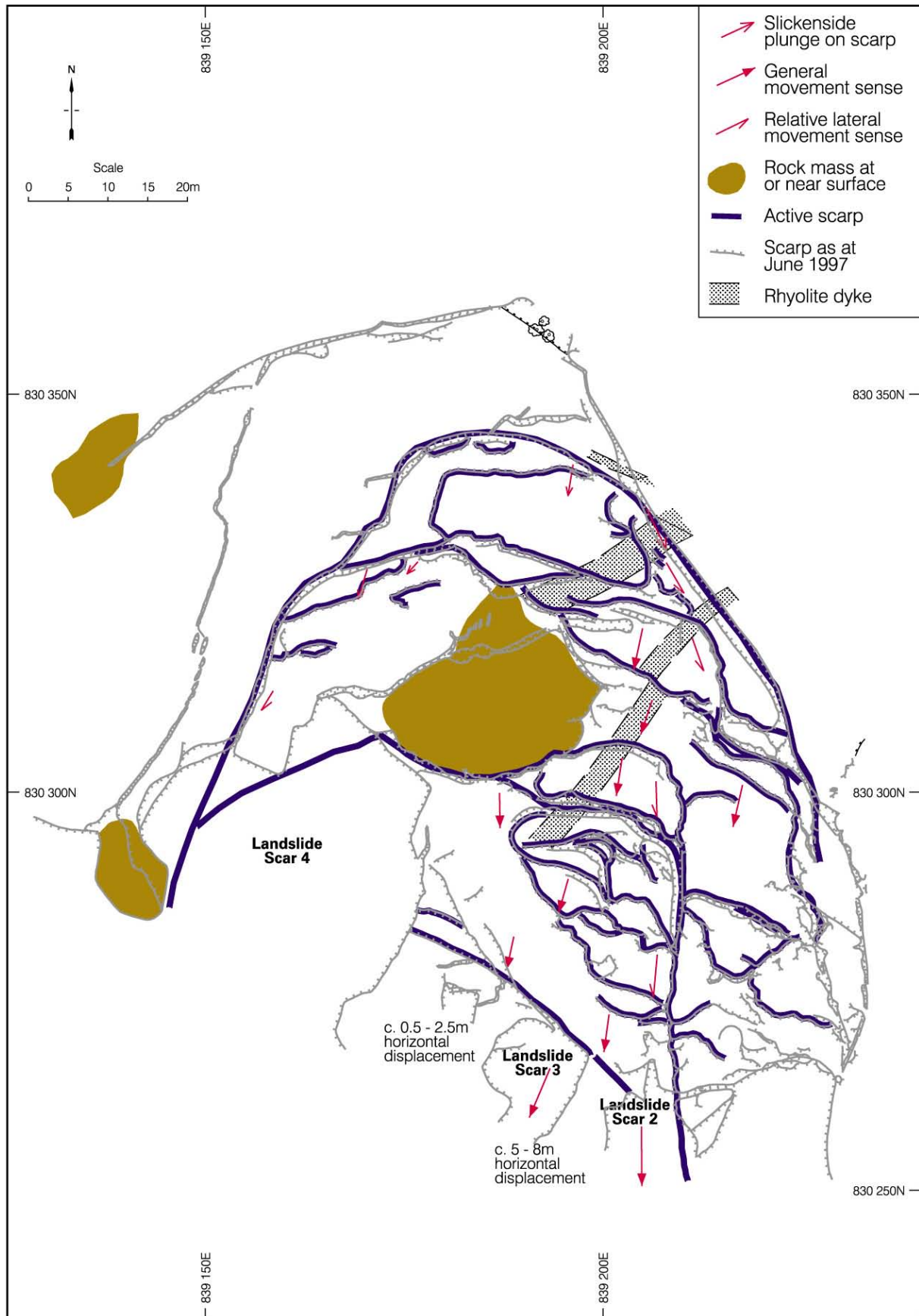


Figure 17 - Composite Landslide Displacement Model - 1983-1987 Including Further Activity Prior to July 1997

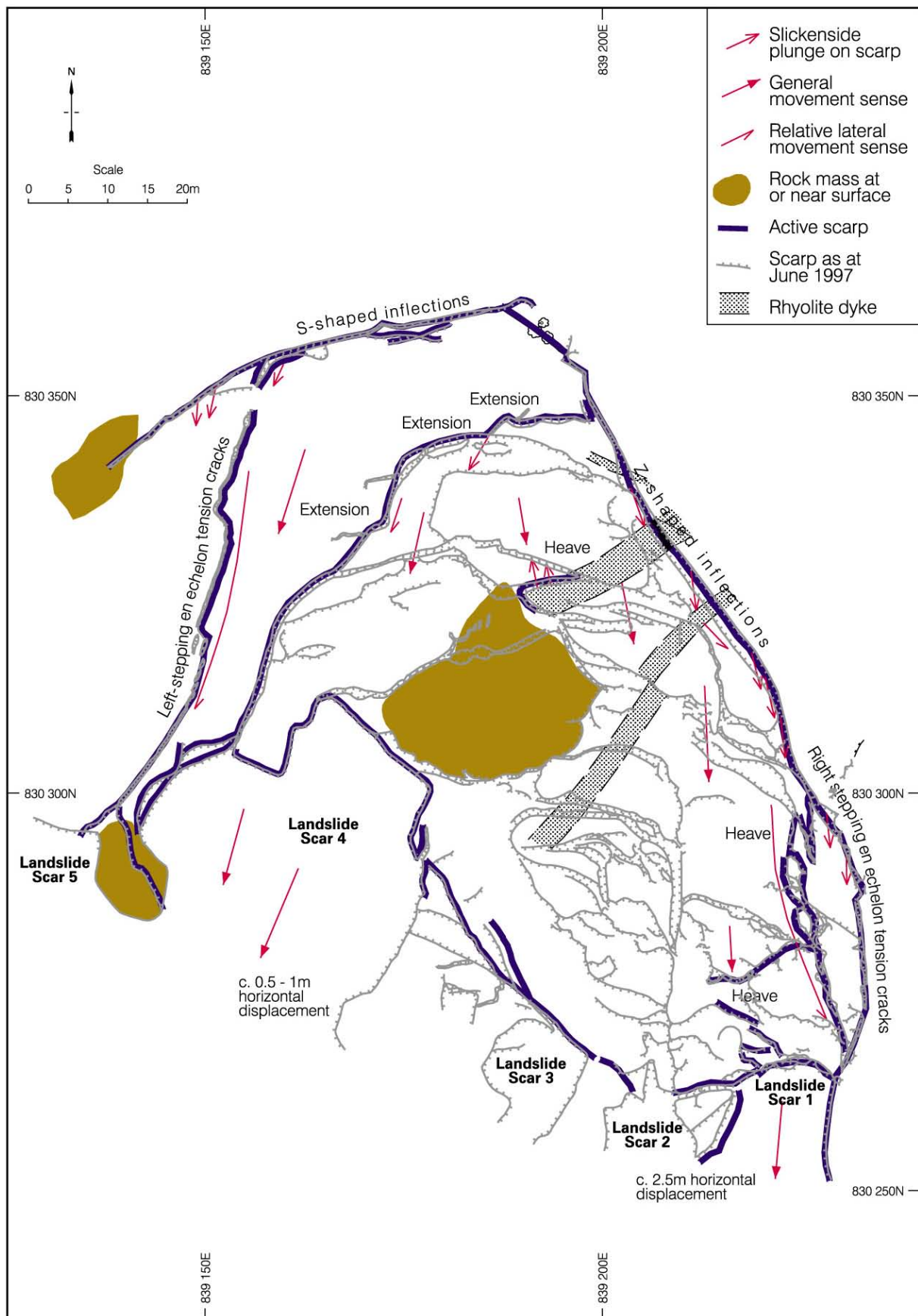


Figure 18 - Composite Landslide Displacement Model - July 1997



LIST OF PLATES

Plate No.		Page No.
1	Oblique Aerial View of Lai Ping Road Landslide Site from the South, Annotated to Show Landslide Scars 1-5, the Approximate Location of the Main Scarp, the Extent of the Debris, Locations of other Minor Failures, the Kau To Shan Borrow Area, the Church Complex and Other Structures (Taken on 4/7/97)	68
2	Oblique Aerial View of Lai Ping Road Landslide from the South-West, Annotated to Show Landslide Scars 1-5 and Associated Debris and Part of the Main Scarp (Taken on 4/7/97)	69
3	Covered Surface Reservoir, Lai Ping Road and Pine Villas in the Valley Base - Viewed from the Crest of Landslide Scar 4A, Looking South (Plate Location Shown on Drawing EG503) (Taken 29/7/97)	70
4	Oblique View of Slope 7NE-C/C95 from the South-West Taken During Construction, Annotated to Show Colluvium Lobe and Zone of Seepage (Taken 3/3/78)	71
5	Lapilli-Bearing Coarse Ash Crystal Tuff (Plate Location Shown on Drawing EG503) (Taken on 7/7/97)	72
6	Flow Banded Quartzphyric Rhyolite Exposed in Landslide Scar 4 (Plate Location Shown on Drawing EG503) (Taken on 6/8/97)	72
7(a)	Intensely Altered Coarse Ash Crystal Tuff Exposed in Landslide Scar 4A (Plate Location Shown on Drawing EG503) (Taken on 6/8/97)	73
7(b)	Southern Face of Block Sample 11 - Intensely Altered Tuff - Note Contorted Relict Joints Infilled with White Kaolin and Manganiferous Deposits (Plate Location Shown on Drawing EG503) (Taken on 21/11/97)	74
8	Main Scarp, Vertical Displacement at this Point is 3.8 m (Plate Location Shown on Drawing EG503) (Taken on 26/9/97)	75
9	Heaved Block of Saprolite or "Pop-Up Structure" within Main and Minor Scarp Complex (Plate Location Shown on Drawing EG503) (Taken on 3/9/97)	76

Plate No.		Page No.
10	Main Scarp Controlled by Relic Joints within Saprolite (Plate Location Shown on Drawing EG503) (Taken on 20/8/97)	76
11	View of Landslide Scar 1 Looking Up Towards the Main Scarp (Plate Location shown on Drawing EG503) (Taken on 30/7/97)	77
12	Planar Slickensided Surface of Rupture Exposed below the Crown of Landslide Scar 1 (Plate Location Shown on Drawing EG503) (Taken on 30/7/97)	78
13	Flat Area of Deposition and Debris Mound in Area Up-Slope of the Intact Debris Raft in Landslide Scar 1 (Plate Location Shown on Drawing EG503) (Taken on 30/7/97)	79
14	View of Landslide Scar 2 Looking Up Towards the Main Scarp (Plate Location Shown on Drawing EG503) (Taken on 14/7/97)	80
15	Corestone Showing Evidence of Rotation Exposed in Right Hand Flank of Landslide Scar 2 (Plate Location Shown on Drawing EG503) (Taken on 10/7/97)	81
16	Made Ground Exposed in the Main Scarp of Landslide Scar 2 (Plate Location Shown on Drawing EG503) (Taken on 7/8/97)	81
17	View of Landslide Scar 3 Looking Down Towards the Left Hand Flank (Plate Location Shown on Drawing EG503) (Taken on 7/7/97)	82
18	Oblique View of Cut Slope 7NE-C/C95 from South Annotated to Show the Approximate Locations of Landslide Scars 3-5, Tension Cracks and Major Soil Pipes (Taken on 10/79 by Maunsell Consultants Asia)	83
19	Landslide Scar 3A Viewed from the South-East (Plate Location Shown on Drawing EG503) (Taken on 7/7/97)	84
20	Counter-Scarp Tension Cracks above Landslide Scar 3A Indicating Possible Toppling Mode of Failure (Plate Location Shown on Drawing EG503) (Taken on 10/7/97)	85

Plate No.		Page No.
21	View of Landslide Scar 4 & 4A (Plate Location Shown on Drawing EG503) (Taken on 12/8/97)	86
22	Left Hand Flank of Landslide Scar 4 Showing Disrupted Rock Mass (Plate Location Shown on Drawing EG503) (Taken on 6/8/97)	87
23	Joint Controlled Surface of Rupture Exposed in Landslide Scar 4 (Plate Location Shown on Drawing EG503) (Taken on 6/8/97)	88
24	Surface of Rupture Through Intact Saprolite Exposed in Landslide Scar 4A - Note Sharp Interface Between Recent Debris and Surface of Rupture (Plate Location Shown on Drawing EG503) (Taken on 27/8/97)	89
25	Debrisflow-Earthflow Lobes from Landslide Scar 4A (Plate Location Shown on Drawing EG503) (Taken on 10/7/97)	89
26	View of Landslide Scar 5 from the South-East (Plate Location Shown on Drawing EG503) (Taken on 12/8/97)	90
27(a)	Main Scarp of Landslide Scar 5 Viewed from the West - Note Older Mottled Colluvium, Dark Brown Staining on Scarp Surface and Sharp Interface Between Colluvium and Saprolite (Taken on 8/8/97)	91
27(b)	Main Scarp of Landslide Scar 5 Viewed from the East - Note Large Soil Pipe. (Plate Location Shown on Drawing EG503) (Taken on 7/7/97)	91
28(a)	A Large 1.5 m Wide Soil Pipe at the Old Colluvium-New Colluvium Interface Exposed in the Main Scarp of Landslide Scar 5 - Note Slight Seepage (Plate Location Shown on Drawing EG503) (Taken on 7/7/97)	92
28(b)	Soil Pipe with Medium Flow (Plate Location Shown on Drawing EG503) (Taken on 8/8/97)	92
28(c)	Soil Pipe with Heavy Flow (Plate Location Shown on Drawing EG503) (Taken on 9/9/97)	93
29	Small 40 mm Diameter Soil Pipes at the Old Colluvium-Saprolite Interface Exposed in Landslide Scar 5 (Plate Location Shown on Drawing EG503) (Taken on 21/7/97)	94

Plate No.		Page No.
30	Rhyolite Dyke Exposed in Landslide Scar 4 - Note Very Closely Spaced Joints with White Kaolin Infill (Plate Location Shown on Drawing EG503) (Taken on 7/7/97)	94
31	Temporary Cut in the Left Hand Flank of Landslide Scar 4 Exposing an Inclined Brittle Dilating Shear Plane within the Partially Weathered Rock Mass (Plate Location Shown on Drawing No. EG503) (Taken on 5/9/97)	95
32	Split 4CMLC Core from Drillhole TT2 Showing Sub-Vertical Relict Joints with Much Manganiferous Staining on the Joint Surface and within the Rock Fabric (Taken on 31/1/98)	96
33	Close-Up of Split Mazier Sample from Drillhole DH97/20 Showing Disrupted Zone Comprising Pockets of Angular Quartz, Feldspar and Moderately Decomposed Tuff, Sand and Gravel, Stiff Brown Silty Clay and Cobbles of Highly Decomposed Tuff (Taken on 6/5/98)	97
34	Close-Up of Split 4CMLC Core from Drillhole TT2A Showing an Anomalous Zone within Grade V Saprolite Interpreted as Being either an Infilled Soil Pipe or a High Permeability Shear Zone (Taken on 6/5/98)	98
35	Minor Scarp Showing at Least Two Phases of Displacement Recognisable by the Vegetation Line of Moss - Scarp Height 1.8 m - Old Displacement 1.6 m - New Displacement 0.2 m (Plate Location Shown on Drawing EG503) (Taken on 24/7/97)	99
36(a)	Main Scarp Showing Vegetation Line Indicating at Least Two Phases of Movement Together with Old and Recent Slickensides on the Scarp Surface and a Rhyolite Dyke Contact (Plate Location Shown on Drawing EG503) (Taken on 26/9/97)	100
36(b)	Close-Up of Old Moss Covered Slickensides (Plate Location Shown on Drawing EG503) (Taken on 26/9/97)	101
37	Re-Growth of Tree Branch Directly up Main Scarp (Plate Location Shown on Drawing EG503) (Taken on 26/9/97)	102





Plate 1 - Oblique Aerial View of Lai Ping Road Landslide Site from the South, Annotated to Show Landslide Scars 1-5, the Approximate Location of the Main Scarp, the Extent of the Debris, Locations of other Minor Failures, the Kau To Shan Borrow Area, the Church Complex and Other Structures (Taken on 4/7/97)

PS 884/11



Plate 2 - Oblique Aerial View of Lai Ping Road Landslide from the South-West, Annotated to Show Landslide Scars 1-5 and Associated Debris and Part of the Main Scarp (Taken on 4/7/97)

PS 885/04





Plate 3 - Covered Surface Reservoir, Lai Ping Road and Pine Villas in the Valley Base - Viewed from the Crest of Landslide Scar 4A, Looking South (Plate Location Shown on Drawing EG503)  
(Taken 29/7/97)

GS 97/83/14-22

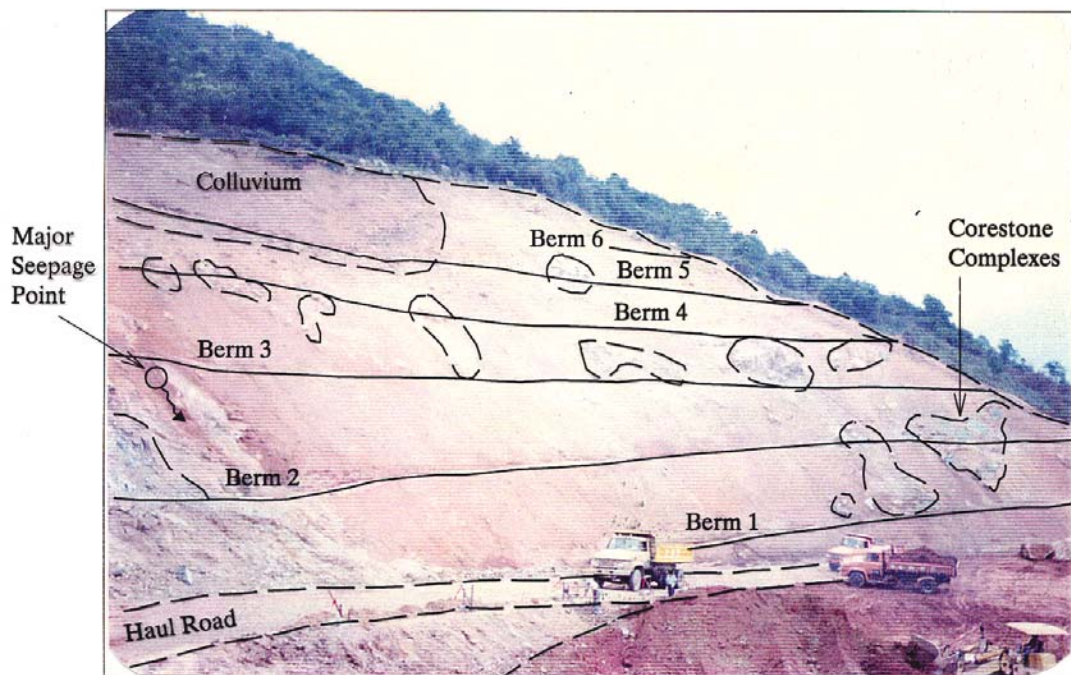


Plate 4 - Oblique View of Slope 7NE-C/C95 from the South-West Taken During Construction, Annotated to Show Colluvium Lobe and Zone of Seepage (Taken 3/3/78).





Plate 5 - Lapilli-Bearing Coarse Ash Crystal Tuff (Plate Location Shown on Drawing EG503) (Taken on 7/7/97)

GS 97/53/09



Plate 6 - Flow Banded Quartzphyric Rhyolite Exposed in Landslide Scar 4 (Plate Location Shown on Drawing EG503) (Taken on 6/8/97)

GS 97/108C/07





Plate 7(a) - Intensely Altered Coarse Ash Crystal Tuff Exposed in Landslide Scar 4A (Plate Location Shown on Drawing EG503) (Taken on 6/8/97)

GS 97/108/21

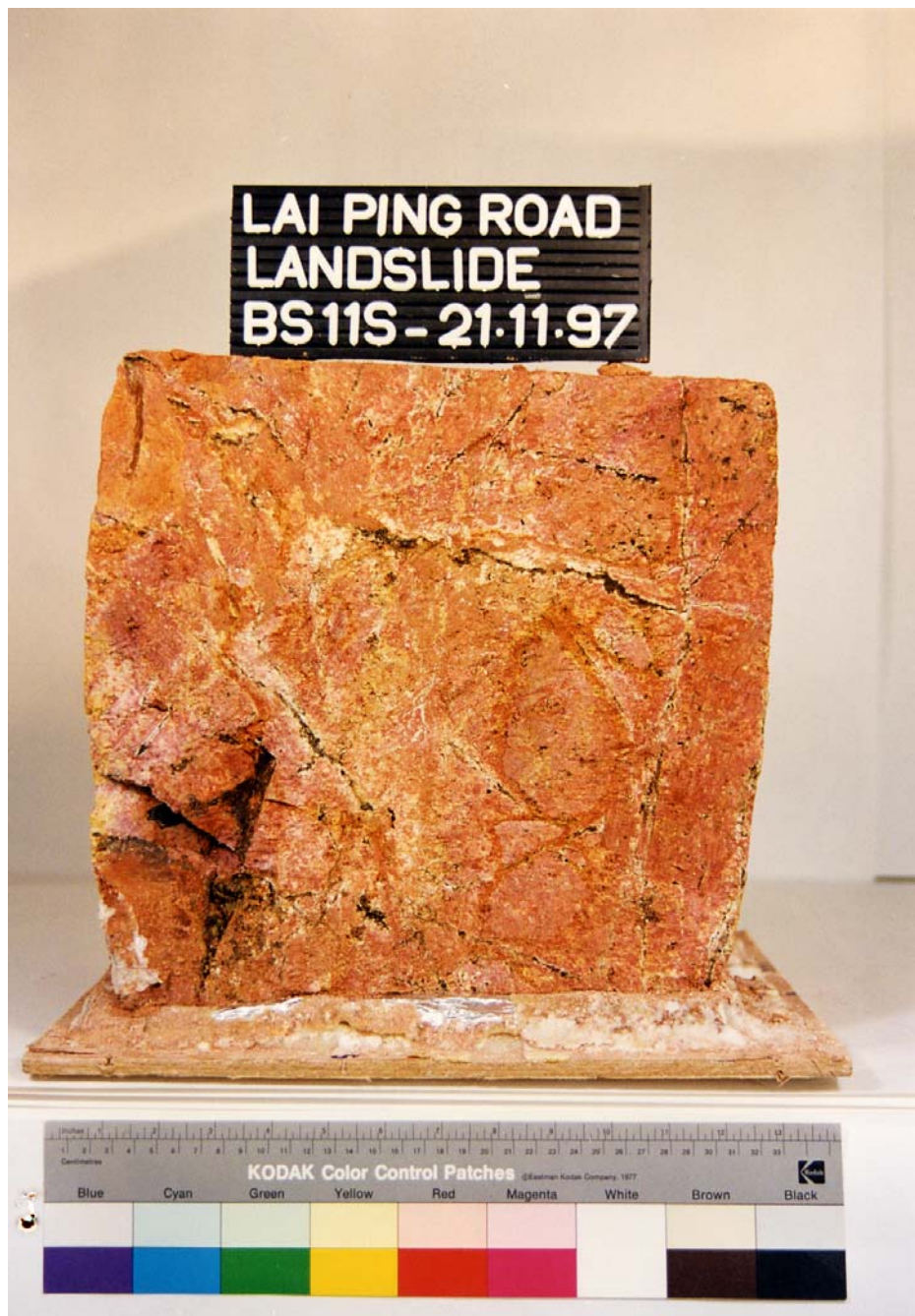


Plate 7(b) - Southern Face of Block Sample 11 - Intensely Altered Tuff -  
Note Contorted Relict Joints Infilled with White Kaolin and  
Manganiferous Deposits (Plate Location Shown on Drawing  
EG503) (Taken on 21/11/97)

EG 97/147/04





Plate 8 - Main Scarp, Vertical Displacement at this Point is 3.8 m  
(Plate Location Shown on Drawing EG503) (Taken on  
26/9/97)

EG 97/117/06





Plate 9 - Heaved Block of Saprolite or “Pop-Up Structure” within Main and Minor Scarp Complex (Plate Location Shown on Drawing EG503)  
(Taken on 3/9/97)

GS 97/119/35



Plate 10 - Main Scarp Controlled by Relic Joints within Saprolite (Plate Location Shown on Drawing EG503) (Taken on 20/8/97)

EG 97/106/22





Plate 11 - View of Landslide Scar 1 Looking Up Towards the Main Scarp (Plate Location shown on Drawing EG503) (Taken on 30/7/97)

EG 97/95/23-35





Plate 12 - Planar Slickensided Surface of Rupture Exposed below the Crown of Landslide Scar 1 (Plate Location Shown on Drawing EG503) (Taken on 30/7/97)

EG 97/96/04





Plate 13 - Flat Area of Deposition and Debris Mound in Area Up-Slope of the Intact Debris Raft in Landslide Scar 1 (Plate Location Shown on Drawing EG503) (Taken on 30/7/97)

EG 97/95/17 - 21





Plate 14 - View of Landslide Scar 2 Looking Up Towards the Main Scarp (Plate Location Shown on Drawing EG503) (Taken on 14/7/97)

GS 97/22/2 - 5





Plate 15 - Corestone Showing Evidence of Rotation Exposed in Right Hand Flank of  
Landslide Scar 2 (Plate Location Shown on Drawing EG503) (Taken on 10/7/97)  
EG 97/89/29



Plate 16 - Made Ground Exposed in the Main Scarp of Landslide Scar 2 (Plate Location  
Shown on Drawing EG503) (Taken on 7/8/97)  
GS 97/93C/14

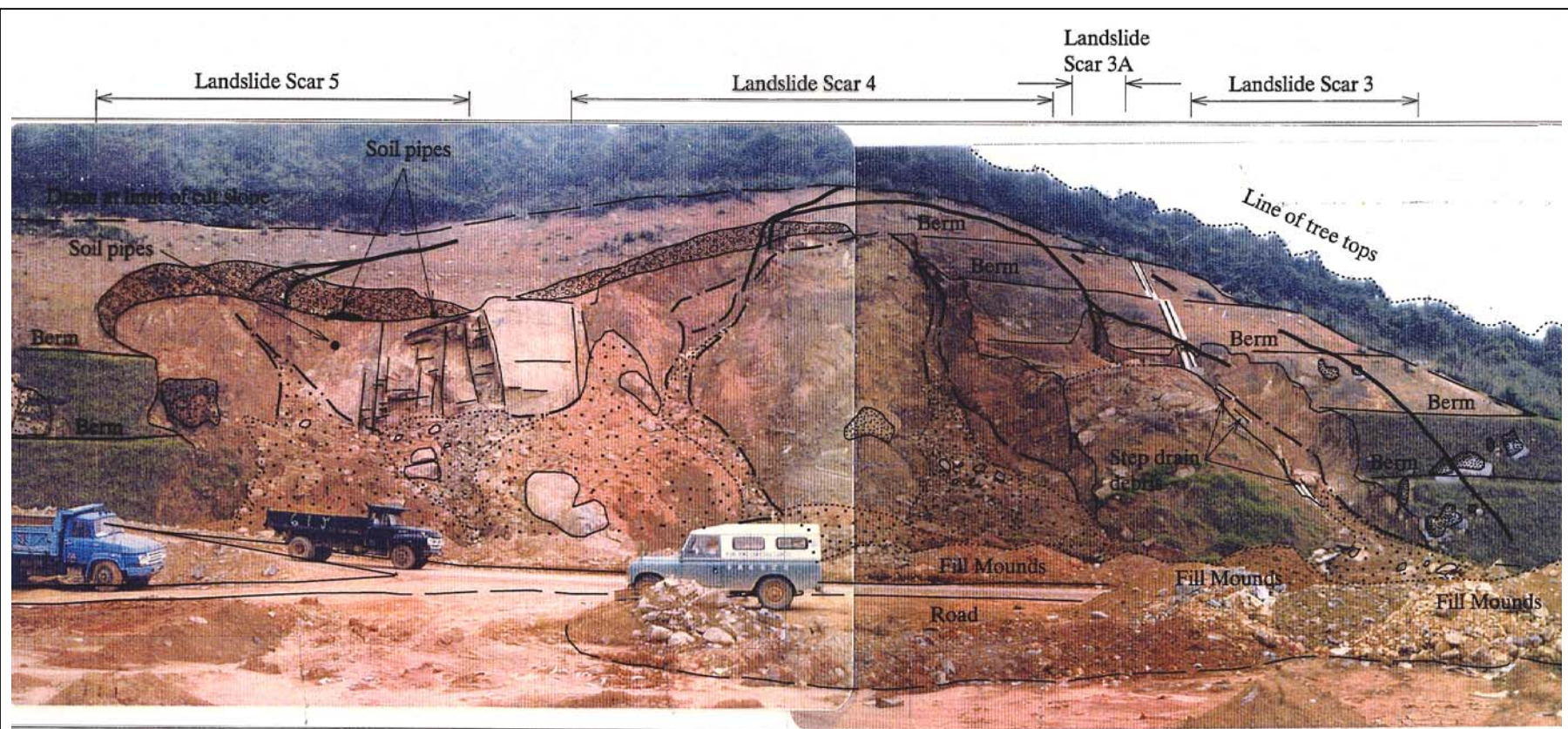




Plate 17 - View of Landslide Scar 3 Looking Down Towards the Left Hand Flank (Plate Location Shown on Drawing EG503) (Taken on 7/7/97)

GS 97/54/7 - 10





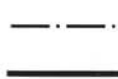
Legend :



Colluvium

Corestones

Landslide debris



Concave break in slope

Tension crack

Plate 18 - Oblique View of Cut Slope 7NE-C/C95 from South Annotated to Show the Approximate Locations of Landslide Scars 3-5, Tension Cracks and Major Soil Pipes (Taken on 10/79 by Maunsell Consultants Asia)





Plate 19 - Landslide Scar 3A Viewed from the South-East (Plate  
Location Shown on Drawing EG503) (Taken on 7/7/97)

GS 97/54/06





Plate 20 - Counter-Scarp Tension Cracks above Landslide Scar 3A  
Indicating Possible Toppling Mode of Failure (Plate  
Location Shown on Drawing EG503) (Taken on 10/7/97)

GS 97/64/17



Plate 21 - View of Landslide Scar 4 & 4A (Plate Location Shown on Drawing EG503)  
(Taken on 12/8/97)

EG 97/104/12 - 13, 22, 24





Plate 22 - Left Hand Flank of Landslide Scar 4 Showing Disrupted Rock Mass (Plate Location Shown on Drawing EG503) (Taken on 6/8/97)

GS 97/108C/23 - 25





Plate 23 - Joint Controlled Surface of Rupture Exposed in Landslide Scar 4 (Plate Location Shown on Drawing EG503) (Taken on 6/8/97)

GS 97/108C/13 - 15





Plate 24 - Surface of Rupture Through Intact Saprolite Exposed in Landslide Scar 4A - Note Sharp Interface Between Recent Debris and Surface of Rupture (Plate Location Shown on Drawing EG503) (Taken on 27/8/97)  
EG 97/109/15



Plate 25 - Debrisflow-Earthflow Lobes from Landslide Scar 4A (Plate Location Shown on Drawing EG503) (Taken on 10/7/97)  
GS 97/64/10 - 11





Plate 26 - View of Landslide Scar 5 from the South-East (Plate Location Shown on Drawing EG503)  
(Taken on 12/8/97)

EG 97/104/14 - 16, 19, 21



Plate 27(a) - Main Scarp of Landslide Scar 5 Viewed from the West - Note Older Mottled Colluvium, Dark Brown Staining on Scarp Surface and Sharp Interface Between Colluvium and Saprolite (Taken on 8/8/97) GS 97/107/33



Plate 27(b) - Main Scarp of Landslide Scar 5 Viewed from the East - Note Large Soil Pipe (Plate Location Shown on Drawing EG503) (Taken on 7/7/97) GS 97/53/15





Plate 28(a) - A Large 1.5 m Wide Soil Pipe at the Old Colluvium-New Colluvium Interface Exposed in the Main Scarp of Landslide Scar 5 - Note Slight Seepage (Plate Location Shown on Drawing EG503) (Taken on 7/7/97)  
GS 97/53/07



Plate 28(b) - Soil Pipe with Medium Flow (Plate Location Shown on Drawing EG503) (Taken on 8/8/97)  
GS 97/107C/30





Plate 28(c) - Soil Pipe with Heavy Flow (Plate Location Shown on Drawing EG503) (Taken on 9/9/97)

GS 97/107C/08





Plate 29 - Small 40 mm Diameter Soil Pipes at the Old Colluvium-Saprolite Interface Exposed in Landslide Scar 5 (Plate Location Shown on Drawing EG503) (Taken on 21/7/97)

EG 97/97/36



Plate 30 - Rhyolite Dyke Exposed in Landslide Scar 4 - Note Very Closely Spaced Joints with White Kaolin Infill (Plate Location Shown on Drawing EG503) (Taken on 7/7/97)



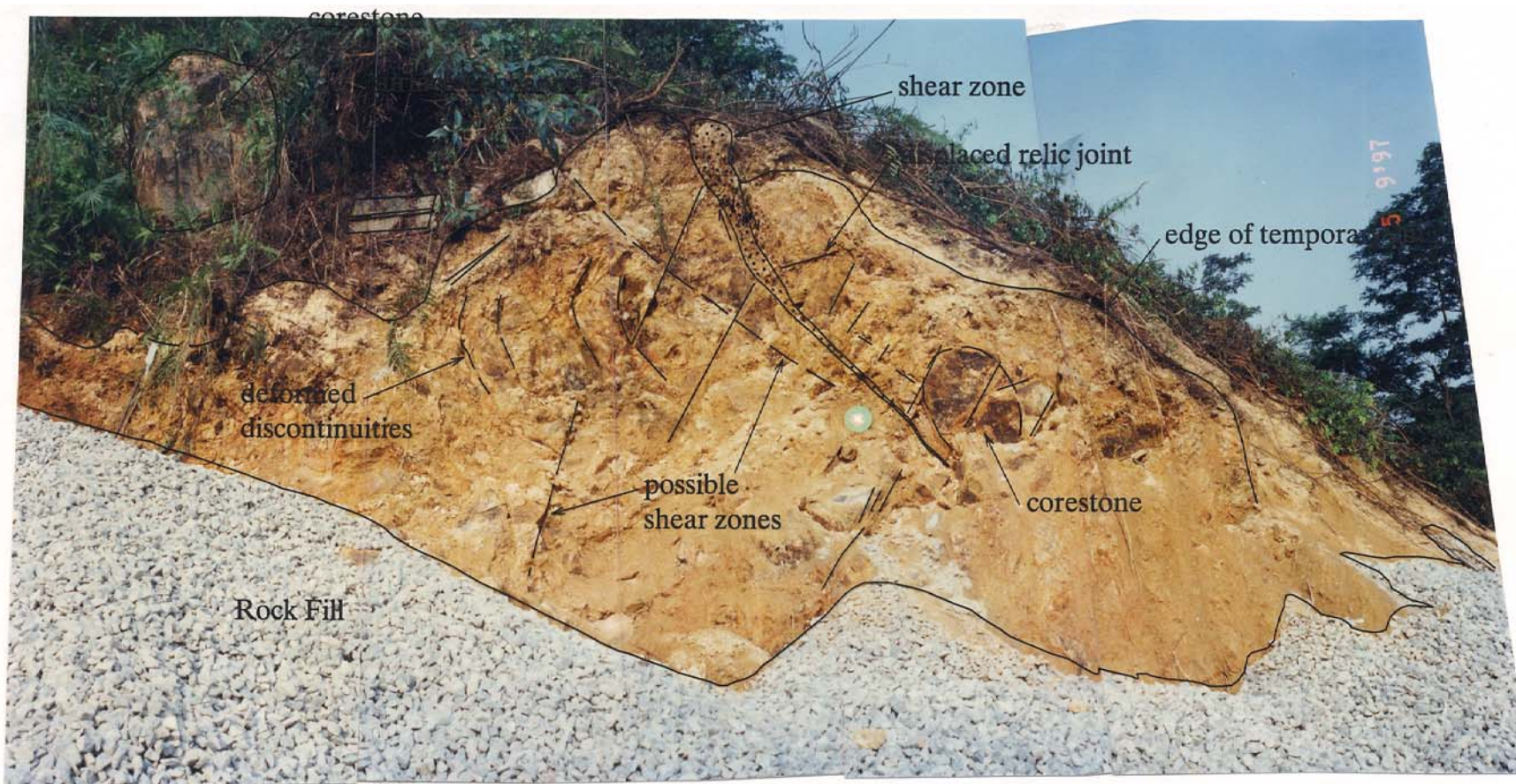


Plate 31 - Temporary Cut in the Left Hand Flank of Landslide Scar 4 Exposing an Inclined Brittle Dilating Shear Plane within the Partially Weathered Rock Mass (Plate Location Shown on Drawing No. EG503) (Taken on 5/9/97)

EG 97/112/9 - 13

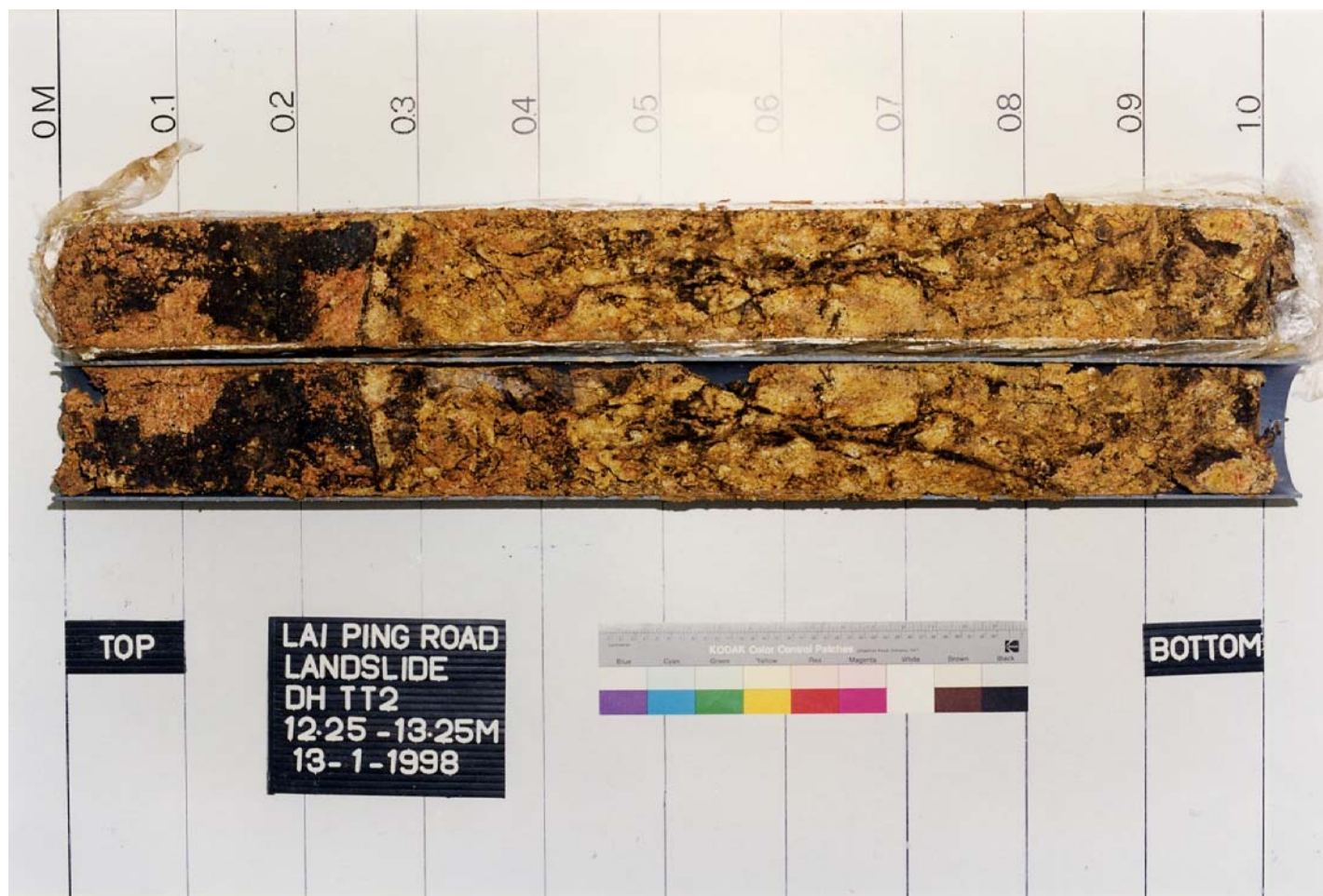


Plate 32 - Split 4CMLC Core from Drillhole TT2 Showing Sub-Vertical Relict Joints with Much Manganiferous Staining on the Joint Surface and within the Rock Fabric (Taken on 31/1/98)

EG 97/05/19



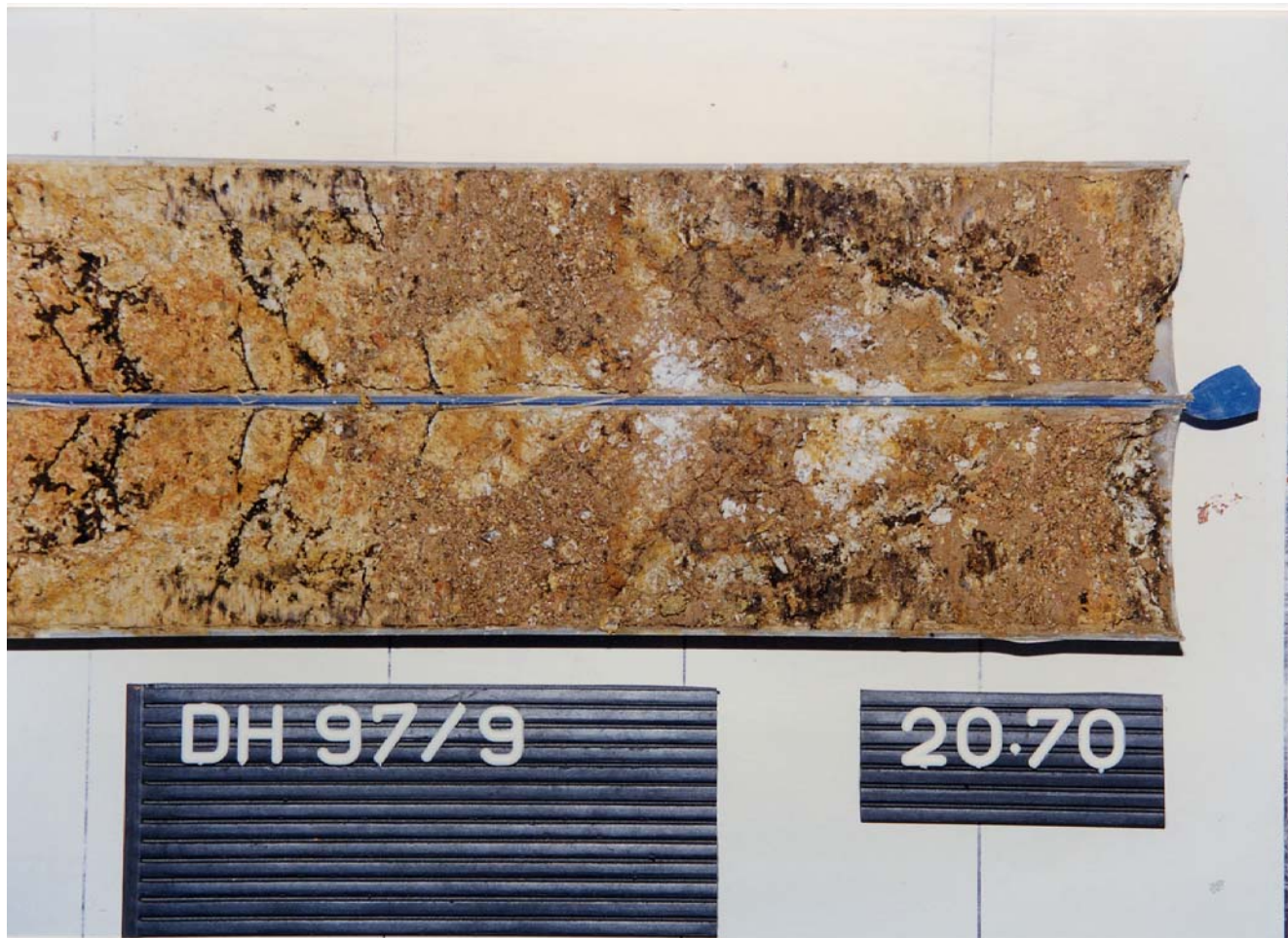


Plate 33 - Close-Up of Split Mazier Sample from Drillhole DH97/20 Showing Disrupted Zone Comprising Pockets of Angular Quartz, Feldspar and Moderately Decomposed Tuff, Sand and Gravel, Stiff Brown Silty Clay and Cobbles of Highly Decomposed Tuff (Taken on 6/5/98)

EG 98/06/28A

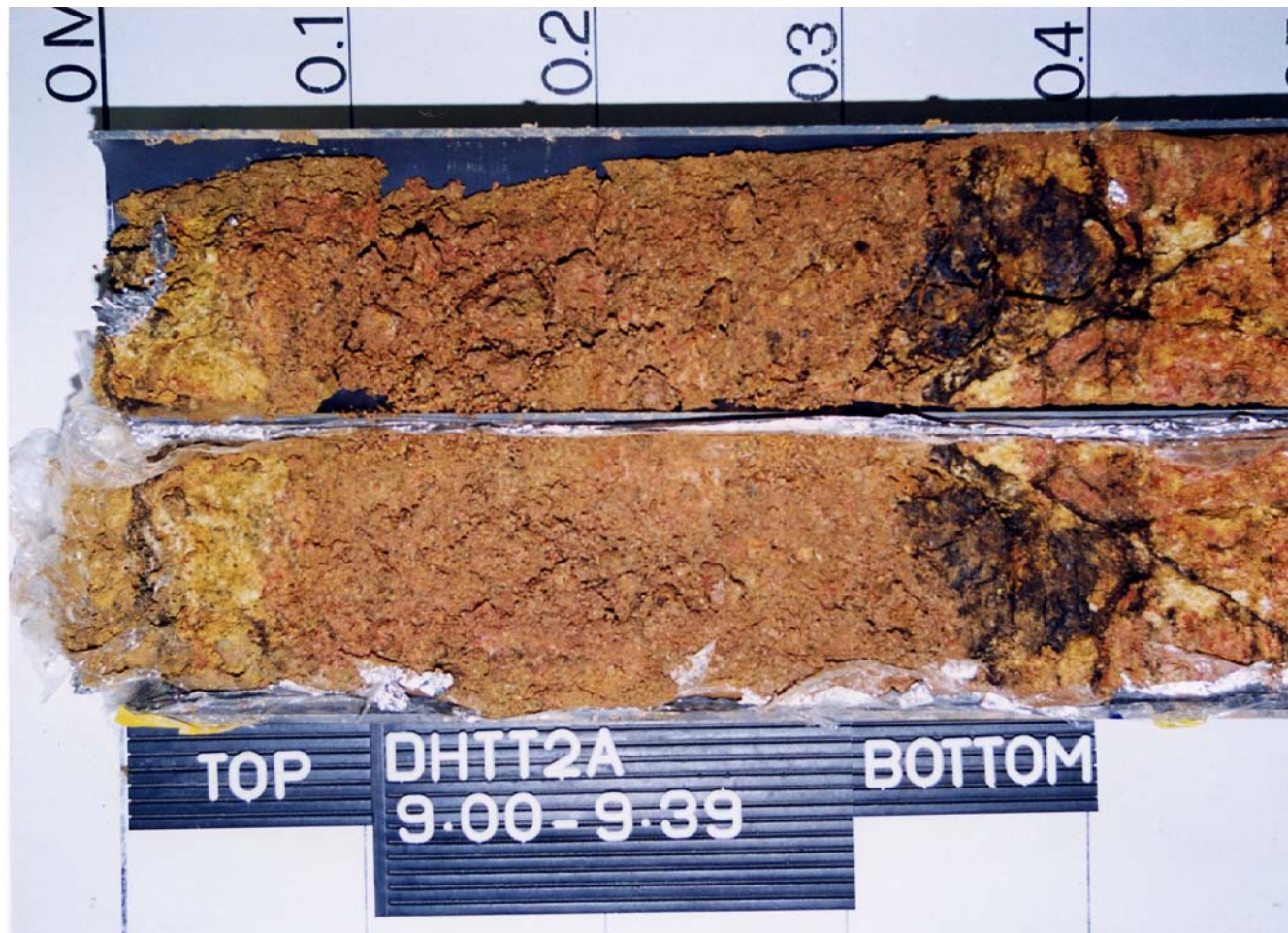


Plate 34 - Close-Up of Split 4CMLC Core from Drillhole TT2A Showing an Anomalous Zone within Grade V Saprolite Interpreted as Being either an Infilled Soil Pipe or a High Permeability Shear Zone (Taken on 6/5/98)

EG 97/18/15





Plate 35 - Minor Scarp Showing at Least Two Phases of Displacement  
Recognisable by the Vegetation Line of Moss - Scarp Height  
1.8 m - Old Displacement 1.6 m - New Displacement 0.2 m  
(Plate Location Shown on Drawing EG503) (Taken on 24/7/97)

GS 97/82/06





Plate 36(a) - Main Scarp Showing Vegetation Line Indicating at Least Two Phases of Movement Together with Old and Recent Slickensides on the Scarp Surface and a Rhyolite Dyke Contact (Plate Location Shown on Drawing EG503) (Taken on 26/9/97)

EG 97/117/24





Plate 36(b) - Close-Up of Old Moss Covered Slickensides (Plate Location Shown on Drawing EG503)  
(Taken on 26/9/97)

EG 97/105/08A





Plate 37 - Re-Growth of Tree Branch Directly up Main Scarp (Plate Location Shown on Drawing EG503)  
(Taken on 26/9/97)

EG 97/117/19



APPENDIX A  
AERIAL PHOTO INTERPRETATION

## 1. SUMMARY

The site was natural terrain (with minor footpaths) comprising a gently sloping concave landform in-between two small ridges prior to the commencement of the borrow area in 1976. A small cut slope, associated with the haul road to Kau To Shan borrow area, was formed in 1976 and was substantially extended, both laterally and vertically, between 1977 and 1978. The haul road alignment, which was further southwest and straighter than Lai Ping Road, was moved in 1978 as part of the development of a cut and fill platform on which the salt water service reservoir was ultimately constructed. Two realignments of the road were constructed during 1978. One, which forms the present alignment of Lai Ping Road, was constructed in part on a ramp. An earlier realignment was constructed even closer to the cut slope, but by the end of 1978, only part of the ramp, below the southeast part of the slope remained intact. Its continuation to the northwest was probably damaged by a failure of the adjacent cut slope and had been removed by late 1978.

The earliest observed slope instability took place in 1977 on the western, uppermost part of the cut slope. The first substantial failure occurred in 1978 and affected the central part of the slope but the extent of this failure is poorly constrained. By the end of 1979, failures had occurred at the eastern bottom edge of the cut slope, and larger slips/erosional features are evident at its western and central areas. Instability recurred on a number of occasions (associated with extensive erosion), mainly on the central western side of the slope, with significant events noted in 1980, 1983, 1987 and 1993. The slope has not had any surface protection applied, although some chunam or grass was placed on the lower eastern side after initial formation into batters. Drainage channels were constructed on the berms on the eastern side. Vegetation has only grown over part of the slope, the upper central and upper eastern sides being the most constantly bare. No apparent remedial works were carried out or surface protection applied following the various failures. Two major tension cracks on the upper eastern side of the cut slope, and subsidiary minor cracks on its lower eastern side, have been clearly visible since 1983. From 1979 onwards, the possible locations of scarps on the natural slope above the cut slope can be inferred on the basis of disturbances of the vegetation.

## 2. SITE HISTORY

The following site history has been interpreted from the available aerial photographs, site visits also having been carried out. The main features are shown on Figure 5:

- |            |   |
|------------|---|
| 6.11.1945  | The area is natural terrain with occasional footpaths. Lai Ping Road has not yet been formed. Relict, very degraded, fully vegetated landslide scars adjacent to the ridgeline north-east of the future slope location. In the vicinity of the future cut slope, the landscape comprises a gently concave slope between two small ridges. |
| 26.1.1963  | No change from 1945 except that a low ridge is also evident between the two ridges seen on the 1945 photographs, and landslide is approximately where the centre/southeast of the cut slope is now.   |
| 16.12.1964 | No change from 1963 (see Figure 2).   |

- 19.12.1975      No change from 1963
- 23.11.1976      The borrow area has been commenced and the haul road (in part the future Lai Ping Road) cut through to Tai Po Road. A small cut slope has been formed approximately where the eastern end of the cut slope now is, and the road is aligned along the toe of this slope (Figure 5) but in a straighter alignment and to the southwest of the current alignment of Lai Ping Road at the landslide site.
- 9.12.1977      The present slope is being formed and has already been considerably extended northwest of the earlier cut slope as well as up-slope to the northeast. The haul road remains in the same position as in 1976. A small scar that may indicate a minor failure is present at the top of the western end of the slope.
- 15.12.1978      The slope excavation has been completed. However, there appears to have been a large failure in its central portion although the northern and western limits of this failure are hard to establish precisely. A cut and fill platform has been constructed on the southwest side of the slope and the route of the haul road has been realigned to its present route. The road is constructed in part along a ramp, and is northeast of its previous alignment, thus avoiding the platform (Figure 5) and nearer the base of the slope. However, yet closer to the slope at its eastern end, there appear to be the remains of an earlier ramp suggesting an earlier road alignment. The ramp extends northwest as far as the approximate location of the slope failure, suggesting that the ramp may originally have continued further along the base of the slope but was damaged by the slope failure and abandoned and either covered by debris or largely removed. The bottom half of the eastern side of the slope appears darker (some chunam or grass protection?) in tone, and three horizontal berms with drainage channels and batters have been formed (Figure 5). The possible failure scar seen on the 1977 photographs appears slightly larger.
- 29.11.1979      A small failure has occurred in the approximate centre of the bottom batter at the eastern side of the slope (Figure 5). A slip/erosion of the eastern slope face also appears to have occurred, cutting vertically through the berms and drainage channels installed. Large scar are evident in the central and western parts of the slope. Intact berms/batters on the western side of the slope help to identify the western limit of the failure. On the natural slope above the cut slope there are paths converging on a possible drill site in the east. In addition, there appear to be some areas of disturbance of the vegetation that could reflect the development of scarps.
- 18.6.1980      Failures across the central part of the slope face, seen on the 1979 aerial photographs, are more prominent. There is also evidence of severe erosion, probably increasing the depth of the failure scars. There does not appear to be much debris at the base of the slope (Figure 5). The upper eastern and lower eastern parts of the slope with berms and batters are distinctly separate now with further deepening of the previous year erosion



in-between. Some revegetation of the slope above the western slip is beginning to occur. Some erosion/instability has also occurred on the western edge of the slope across the partially formed berms. Further indications of disturbance of the vegetation on the natural slope above the cut slope could be interpreted as evidence of scarp development.

- 27.10.1981 No real change from 1980 apart from some re-vegetation of the original cut slope above the central western slip scar. No remedial works appear to have been carried out to the failed sections of the slope face.
- 10.10.1982 No change apart from some further re-vegetation, especially on the western part of the slope. Perhaps some localised further erosion of the central scars.
- 22.12.1983 The small failure on the eastern side has advanced up to the top of the second batter, but has not really increased in width. Two open fractures have developed across part of the top of the cut slope, above and further to the east of the central/eastern slip/erosion scar (Figure 5). These are interpreted as tension cracks. Some re-vegetation of the lower parts of the central slip/erosion scars is evident.
- 22.10.1984 More extensive re-vegetation of the lower and far western part of the slope and above the remains of the central western slip scar (which still has clearly defined edges). Erosion is still ongoing in-between the berms on the eastern side of the slope. The tension cracks previously seen at the top of the cut slope appear to have opened further and are more easily visible. In addition, further smaller tension cracks are visible in the lower eastern part of the cut slope. Vegetation disturbance on the natural slope above the main tension cracks may be related to the development of similarly-orientated tension cracks. Other obviously identifiable vegetation disturbance is now less evident.
- 28.4.1986 No real change apart from further re-vegetation of the slope and slip scars. The tension cracks are not as clearly defined as previously.
- 21.12.1986 No change from earlier in the year.
- 10.12.1987 Further movement/erosion? has occurred within the central western slip over the left hand side of the scar. There appears to be a slight regression of the scar up-slope, with a slight widening on the western edge and some deepening as well (Figure 5). The tension cracks are still very well defined and the eastern and western parts of the slope are well re-vegetated now (the scar of the small slip in the berms on the eastern side is quite well re-vegetated). The central part of the slope has also got more vegetation. Some landslide debris has been washed along the base of the slope. On the natural slope above the cut slope, disturbance of the vegetation appears to be consistent with renewed development of arcuate and linear scarps, especially above the central portion of the cut slope.

- 4.11.1988 No change from the previous year apart from some minor vegetation growth on the scars. No remedial work appears to have been carried out. The tension cracks are still clearly visible. The old failure scar in the eastern berms is almost completely re-vegetated now.
- 17.1.1989 No change apart from further re-vegetation.
- 21.3.1990 Further instability/erosion? across the central western scar almost across the whole original (1980) width. The tension cracks appear to be wider apart, but there are no other signs of instability. There are suggestions of vegetation disturbance along linear trends on the natural slope above the cut slope, possibly associated with renewed scarp development.
- 19.9.1991 No change apart from some re-vegetation of the central western scar. Also some re-vegetation across the upper part of the slope.
- 15.4.1992 No change apart from further re-vegetation.
- 6.10.1992 Some further erosion in the central western scar and across the upper central part of the slope and the tension cracks are more visible than earlier in the year. On the natural slopes above the cut slope, there are suggestions of linear and arcuate features, including a laterally persistent feature in the approximate location of the present north-east flank of the main scarp.
- 30.5.1993 No change. Some evidence of possible seepage/runoff? from the central western scar with a lighter colour trail running down to the base of the slope. Also some further erosion over the middle of the western side of the slope
- 6.12.1993 Further instability/erosion? across the central western scar clearing away the vegetation. The eastern side erosion which had split the part of the slope with berms in 1979 (Figure 5) has also moved further up-slope (another possible slip scar) to the edge of the original cut. The tension cracks are still visible. Construction of the service reservoir south of Lai Ping Road has commenced.
- 17.10.1994 No change apart from minor re-vegetation.
- 30.8.1995 No change apart from further minor re-vegetation. Some vegetation along the tension cracks. On the natural slope above the cut slope, linear zones of disturbance in the vegetation are again evident. The service reservoir is fully complete (Figure 5).
- 26.4.1996 No change except more re-vegetation (including the tension cracks).
- 24.10.1996 No change, apart from further re-vegetation, especially on the slope around the tension cracks. Small channel observed (seepage/surface water?) down central west slip scar.

3. AERIAL PHOTOGRAPHS.

Aerial photographs examined (black and white except where indicated\*):

<u>Date</u>	<u>Altitude</u>	<u>Photograph Number</u>
6.11.45	20,000'	Y00740 & 41
26.1.63	3,900'	Y08768 & 69
16.12.64	1,800'	Y12387 & 88
28.2.74	12,500'	8246 & 47
19.12.75	12,500'	11723 & 24
23.11.76	12,500'	16482 & 83
9.12.77	12,500'	19895 & 96
15.12.78	12,500'	24560 & 61
29.11.79	10,000'	28204 & 05
18.6.80	4,000'	30757 & 58
27.10.81	10,000'	39217 & 18
10.10.82	10,000'	44627 & 28
22.12.83	10,000'	52215 & 16
22.10.84	4,000'	56843 & 44
28.4.86	4,000'	A04857 & 58
21.12.86	10,000'	A08097 & 98
10.12.87	4,000'	A11124 & 25
4.11.88	4,000'	A15393 & 94
17.1.89	4,000'	A16153 & 54
21.3.90	4,000'	A21029 & 30
19.9.91	4,000'	A27115 & 16
15.4.92	4,000'	A30135 & 36
6.10.92	4,000'	A31936 & 37
30.5.93	4,000'	A34655 & 56
6.12.93	10,000'	CN5602 & 03
17.10.94	4,000'	A39081 & 82
30.8.95	3,500'	CN10698 & 99*
26.4.96	3,500'	CN13340 & 41*
24.10.96	4,000'	CN14935 & 36*



## APPENDIX B

### DETAILED CORE DESCRIPTIONS AND PHOTOGRAPHS



Plate B1 - Drillhole 97/20 - Split Maizier 4.30 m to 4.70 m Transition Zone from Residual Soil into Saprolite.

4.30 m - 4.45 m. Stiff orangish-brown occasionally mottled yellow and pinkish-red very silty CLAY with much angular coarse quartz sand and fine angular gravel (RESIDUAL SOIL) with zones of extremely weak yellow mottled white completely decomposed coarse ash TUFF.

4.45 m to 4.70 m. Very weak brownish-orangish-yellow mottled purplish-red highly decomposed coarse ash TUFF.

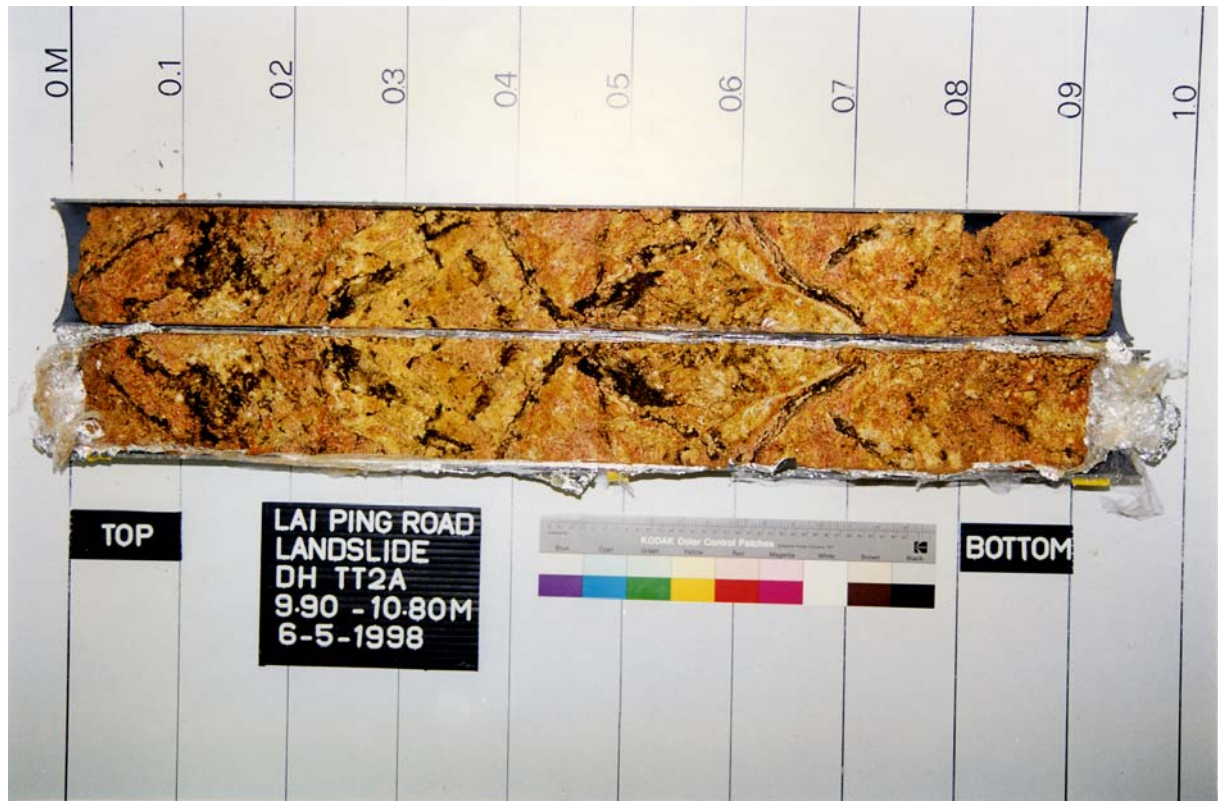


Plate B2 - Drillhole TT2A - Split 4CMLC Core 9.90 m to 10.80m. Typical Completely Decomposed Tuff.

9.90 m to 10.80 m. Extremely weak yellowish-brown mottled reddish-pinkish-brown, white and black and streaked black completely decomposed coarse ash TUFF with very closely-spaced, rough planar, extremely narrow,  $70^\circ$  joints infilled with manganiferous deposits and white clay (kaolin).  $30^\circ$  -  $40^\circ$  moderately spaced joint set with up to 10mm of intercolated white clay and manganiferous deposits between 10.30 m and 10.60 m (clayey SILT with much angular coarse quartz sand and fine angular gravel).





Plate B3 - Drillhole TT2 - Split 4CMLC Core 14.25 m to 15.25 m. Typical Sub-vertical Joint in Completely Decomposed Tuff.

14.25 m to 15.25 m. Extremely weak yellowish-brown mottled pinkish-red and white, completely decomposed coarse ash TUFF (clayey SILT with much angular coarse quartz sand and fine angular gravel). with sub-vertical slickensided undulating, narrow joint with up to 18 mm of white clay (kaolin) and 1 mm manganiferous deposit infill at 14.25 m to 14.55 m with managniferous deposits becoming dominant below 14.55 m. At 15.00 m, 3 mm of manganiferous deposits and no kaolin. Occasional sub-horizontal joints displaced along main sub-vertical joint.



Plate B4 - Drillhole DH 97/9 - Split Maizier 17.50 m to 18.60 m. Sharp Junction between Completely Decomposed Tuff and Highly Altered Completely Decomposed Tuff.

17.50 m to 17.60 m. Disturbed Sample.

17.60 m to 18.05 m. Extremely weak brown mottled dark brown and ginger and striped dark brown completely decomposed coarse ash TUFF (clayey SILT with much angular coarse quartz sand and fine angular gravel).with very closely-spaced sub-horizontal to 45° very narrow relic joints infilled with white clay (kaolin) and manganiferous deposits.

18.05 m to 18.60 m. Extremely weak reddish-purple mottled white, ginger and dark brown and spotted grey completely decomposed coarse ash TUFF (Highly Altered Tuff - stiff silty CLAY) with very closely-spaced 40° to 70° very narrow relic joints infilled with white clay (kaolin) and manganiferous deposits. Where present the kaolin surrounds the manganiferous joint infill deposits.

APPENDIX C  
TRIAL PIT LOGS



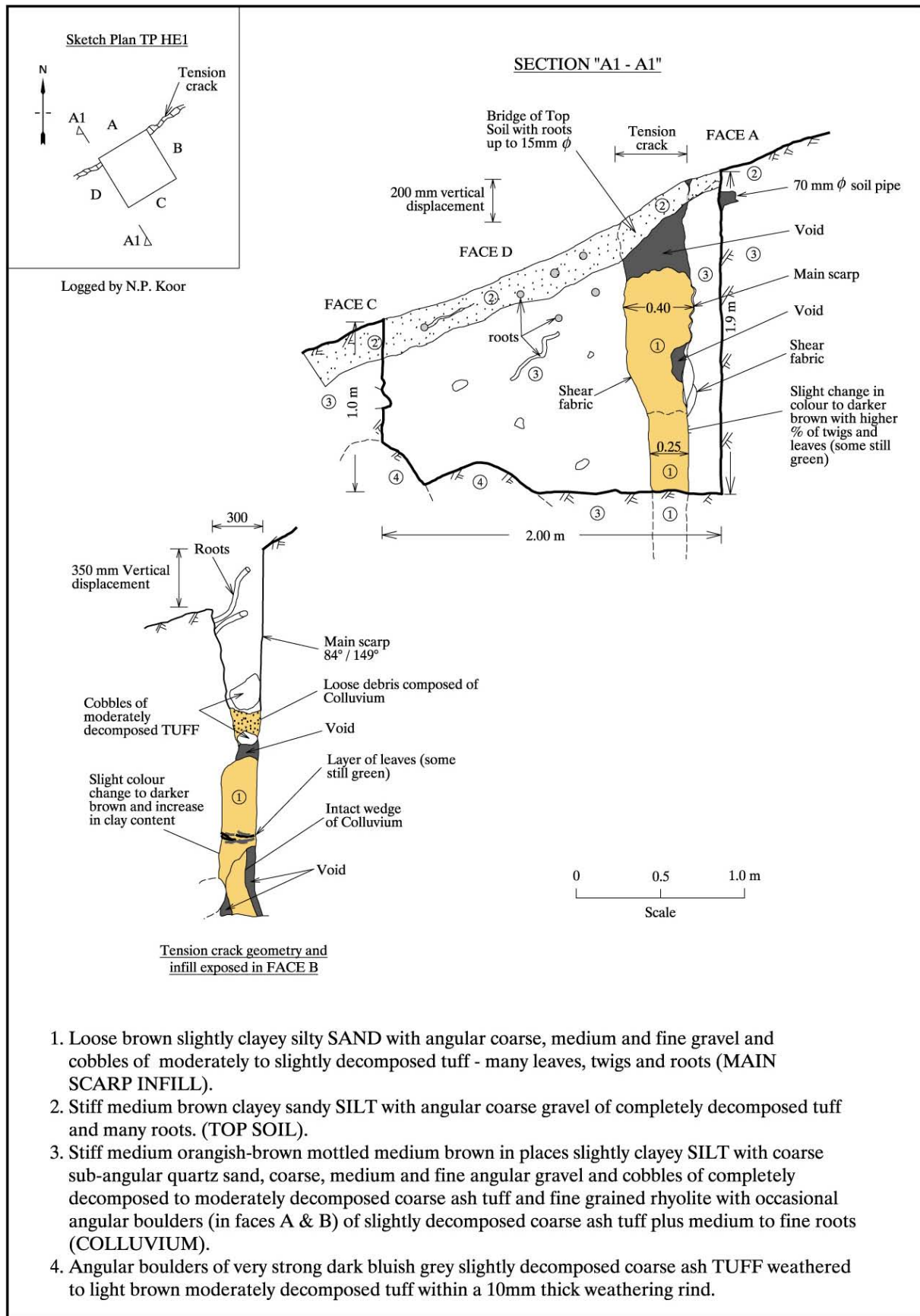


Figure C1 - Lai Ping Road Land Investigation Trial Pit HE1 - Section "A1 - A1"

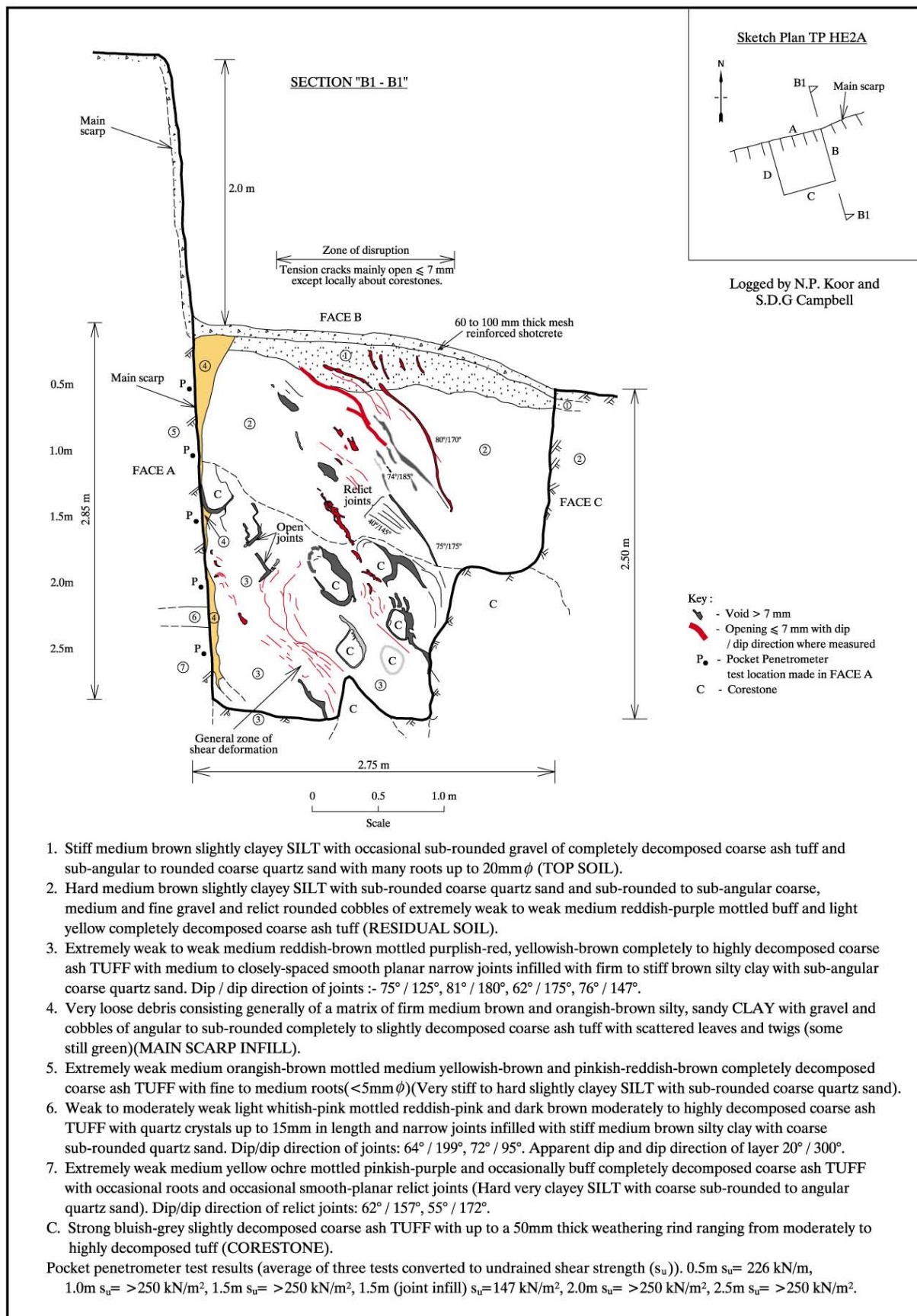


Figure C2 - Lai Ping Road Land Investigation - TP HE2A - Section "B1-B1"

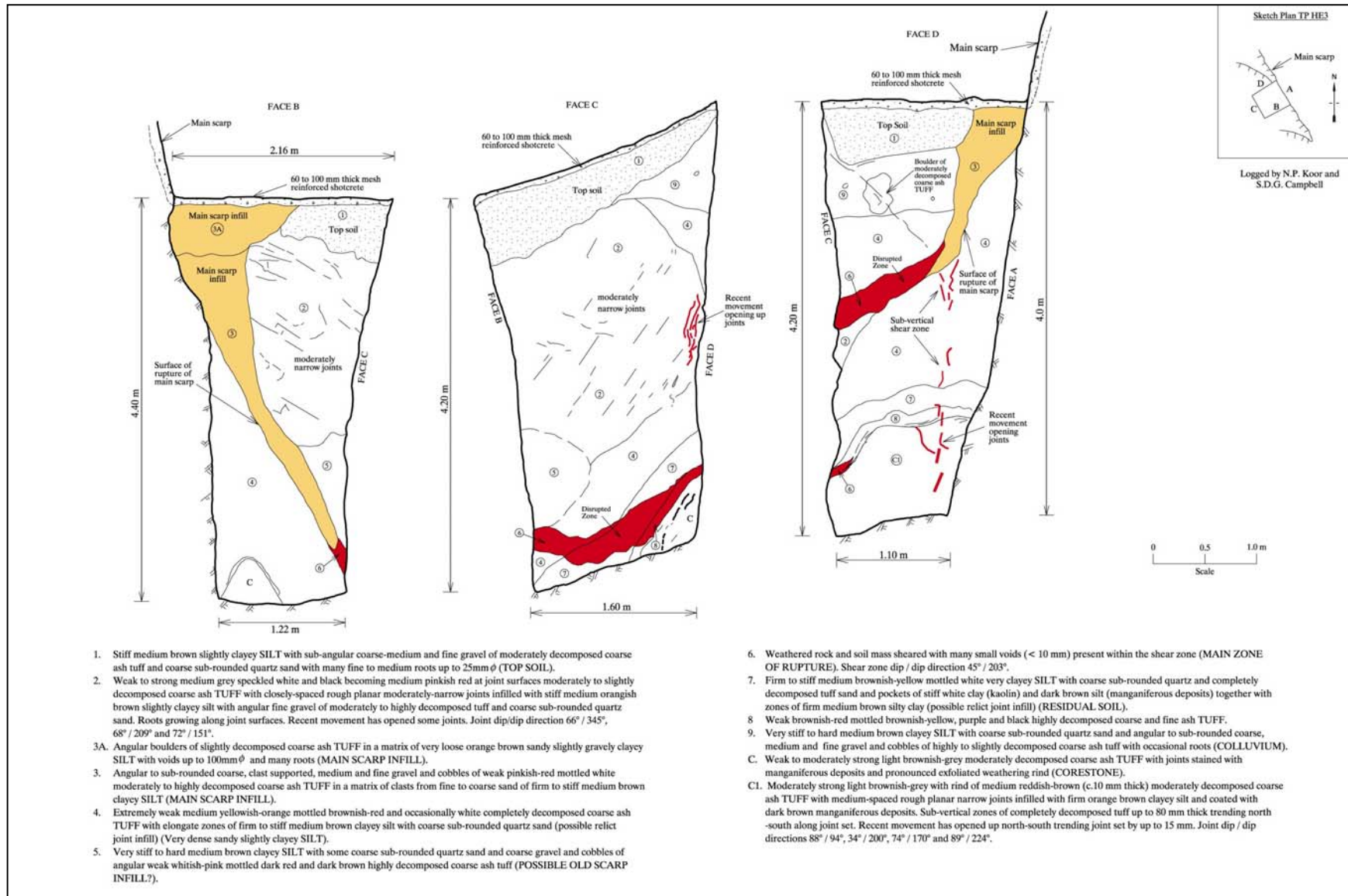


Figure C3 - Lai Ping Road Land Investigation Trial Pit HE3



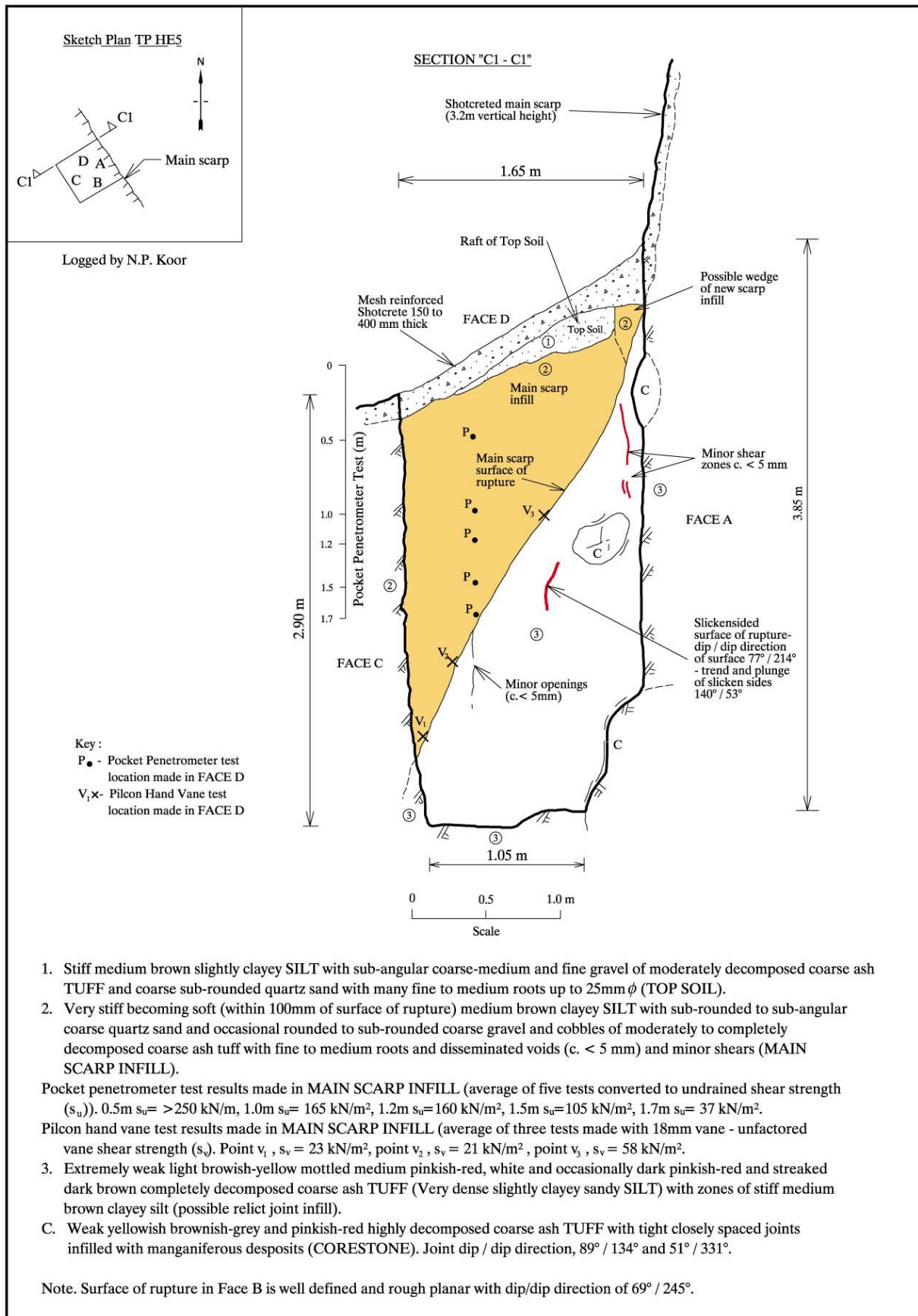


Figure C4 - Lai Ping Road Landslide Investigation - Trial Pit HE5 - Section "C1 - C1"

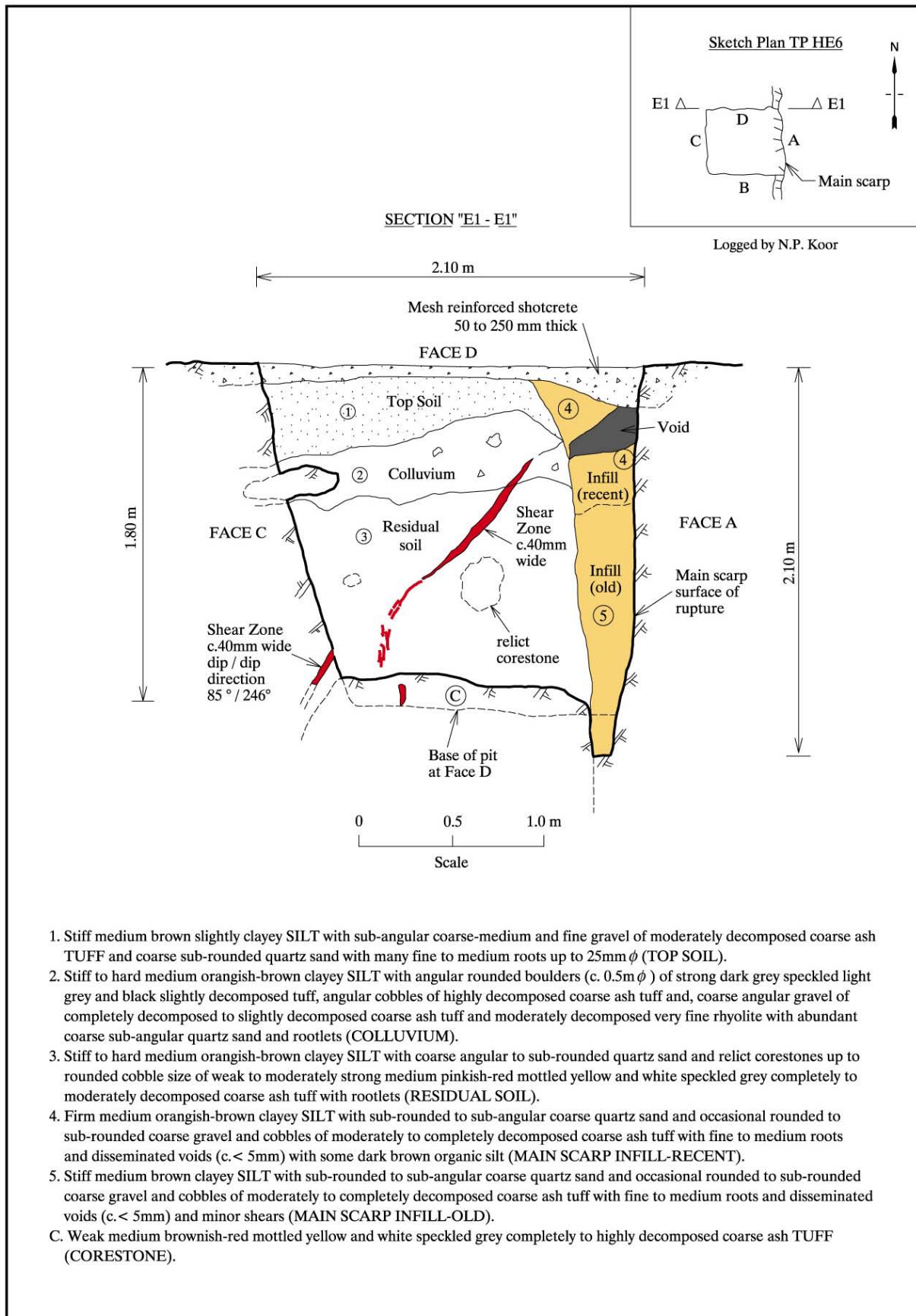


Figure C5 - Lai Ping Road Land Investigation Trial Pit HE6 - Section "E1 - E1"

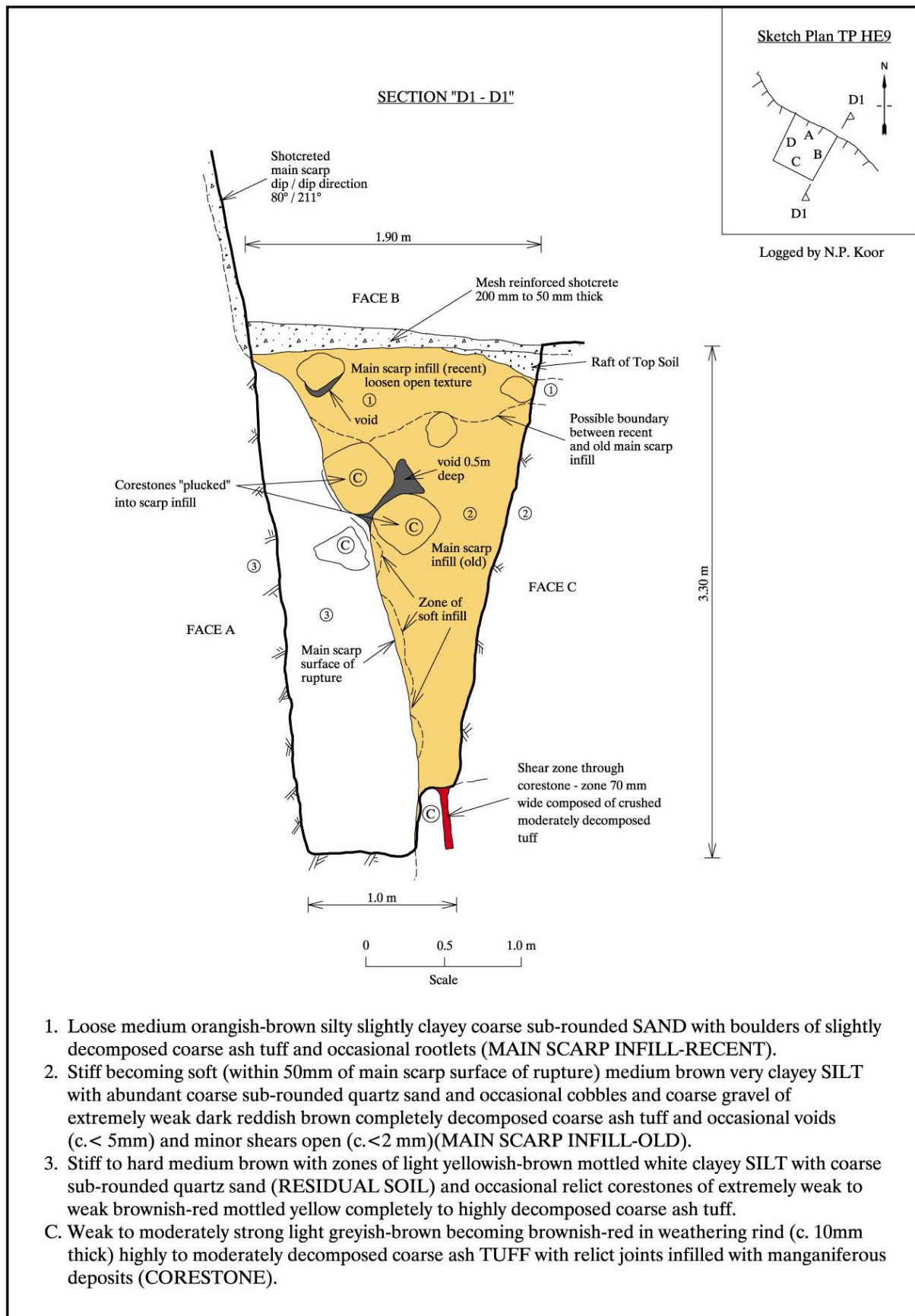


Figure C6 - Lai Ping Road Landslide Investigation - Trial Pit HE9 - Section "D1 - D1"



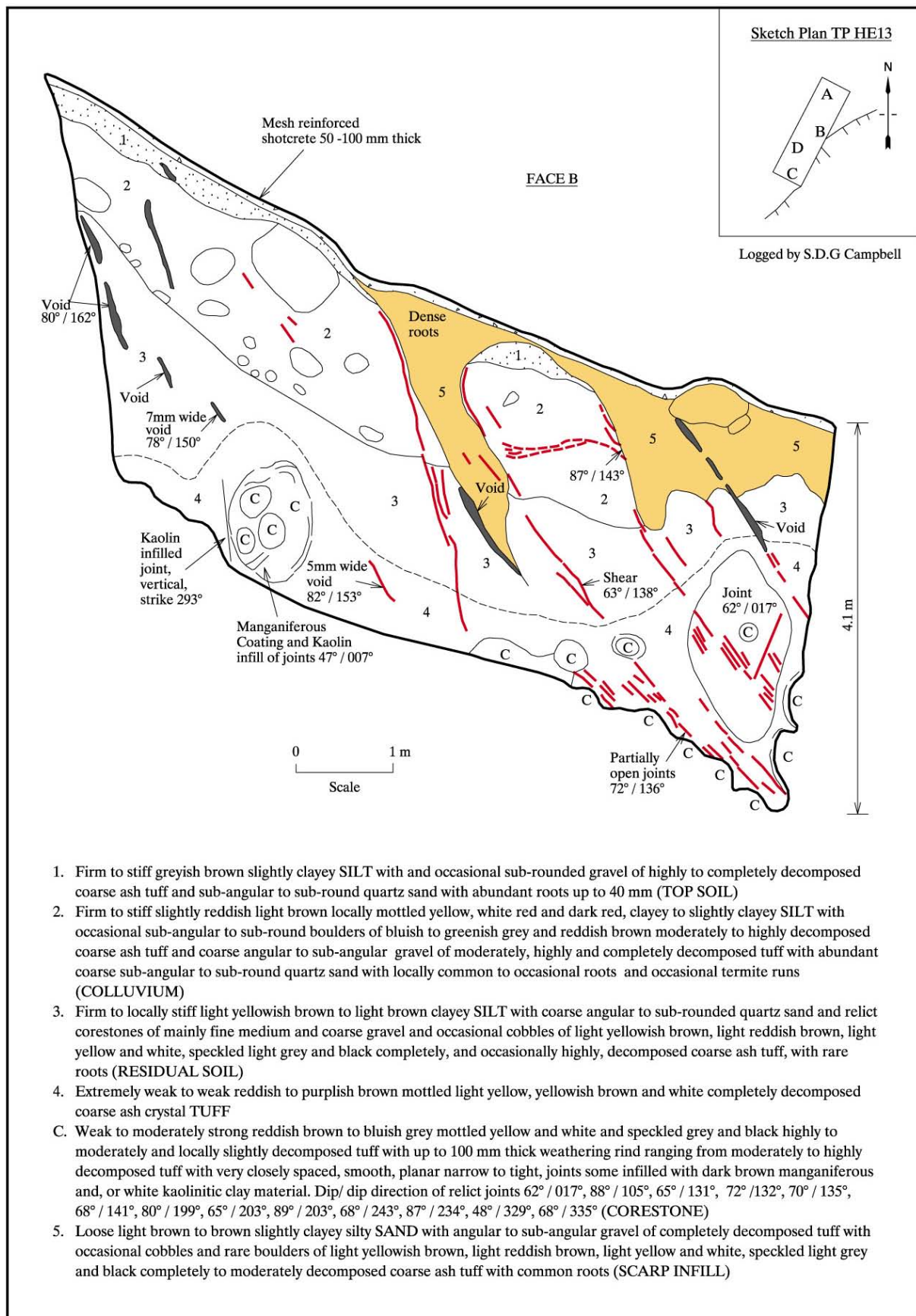


Figure C7 - Lai Ping Road Landslide Investigation - Trial Pit HE13 - Face B

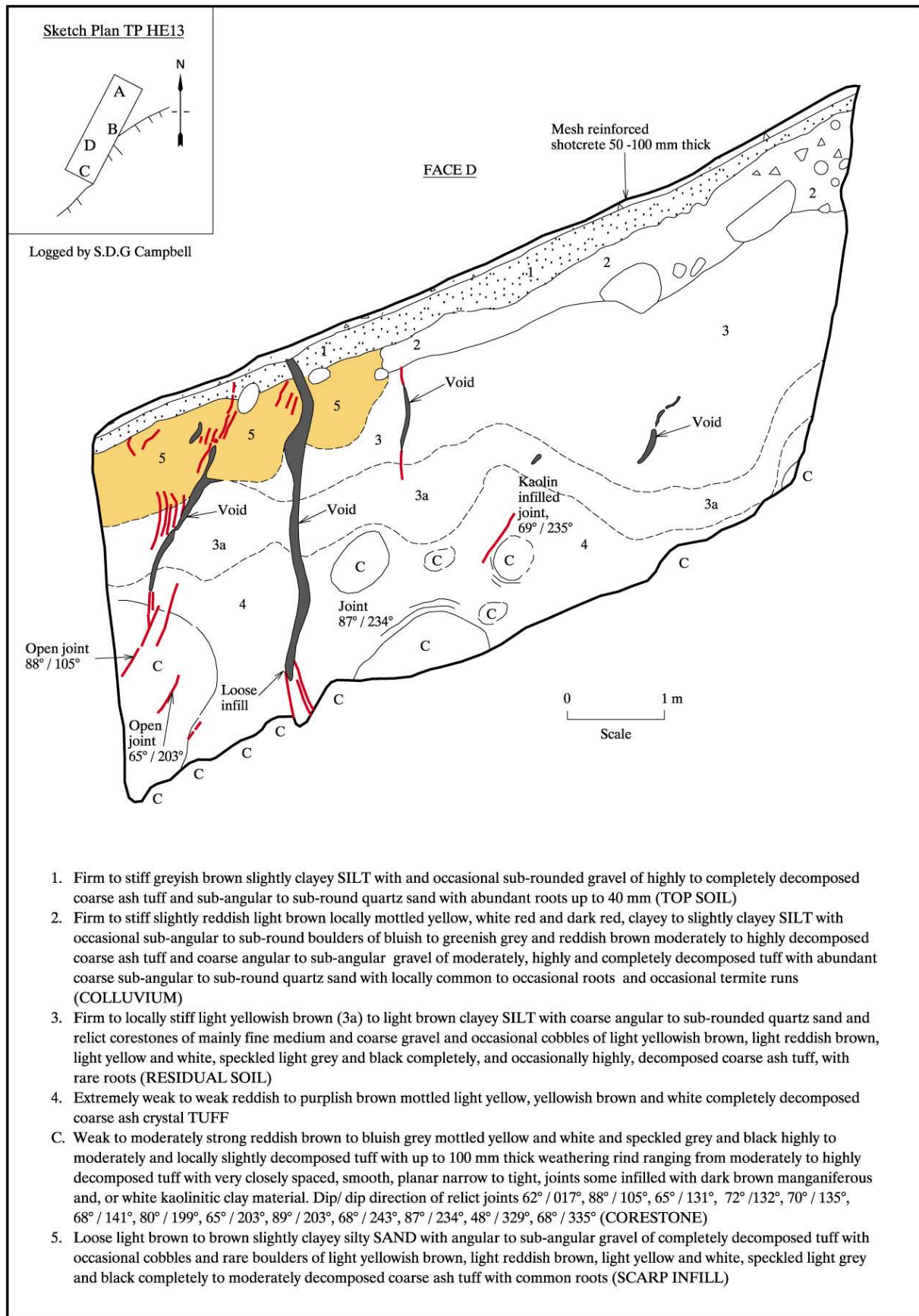


Figure C8 - Lai Ping Road Landslide Investigation - Trial Pit HE13 - Face D

## APPENDIX D

### BLOCK SAMPLE DESCRIPTIONS AND PHOTOGRAPHS



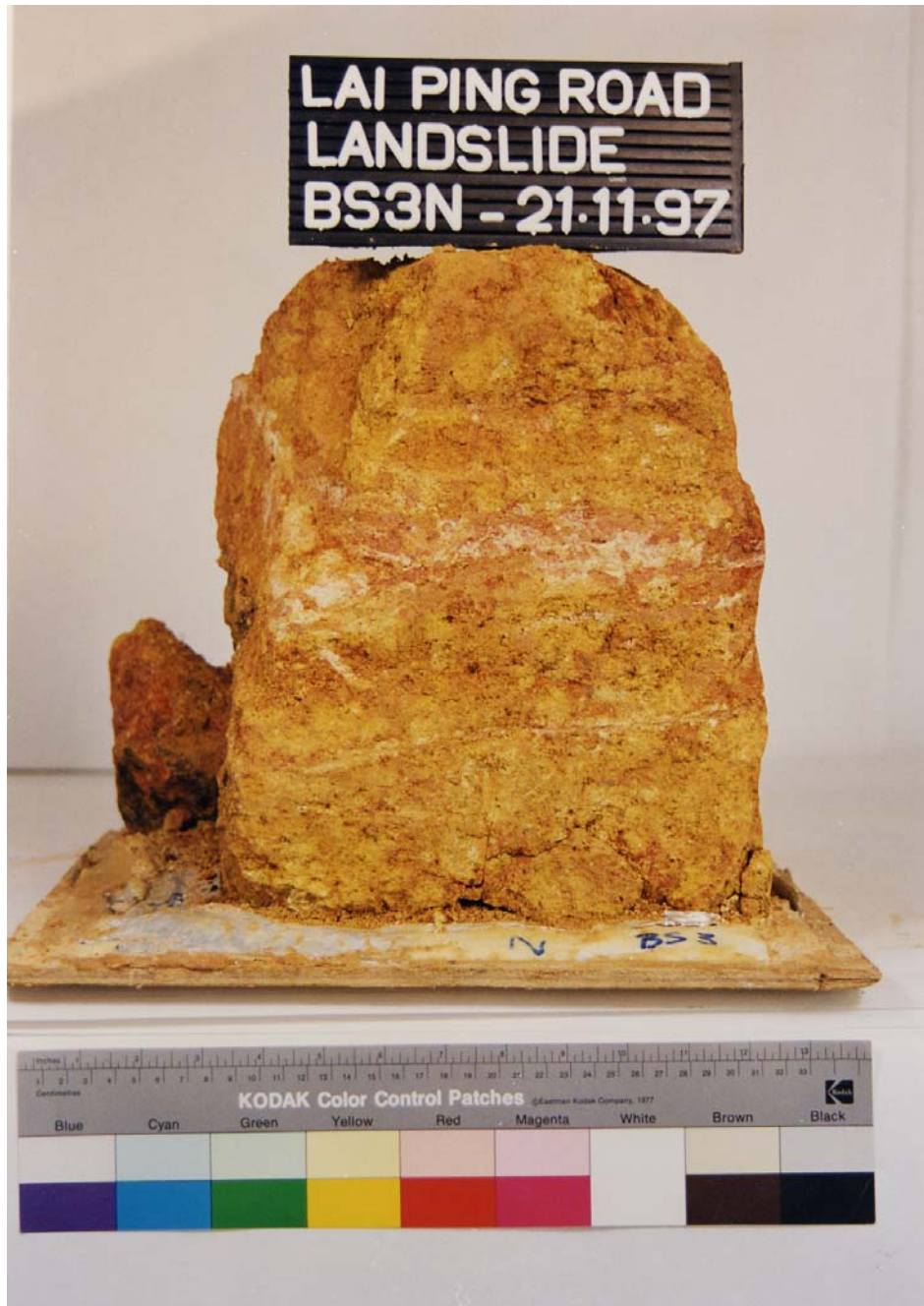


Plate D1 - Block Sample BS 3 - North Face

### Lai Ping Road Landslide Investigation - Block Sample Description

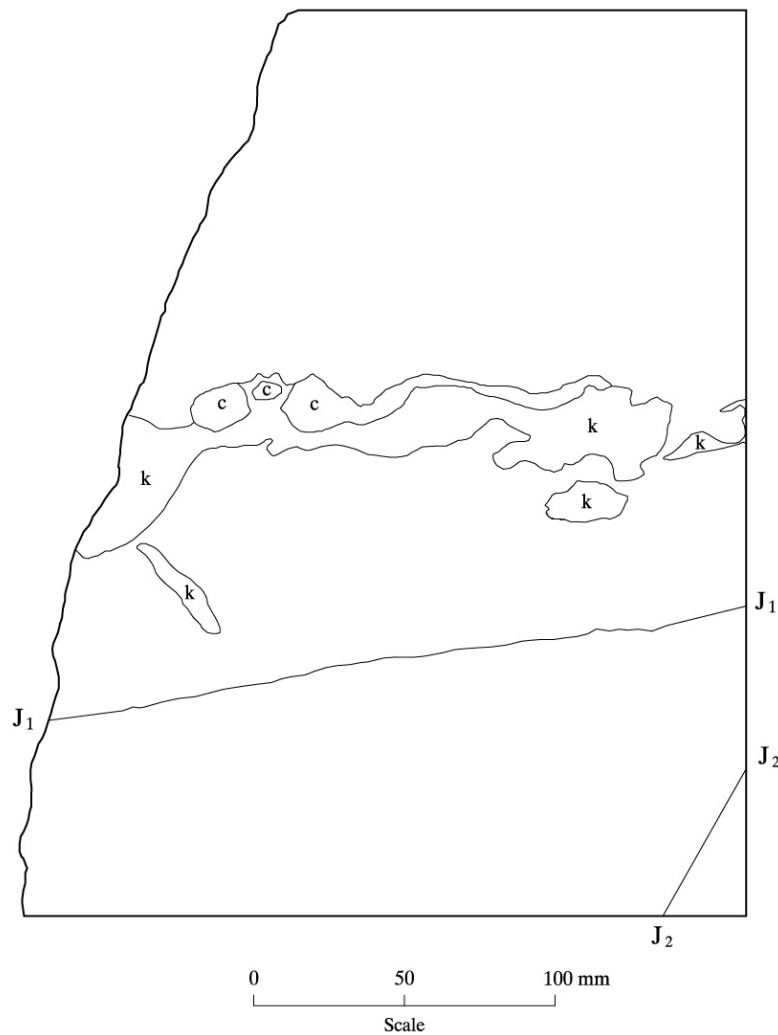
Block Sample BS 3 - North Face

Sample taken - 5-9-97

First Unpacked - 20-10-97

Date Described - 24-10-97 by N.P. Koor and S.D.G. Campbell

Sample Condition - Sample not waxed and beginning to dry out. East face collapse along inclined joint.



General Description - Very weak medium yellowish brown occasionally mottled buff and dark reddish brown highly decomposed coarse ash TUFF.

k - Deformed strings of light pinkish white clay (KAOLIN) with layers of dark pinkish red manganiferous deposits (<0.5mm).

c - Soft to firm light brown to buff silty CLAY.

J<sub>1</sub> - Extremely narrow joint infilled with white clay and reddish brown silt.

J<sub>2</sub> - Very narrow joint infilled with stiff dark brown silty clay with occasional whisps and lenses of white clay.

Figure D1 - Block Sample BS 3 - Description of North Face

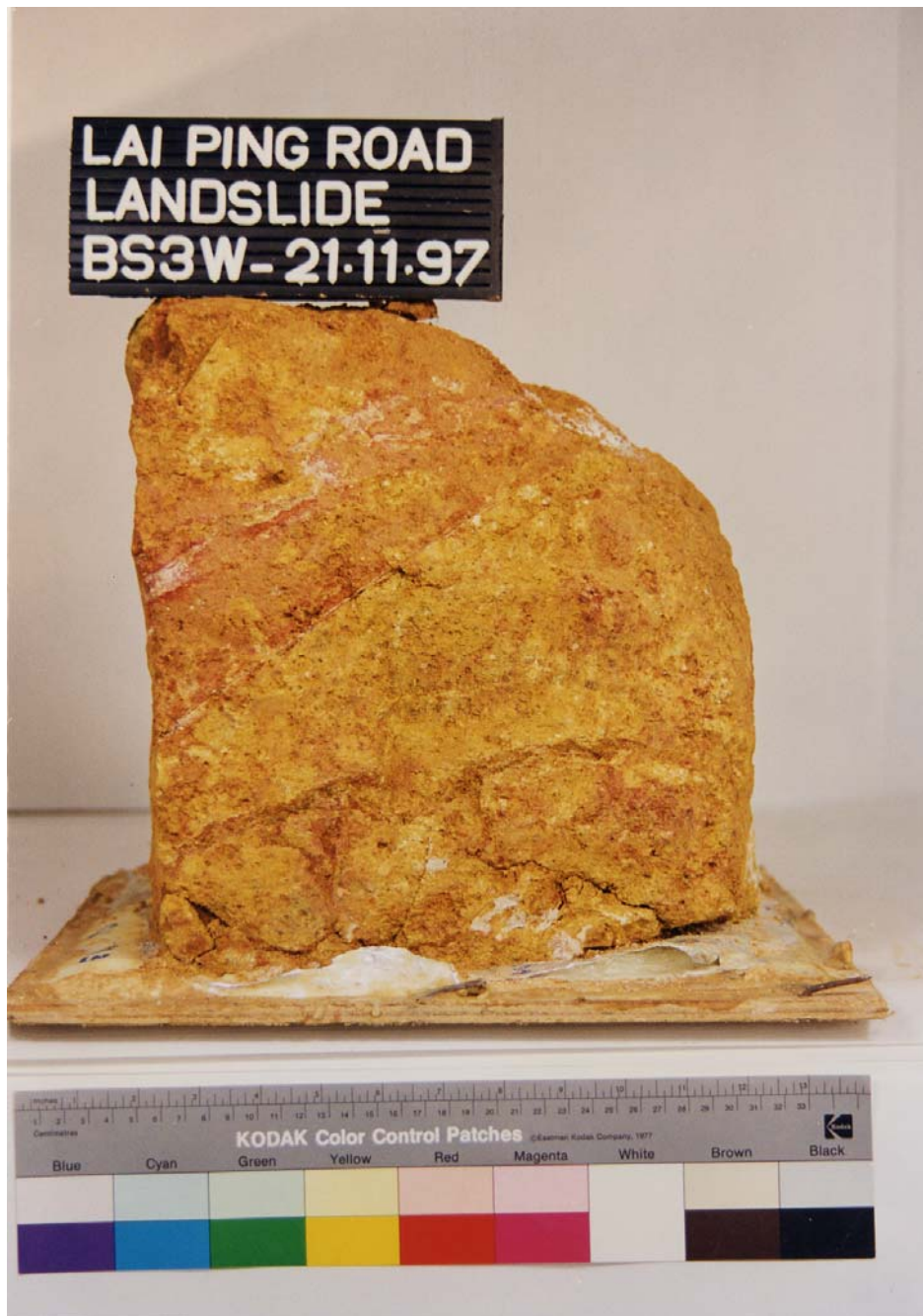


Plate D2 - Block Sample BS 3 - West Face



### Lai Ping Road Landslide Investigation - Block Sample Description

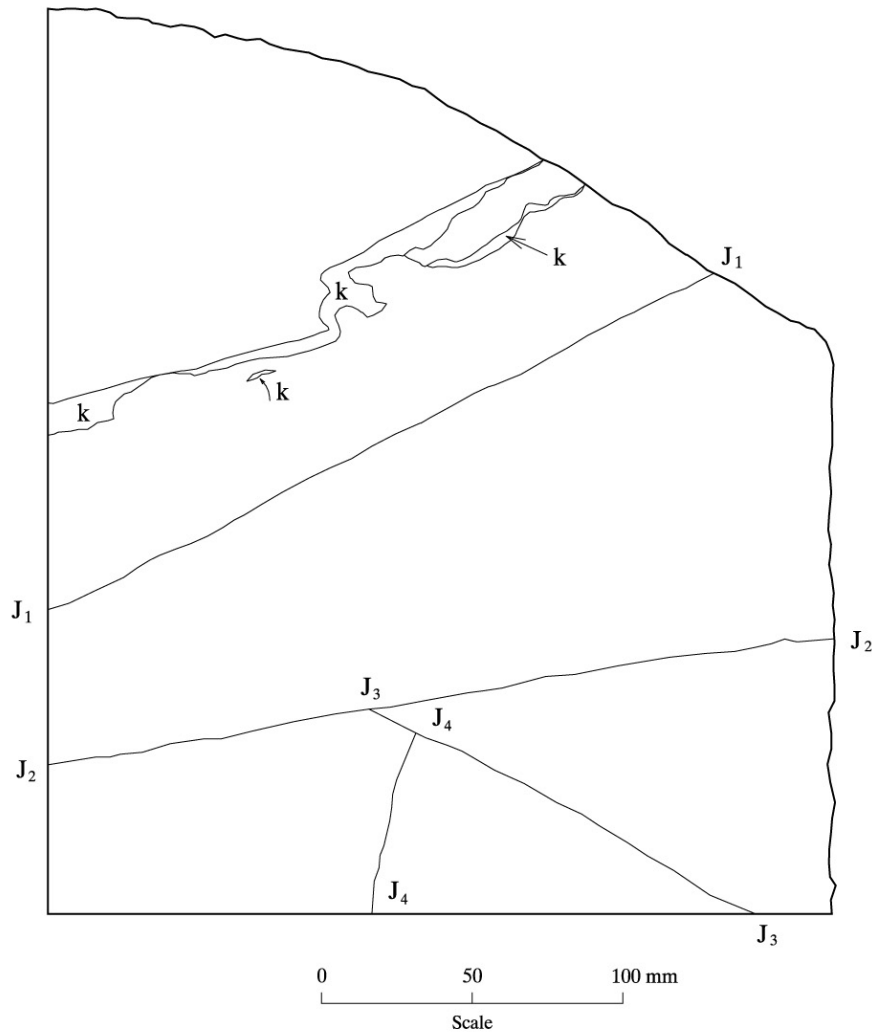
Block Sample BS 3 - West Face

Sample taken - 5-9-97 by Enpack

First Unpacked - 20-10-97

Date Described - 24-10-97 by N.P. Koor and S.D.G. Campbell

Sample Condition - Sample not waxed and beginning to dry out. East face collapsed along inclined joint.



General Description - Very weak medium yellowish brown occasionally mottled buff and dark reddish brown highly decomposed coarse ash TUFF (Stiff clayey sandy SILT).

k - Deformed strings of light pinkish white clay (KAOLIN) with layers of dark pinkish red manganiferous deposits (<0.5mm).

J<sub>1</sub> - Extremely narrow joint infilled with white clay and reddish brown silt.

J<sub>2</sub> - Very narrow joint infilled with stiff dark brown silty clay with occasional whisps and lenses of white clay.

J<sub>3</sub> - Very narrow joint infilled with stiff dark brown silty clay with occasional whisps and lenses of white clay.

J<sub>4</sub> - Extremely narrow with a coating of white clay.

Figure D2 - Block Sample BS 3 - Description of West Face



Plate D3 - Block Sample BS 4 - North Face

### Lai Ping Road Landslide Investigation - Block Sample Description

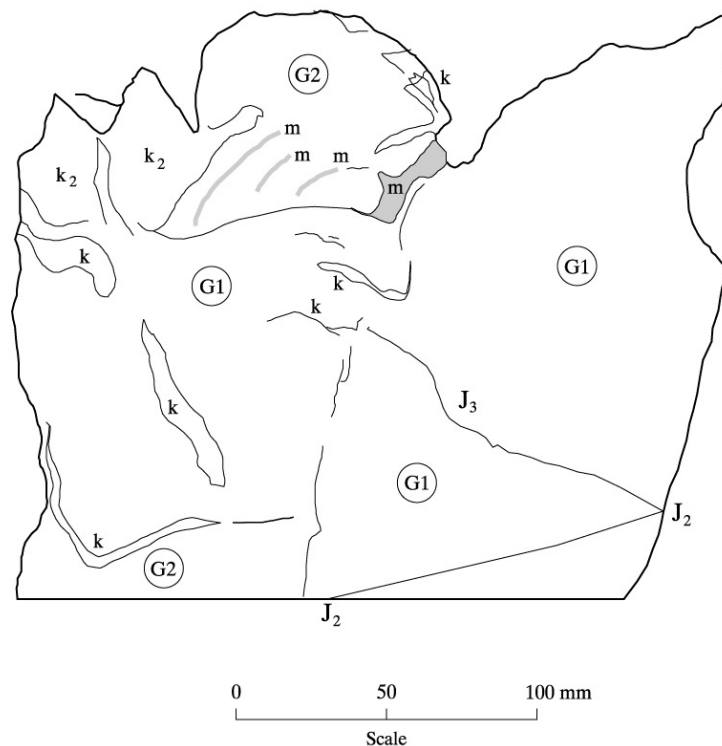
Block Sample BS 4 - North Face

Sample taken - 5-9-97

First Unpacked - 20-10-97

Date Described - 24-10-97 by N.P. Koor and S.D.G. Campbell

Sample Condition - Sample not waxed and beginning to dry out.



- ⒺG1)- Extremely weak medium yellow brown and reddish brown completely decomposed coarse ash TUFF (Stiff clayey slightly sandy SILT).
- ⒺG2)- Extremely weak medium pinkish red mottled white completely decomposed coarse ash lappili TUFF (Stiff clayey SILT).
- k - Firm to stiff white silty CLAY (KAOLIN).
- k<sub>2</sub> - Firm buff silty CLAY (KAOLIN).
- m - Firm dark brown SILT (MANGANIFEROUS DEPOSITS).
- J<sub>2</sub> - Extremely narrow joint infilled with manganiferous deposits and white kaolin.
- J<sub>3</sub> - Tight joint.

Figure D3 - Block Sample BS 4 - Description of North Face





Plate D4 - Block Sample BS 4 - East Face

### Lai Ping Road Landslide Investigation - Block Sample Description

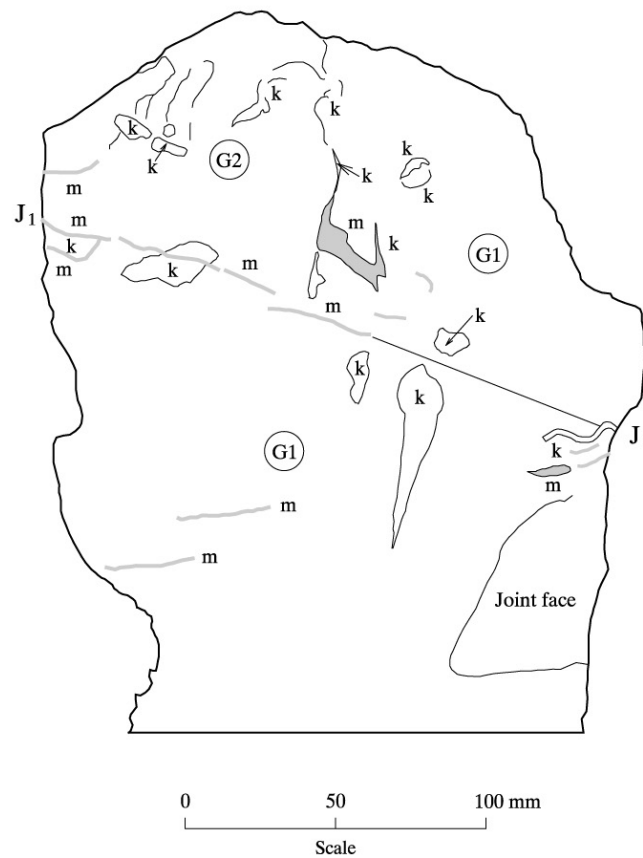
Block Sample BS 4 - East Face

Sample taken - 5-9-97

First Unpacked - 24-10-97

Date Described - 24-10-97 by N.P. Koor and S.D.G. Campbell

Sample Condition - Very poor. 1/3 sample collapse along sampling induced fractures.



- ⒸG1 - Extremely weak medium yellow brown and reddish brown completely decomposed coarse ash TUFF (Stiff clayey slightly sandy SILT).
- ⒸG2 - Extremely weak medium pinkish red mottled white completely decomposed coarse ash lappili TUFF (Stiff clayey SILT).
- k - Firm to stiff white silty CLAY (KAOLIN).
- m - Firm dark brown SILT (MANGANIFEROUS DEPOSITS).
- J<sub>1</sub> - Extremely narrow joint infilled with manganiferous deposits.

Figure D4 - Block Sample BS 4 - Description of East Face



Plate D5 - Block Sample BS 5 - North Face



### Lai Ping Road Landslide Investigation - Block Sample Description

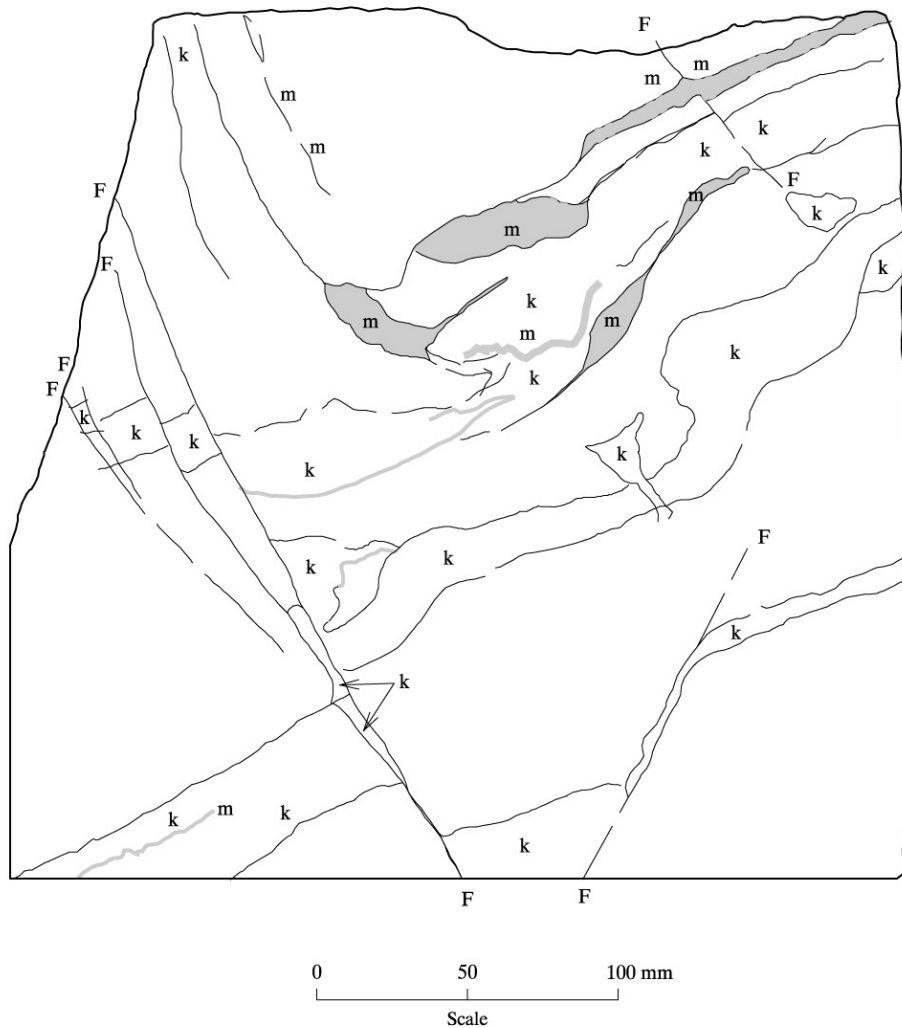
Block Sample BS 5 - North Face

Sample taken - 5-9-97

First Unpacked - 24-10-97

Date Described - 24-10-97 by N.P. Koor and S.D.G. Campbell

Sample Condition - Sample not waxed - dried out - with many fractures.



General Description - Extremely weak medium orangish brown mottled pinkish red inequigranular completely decomposed coarse ash TUFF with deformed and faulted layers 5-70 mm thick of stiff white and buff CLAY (Stiff sandy slightly clayey SILT).

k - Stiff off white and buff mottled pinkish red slightly silty CLAY (KAOLIN).

m - Firm dark brown SILT (MANGANIFEROUS DEPOSITS).

F - Micro-faults.

Figure D5 - Block Sample BS 5 - Description of North Face



Plate D6 - Block Sample BS 5 - West Face

### Lai Ping Road Landslide Investigation - Block Sample Description

Block Sample BS 5 - West Face

Sample taken - 5-9-97

First Unpacked - 20-10-97

Date Described - 24-10-97 by N.P. Koor and S.D.G. Campbell

Sample Condition - Sample not waxed and beginning to dry out - with many fractures.



General Description - Extremely weak medium orangish brown mottled pinkish red inequigranular completely decomposed coarse ash TUFF with deformed layers 5-70 mm thick of stiff white and buff faulted CLAY (Stiff sandy slightly clayey SILT).

k - Stiff off white and buff mottled pinkish red slightly silty CLAY (KAOLIN).

m - Firm dark brown SILT (MANGANIFEROUS DEPOSITS).

Fr - Fracture in sample.

Figure D6 - Block Sample BS 5 - Description of West Face





Plate D7 - Block Sample BS 6 - East Face

### Lai Ping Road Landslide Investigation- Block Sample Description

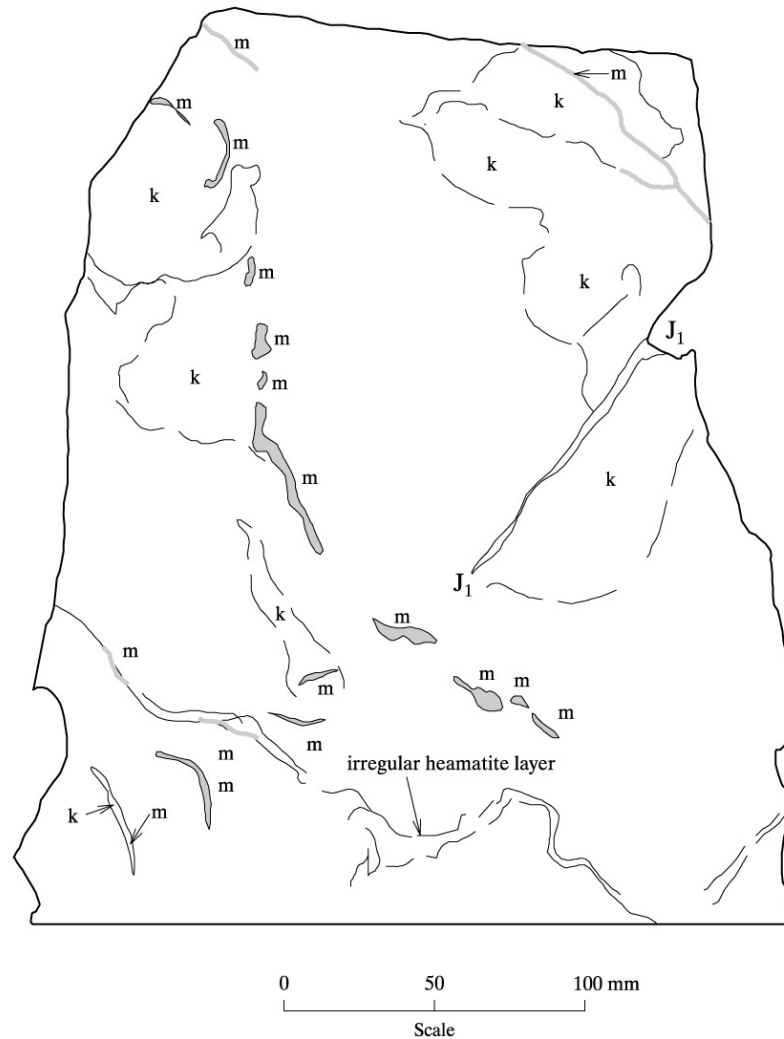
Block Sample BS 6 - East Face

Sample taken - 5-9-97

First Unpacked - 27-10-97

Date Described - 27-10-97 by N.P. Koor and S.D.G. Campbell

Sample Condition - Very poor, split along vertical and diagonal fractures.



General Description - Extremely weak medium reddish brown mottled light pinkish white, brownish yellow streaked black completely decomposed coarse ash TUFF (Stiff slightly sandy clayey SILT).

k - Firm white mottled reddish brown and pink silty occasionally sandy CLAY (KAOLIN).

m - Firm dark brown SILT (MANGANIFEROUS DEPOSITS).

J<sub>1</sub> - Extremely narrow joint infilled with firm brown clay, kaolin and manganiferous deposits.

Figure D7 - Block Sample BS 6 - Description of East Face



Plate D8 - Block Sample BS 7 - North Face



### Lai Ping Road Landslide Investigation - Block Sample Description

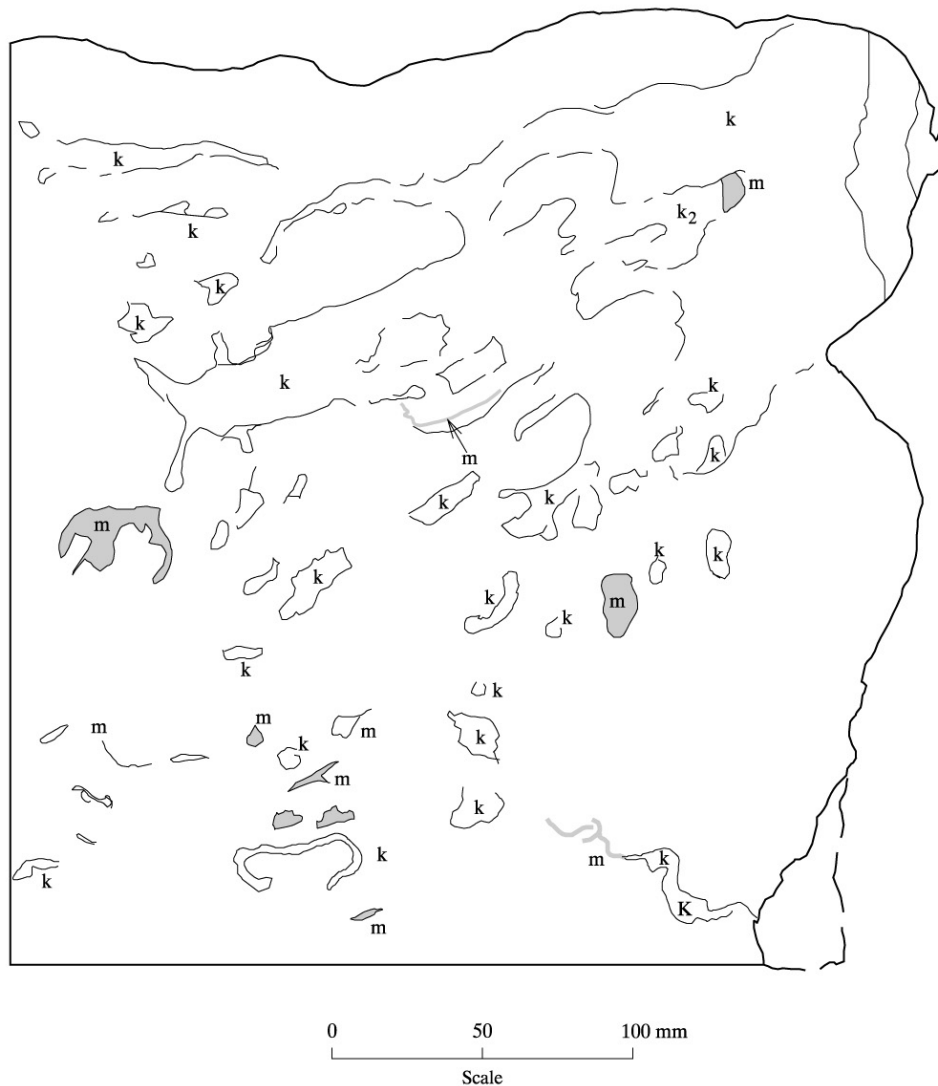
Block Sample BS 7 - North Face

Sample taken - 5-9-97

First Unpacked - 24-10-97

Date Described - 24-10-97 by N.P. Koor and S.D.G. Campbell

Sample Condition - Sample not waxed. Some disturbance in form of micro - shears.



**General Description** - Extremely weak reddish brown and yellow brown mottled dark brown and white completely decomposed coarse ash lapilli TUFF (Stiff silty slightly sandy CLAY).

k - Firm white marbled reddish-pinkish brown slightly silty CLAY (KAOLIN).

k<sub>2</sub> - Firm to stiff medium yellow brown silty CLAY.

m - Firm dark brown SILT(MANGANIFEROUS DEPOSITS).

Figure D8 - Block Sample BS 7 - Description of North Face

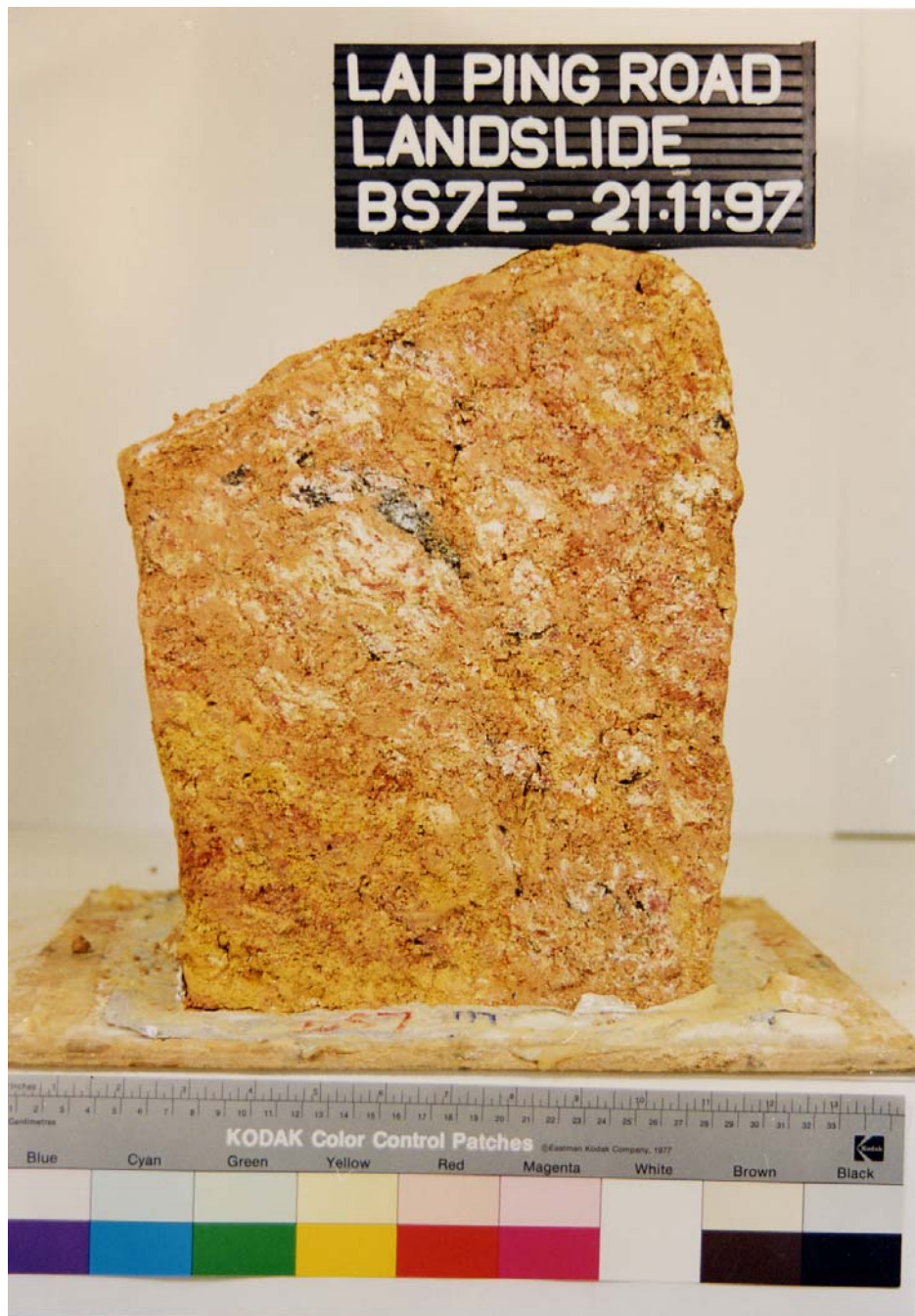


Plate D9 - Block Sample BS 7 - East Face

### Lai Ping Road Landslide Investigation - Block Sample Description

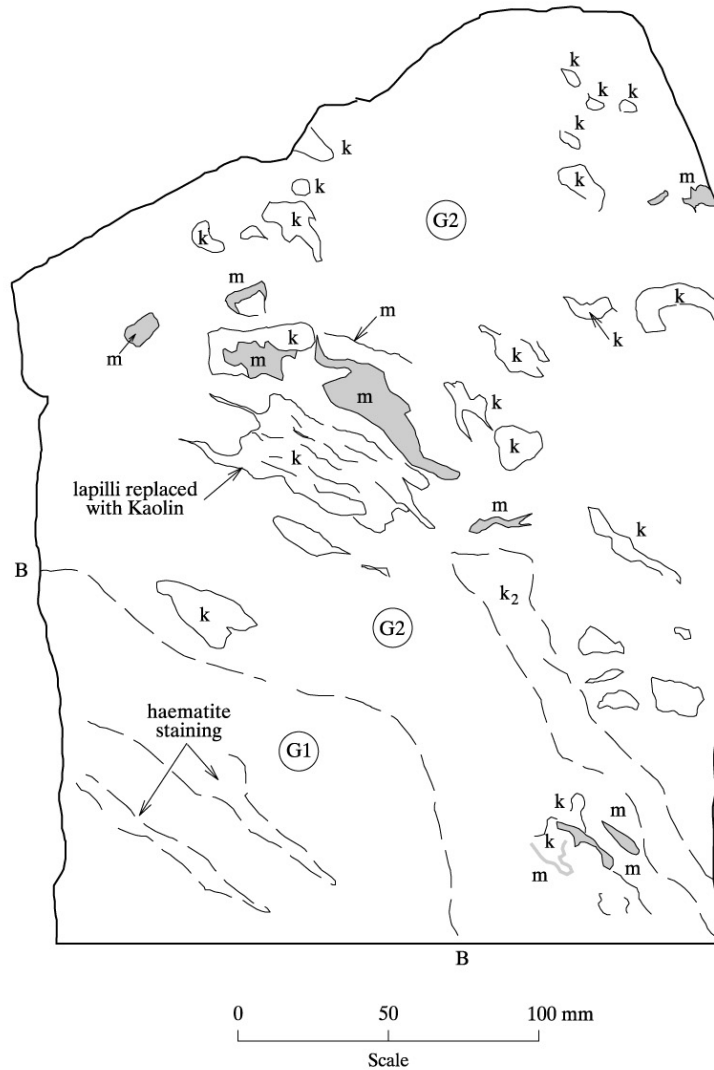
Block Sample BS 7 - East Face

Sample taken - 5-9-97

First Unpacked - 24-10-97

Date Described - 24-10-97 by N.P. Koor and S.D.G. Campbell

Sample Condition - Sample not waxed. Some disturbance in form of micro-shears.



- ⒺG1- Extremely weak medium yellow brown dappled reddish brown completely decomposed coarse ash TUFF (Stiff silty slightly sandy CLAY).
- ⒺG2- Extremely weak medium reddish-pinkish brown mottled whitish pink and dark brown completely decomposed coarse ash lapilli TUFF (Stiff silty slightly sandy CLAY).
- k - Firm white marbled reddish-pinkish brown slightly silty CLAY (KAOLIN).
- k<sub>2</sub> - Firm to stiff medium yellow brown silty CLAY.
- m - Firm dark brown SILT (MANGANIFEROUS DEPOSITS).
- B - Possible interface between lapilli and non-lapilli bearing tuff.

Figure D9 - Block Sample BS 7 - Description of East Face



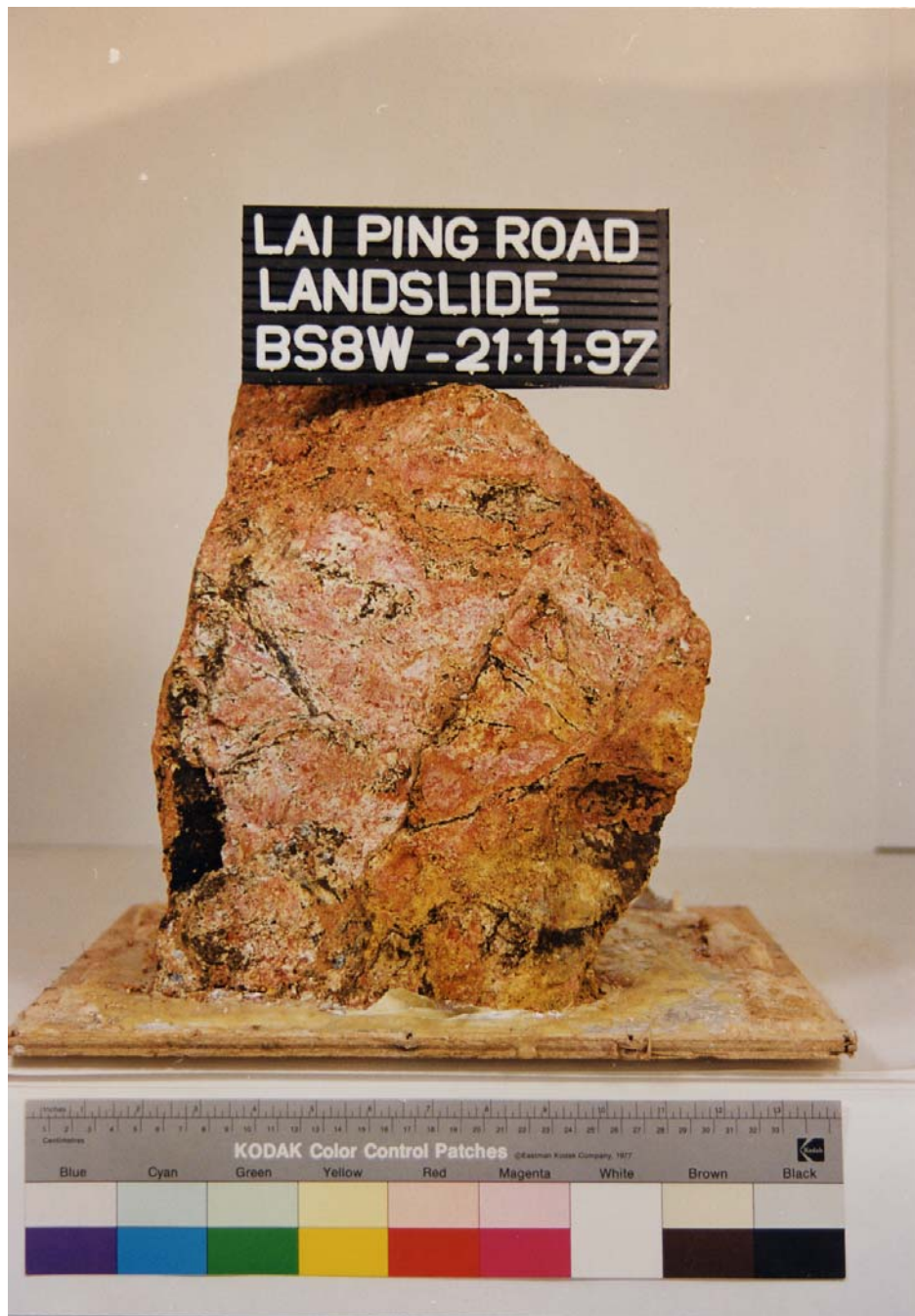


Plate D10 - Block Sample BS 8 - West Face

### Lai Ping Road Landslide Investigation - Block Sample Description

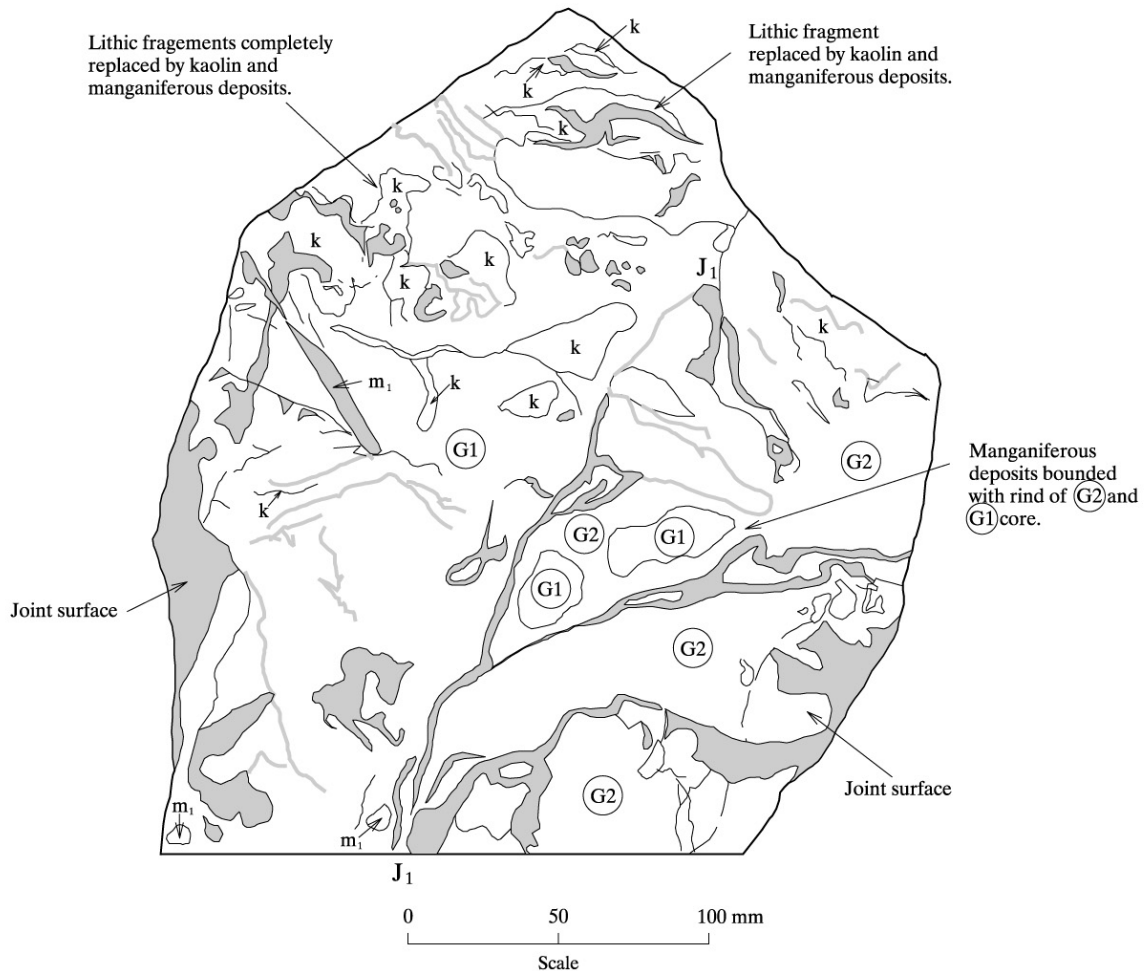
Block Sample BS 8 - West Face

Sample taken - 9-9-97

First Unpacked - 24-10-97

Date Described - 24-10-97 and 27-10-97 by N.P. Koor and S.D.G. Campbell

Sample Condition - Some disturbance, faces not parallel - not waxed.



- ⒺG1- Extremely weak medium reddish pink mottled white and orange brown and streaked black completely decomposed coarse ash TUFF (Stiff clayey SILT).
- ⒺG2- Extremely weak medium reddish orangish brown mottled reddish brown and streaked black completely decomposed coarse ash TUFF (Stiff clayey SILT).
- k - Firm light pinkish white sometimes mottled reddish brown silty CLAY (KAOLIN) often enclosing dark brown crinulated manganiferous deposits.
- - Firm dark brown SILT (MANGANIFEROUS DEPOSITS).
- ~ - Firm dark brown SILT < 1 mm thick.
- m<sub>1</sub> - Firm silver grey slightly clayey SILT (disseminated manganiferous deposits and kaolin).
- J<sub>1</sub> - Extremely narrow joint infilled with stiff brown clay and manganiferous deposits.

Figure D10 - Block Sample BS 8 - Description of West Face



Plate D11 - Block Sample BS 9 - East Face

### Lai Ping Road Landslide Investigation - Block Sample Description

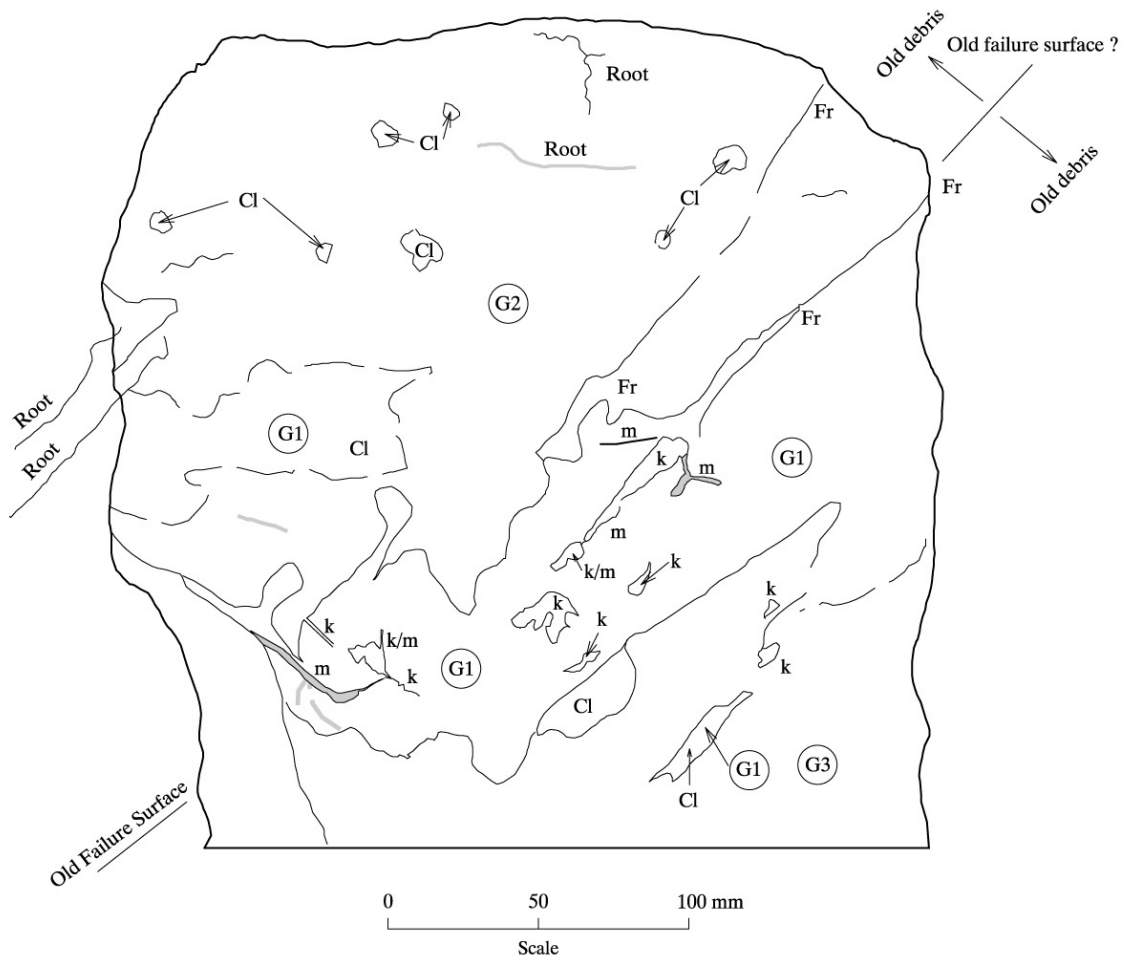
Block Sample BS 9 - East Face

Sample taken - 9-9-97

First Unpacked - 27-10-97

Date Described - 27-10-97 by N.P. Koor and S.D.G. Campbell

Sample Condition - Sample not waxed. Some micro-fractures present



- ① G1 Dense medium pinkish red very sandy clayey SILT (LANDSLIDE DEBRIS CLAST) with whisps of white clay and crinulated extremely narrow very dark brown manganiferous deposits infilled joints.
- ② G2 Firm to stiff medium brown mottled reddish brown very clayey SILT with occasional angular to sub-rounded coarse, medium and fine gravel of stiff red silt and moderately decomposed coarse ash tuff and occasional fine roots (LANDSLIDE DEBRIS MATRIX).
- ③ G3 Firm light brownish yellow sandy very clayey SILT (RESIDUAL SOIL).
- k - Firm white silty CLAY (KAOLIN) - Kaolin often rimmed with manganiferous deposits.
- m - Firm dark brown SILT (MANGANIFEROUS DEPOSITS).
- Fr - Fracture in sample.
- Cl - Debris clast.

Figure D11 - Block Sample BS 9 - Description of East Face





Plate D12 - Block Sample BS 12 - Northeast Face

### Lai Ping Road Landslide Investigation - Block Sample Description

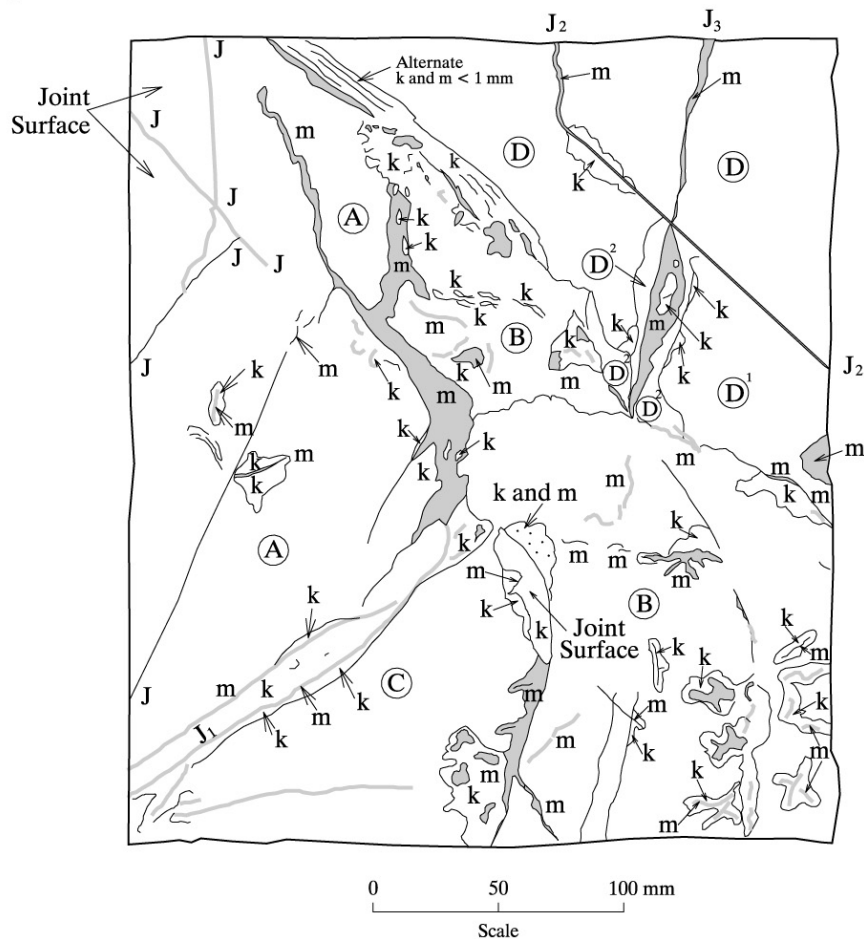
Block Sample BS 12 - Northeast Face

Sample taken - 30-10-97

First Unpacked - 21-11-97

Date Described - 21-11-97 by N.P. Koor

Sample Condition - Good.



- (A) - Extremely weak dark brownish red mottled pink and white completely decomposed fine ash TUFF with tight manganiferous deposits infilled joints (J) often surrounded by thin veneer of white clay (Dense slightly clayey SILT with very occasional coarse sub-rounded quartz sand).
- (B) - Stiff light pink mottled white occasionally light brown and black silty CLAY with very occasional coarse sub-rounded quartz sand (Highly altered tuff appears to have been replaced with white and pink clay. Manganiferous deposits infill to contorted joints often surrounded by white clay.
- (C) - As (A) but becoming light pink adjacent to J<sub>1</sub>.
- (D) - Extremely weak medium orangish brown becoming pinkish red in (D<sub>1</sub>) spotted white and medium brown in (D<sub>2</sub>) completely decomposed fine ash TUFF with very narrow manganiferous deposits infilled joints (J<sub>2</sub> + J<sub>3</sub>).
- k - Firm white to pinkish white CLAY (KAOLIN).
- m - Dark brown SILT (MANGANIFEROUS DEPOSITS).

Figure D12 - Block Sample BS 12 - Description of Northeast Face

## APPENDIX E

DISCONTINUITY DATA OBTAINED WITH BOTH  
IMPRESSION PACKER AND ACOUSTIC TELEVIEWER

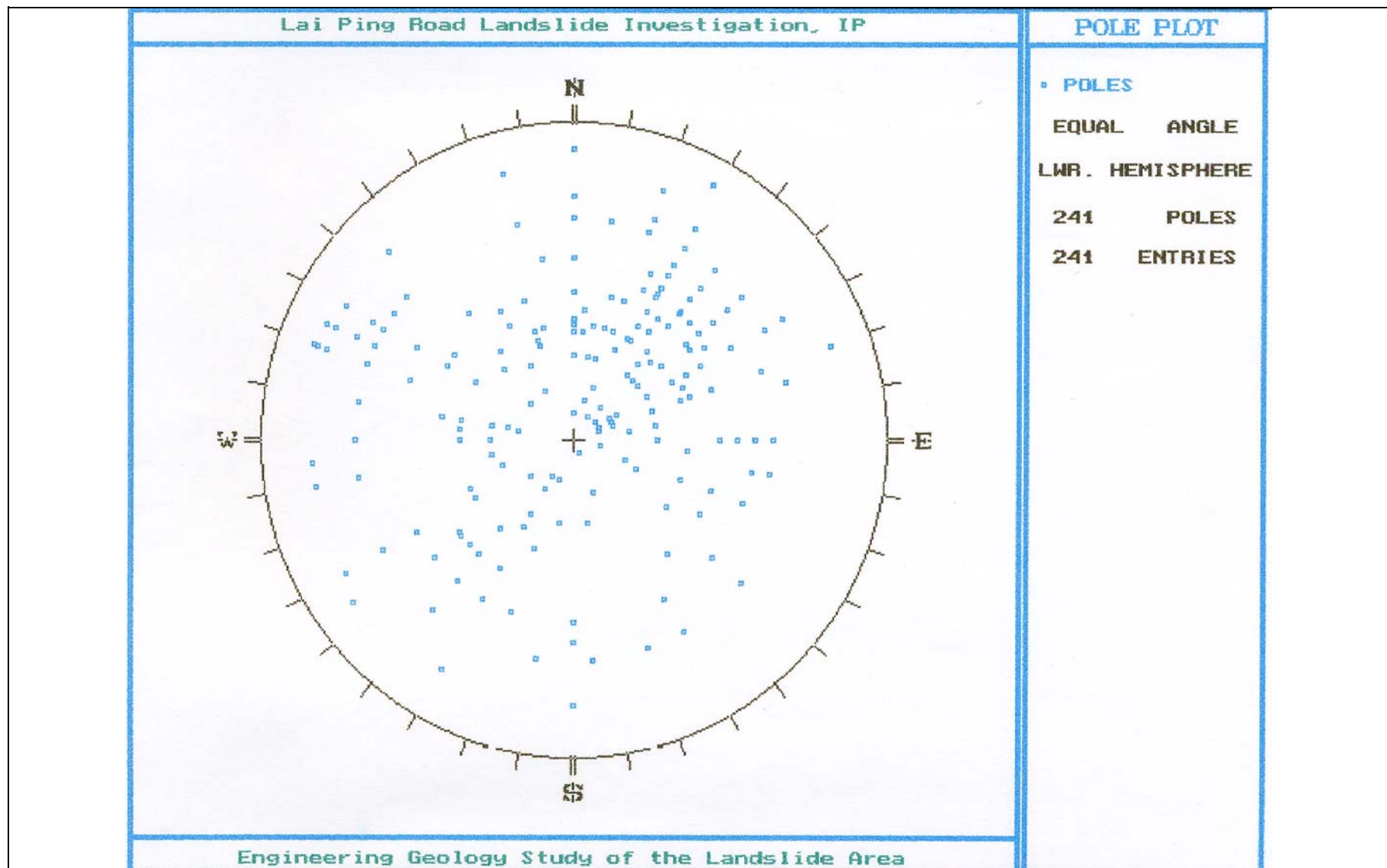


Figure E1 - Pole Plot of Discontinuity Data Obtained from Impression Packer Tests



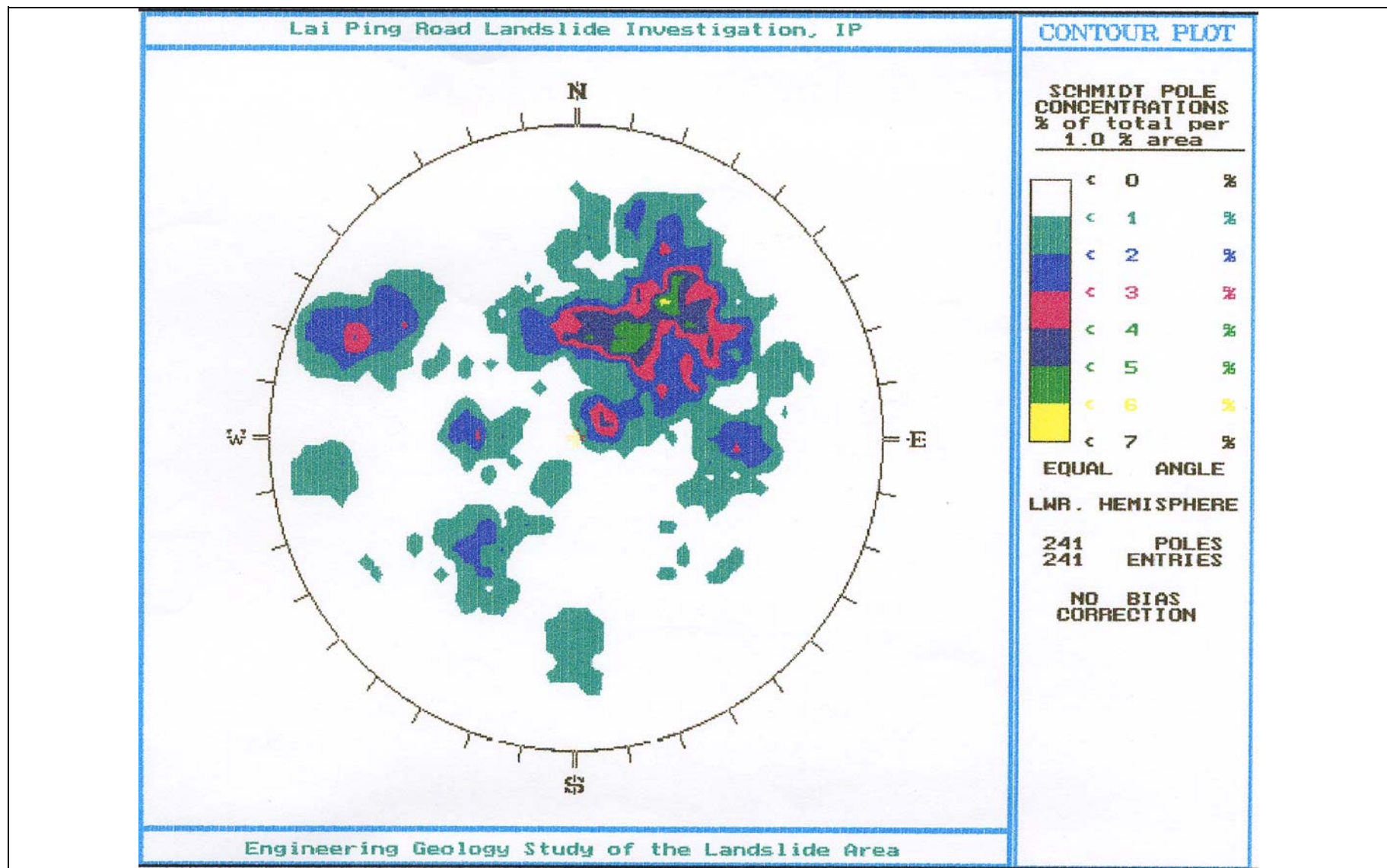


Figure E2 - Contour Plot of Discontinuity Data Obtained from Impression Packer Tests

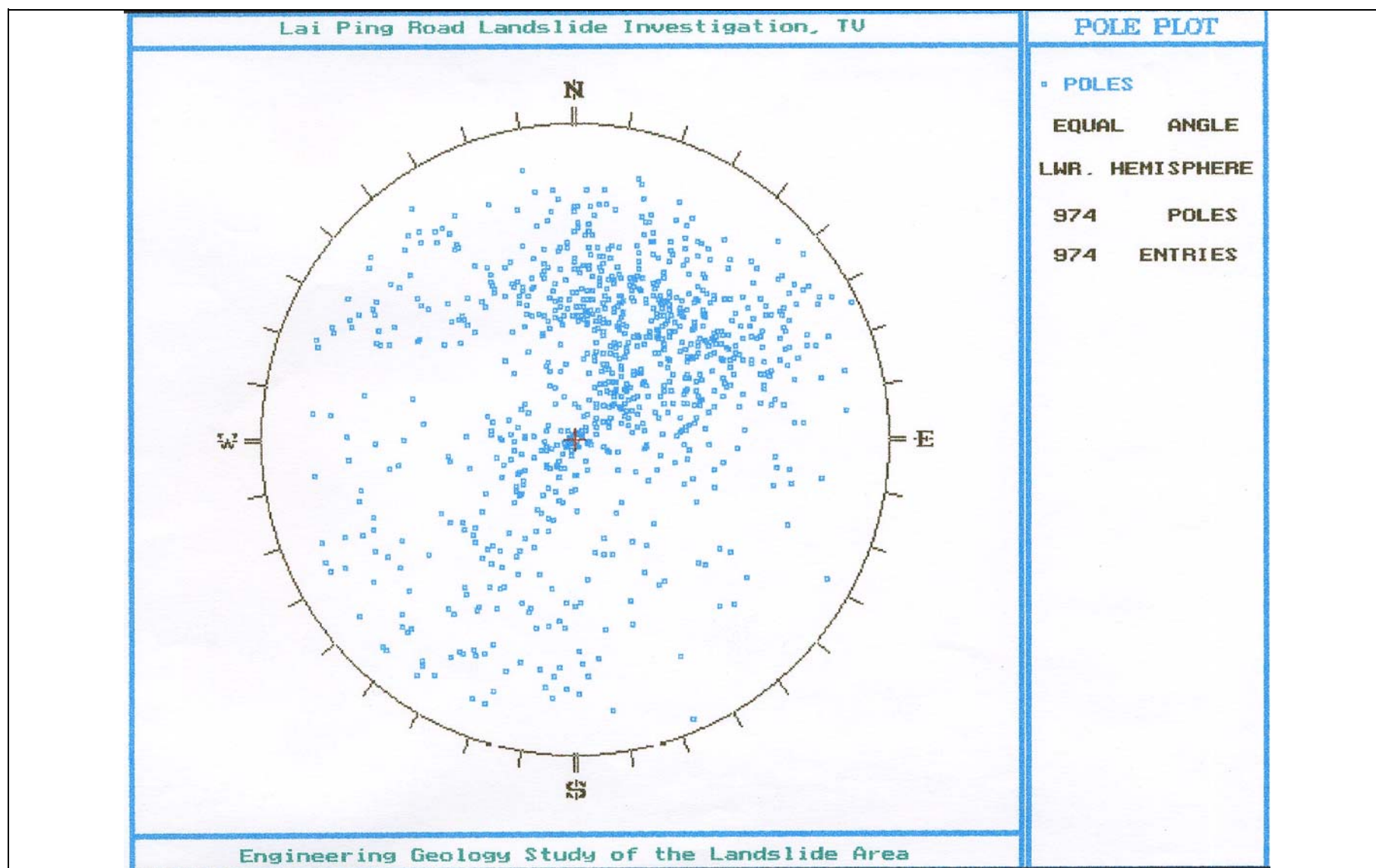


Figure E3 - Pole Plot of Discontinuity Data Obtained from Acoustic Televiewer Tests

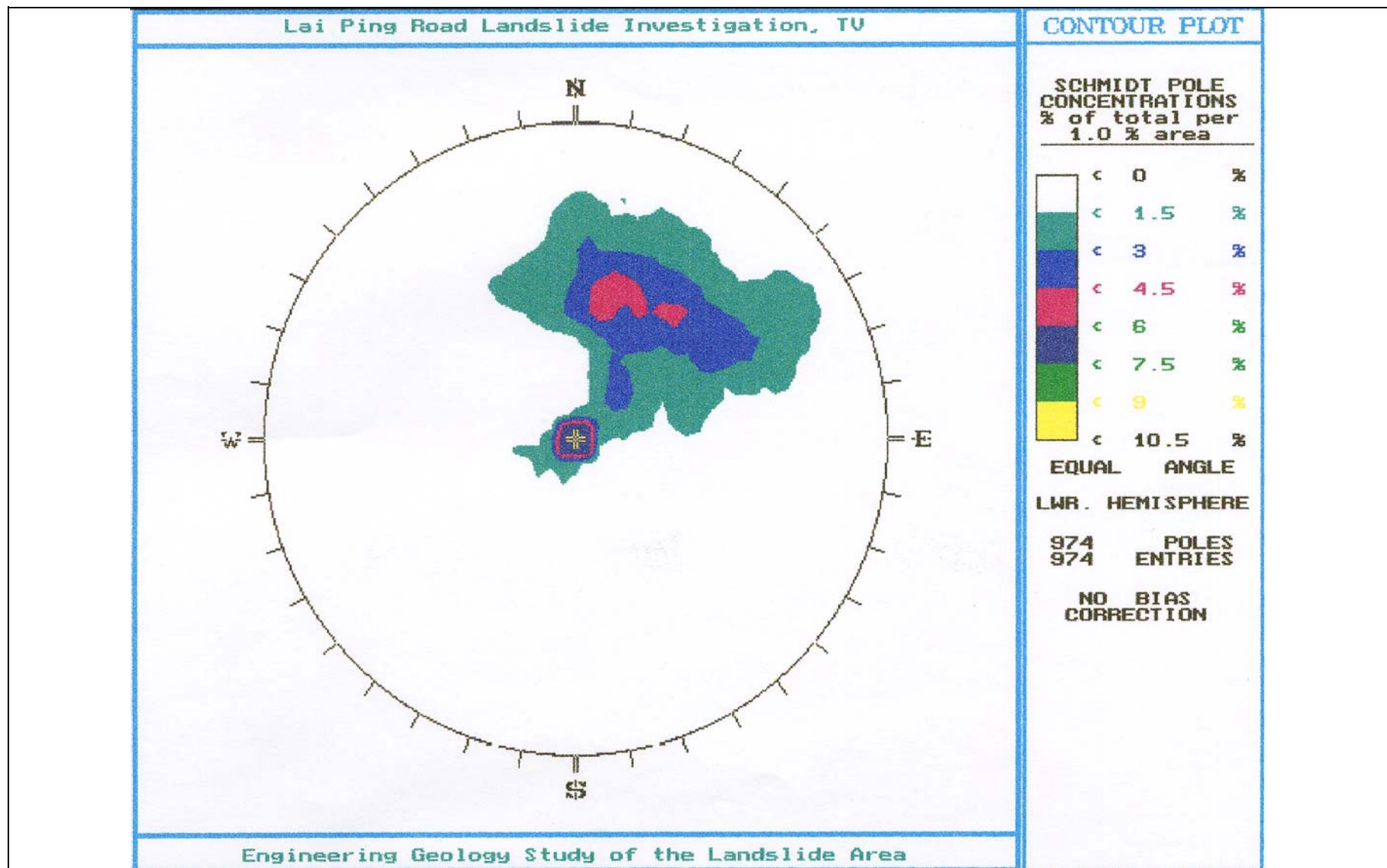


Figure E4 - Contour Plot of Discontinuity Data Obtained from Acoustic Televiewer Tests

APPENDIX F  
MINERALOGICAL AND MICROTTEXTURAL REPORT



Version 1

**BRITISH GEOLOGICAL SURVEY  
TECHNICAL REPORT  
Mineralogy & Petrology Series**

**REPORT NO. WG/98/25C**

**A MINERALOGICAL AND MICROTTEXTURAL  
STUDY OF THE LAI PING ROAD  
LANDSLIDE, HONG KONG**

**R J Merriman, S J Kemp, V L Hards and H A Murphy**

**Date**

October 6, 1998

**Classification**

Commercial-in-confidence

**Geographical index**

Hong Kong

**Bibliographic reference**

Merriman, R J, Kemp, S J, Hards, V L & Murphy, H.A. 1998.

A mineralogical and microtextural study of the Lai Ping Road landslide, Hong Kong

*British Geological Survey Technical Report WG/98/25C*

British Geological Survey, Keyworth, Nottingham NG12 5GG, UK.

## CONTENTS

	Page
<b>1. INTRODUCTION</b>	<b>1</b>
<b>2. GEOLOGY AND SAMPLE LOCATION</b>	<b>2</b>
<b>3. MINERALOGICAL ANALYSIS</b>	<b>3</b>
<b>3.1. Sample preparation</b>	<b>3</b>
<b>3.2. X-ray diffraction analysis</b>	<b>3</b>
<b>3.3. Results</b>	<b>4</b>
<b>4. MICROTTEXTURAL ANALYSIS</b>	<b>5</b>
<b>4.1. Sample preparation</b>	<b>5</b>
<b>4.2. Microtextural descriptions</b>	<b>5</b>
4.2.1. Sample BS5/A5/D	5
4.2.2. Sample BS7/A7/C	6
4.2.3. Sample BS8/A8/B.	6
4.2.4. Sample BS12/B1/A.	7
4.2.5. Sample BS12/B1/B.	8
<b>5. DISCUSSION</b>	<b>9</b>
<b>6. CONCLUSIONS</b>	<b>11</b>
<b>7. REFERENCES</b>	<b>12</b>

## TABLES

<b>Table 1. Sample Descriptions</b>	<b>2</b>
<b>Table 2. Estimated proportions of clay minerals in the sample fine-fractions from XRD analyses</b>	<b>4</b>

## FIGURES

	Page
<b>Figure 1. Site plan showing the landslide scars at Lai Ping Road and the location of samples studied for this report.</b>	<b>13</b>
<b>Figure 2. XRD traces illustrating the effects of formamide intercalation on sample BS5/A5/D (black trace = wet run, red trace = formamide intercalation, green trace = heated at 110 °C/90 minutes)</b>	<b>14</b>
<b>Figure 3. XRD traces illustrating the effects of formamide intercalation on sample BS7/A7/C (black trace = wet run, red trace = formamide intercalation, green trace = heated at 110 °C/90 minutes)</b>	<b>14</b>
<b>Figure 4. XRD traces illustrating the effects of formamide intercalation on sample BS8/A8/B (black trace = wet run, red trace = formamide intercalation, green trace = heated at 110 °C/90 minutes)</b>	<b>15</b>
<b>Figure 5. XRD traces illustrating the effects of formamide intercalation on sample BS12/B1/A (black trace = wet run, red trace = formamide intercalation, green trace = heated at 110 °C/90 minutes)</b>	<b>15</b>
<b>Figure 6. XRD traces illustrating the effects of formamide intercalation on sample BS12/B1/B (black trace = wet run, red trace = formamide intercalation, green trace = heated at 110 °C/90 minutes)</b>	<b>16</b>

## PLATES

<b>Plate 1.</b>	<b>Page</b>
1A. Sample BS5/A5/D. Lai Ping Road landslide. Optical photomicrograph of clay-rich saprolite with dark-brown fragments of ferromanganese minerals. The clay is impregnated with blue-stained resin (plane-polarized light; field width 9 mm).	17
1B. Sample BS5/A5/D. Lai Ping Road landslide. Optical photomicrograph of igneous grain partially replaced by intergrowths of yellow-brown biotite (cross-polarized light; field width 4.5 mm).	17
1C. Sample BS5/A5/D. Lai Ping Road landslide. Optical photomicrograph of deformed kaolinite 'books' in the clay matrix. (cross-polarized light; field width 1.1 mm).	17
<b>Plate 2.</b>	
2A. Sample BS5/A5/D. Lai Ping Road landslide. Optical photomicrograph showing replacement of planar kaolinite crystals in a book by fibrous ?halloysite. Clay minerals are stained yellow by ferromanganese mineral (cross-polarized light; field width 0.45 mm).	18
2B. Sample BS7/A7/C. Lai Ping Road landslide. Optical photomicrograph of deformed quartz grain showing mortar texture (cross-polarized light; field width 4.5 mm).	18
2C. Sample BS7/A7/C. Lai Ping Road landslide. Optical photomicrograph of deformed kaolin-filled vein (cross-polarized light; field width 1.1 mm).	18



# **PLATES (continued)**

<b>Plate 3</b>	<b>Page</b>
3A. Sample BS7/A7/C. Lai Ping Road landslide. Backscattered secondary electron photomicrograph of deformed kaolinite book in the clay matrix.	19
3B. Sample BS7/A7/C. Lai Ping Road landslide. Backscattered secondary electron photomicrograph of deformed book-like kaolinite plates partially replaced by fibrous ?halloysite.	19
3C. Sample BS8/A8/B. Lai Ping Road landslide. Backscattered secondary electron photomicrograph of slip clay fragment. Dark-grey kaolin-rich clay is highly contorted; associated ferromanganese minerals are bright grey or white.	19
3D. Sample BS8/A8/B. Lai Ping Road landslide. Backscattered secondary electron photomicrograph of slip clay fragment. Dark-grey kaolin-rich clay generated by slip contains white laminae of Mn-oxide precipitated by fluid movement on a slip plane. The clay matrix consists of numerous kaolinite books.	19
3E. Sample BS8/A8/B. Lai Ping Road landslide. Backscattered secondary electron photomicrograph of Mn-oxide showing concentric growth of thin platy crystals.	19
3F. Sample BS8/A8/B. Lai Ping Road landslide. Backscattered secondary electron photomicrograph of Mn-oxide showing radial clusters of thin platy crystals.	19
<b>Plate 4</b>	
4A. Sample BS8/A8/B. Lai Ping Road landslide. Optical photomicrograph of highly fractured quartz phenocryst with blue-stained clay filling cracks (cross-polarized light; field width 4.5 mm).	20
4B. Sample BS8/A8/B. Lai Ping Road landslide. Optical photomicrograph of a compound slip clay fragment in the clay matrix. The folded bluish-white kaolin with associated dark-brown Mn-oxide is an early slip clay; the green-stained kaolin is a later slip clay. Resin is deep blue (plane-polarized light; field width 4.5 mm).	20
4C. Sample BS12/B1/A. Lai Ping Road landslide. Optical photomicrograph of an early clay gouge with associated slip planes. Slip clays form green-stained diagonal lines bottom right and top left. Dark-brown ferromanganese minerals stain a detached and disrupted slip clay fragment in the gouge (centre). Thin tensional veins cut the fragment and quartz grains (plane-polarized light; field width 9 mm).	20

**PLATES (continued)**

<b>Plate 5.</b>	<b>Page</b>
5A. Sample BS12/B1/A. Lai Ping Road landslide. Optical photomicrograph of a fractured quartz grain in a clay gouge. Dark-brown ferromanganese minerals with thin green-stained clays attached are slip clay fragments. Blue-stained kaolin forms the matrix of the gouge. (plane-polarized light; field width 9 mm).	21
5B. Sample BS12/B1/A. Lai Ping Road landslide. Optical photomicrograph of a slip plane. Slip clays are pale-blue or green-stained in association with dark-brown laminae of ferromanganese minerals. Resin is deep blue. (plane-polarized light; field width 1.1 mm).	21
5C. Sample BS12/B1/A. Lai Ping Road landslide. Optical photomicrograph of a slip plane. Tensional veins (bottom right) formed normal to the slip plane are filled with ferromanganese minerals (plane-polarized light; field width 4.5 mm).	21
<b>Plate 6.</b>	
6A. Sample BS8/A8/B. Lai Ping Road landslide. Backscattered secondary electron photomicrograph of orientated domains of kaolin clay with overgrowths of fibrous halloysite.	22
6B. Sample BS8/A8/B. Lai Ping Road landslide. Backscattered secondary electron photomicrograph of kaolinite books with overgrowths of fibrous halloysite.	22
6C. Sample BS8/A8/B. Lai Ping Road landslide. Backscattered secondary electron photomicrograph of the halloysite fibres forming overgrowths on kaolinite. Note the curvature of some end sections of the fibres.	22
6D. Sample BS12/B1/A. Lai Ping Road landslide. Backscattered secondary electron photomicrograph of kaolinite books with overgrowths of halloysite fibres.	22
6E. Sample BS12/B1/A. Lai Ping Road landslide. Backscattered secondary electron photomicrograph showing deformed and disrupted ferromanganese laminae (bright grey) and quartz grains (mid-grey).	22
6F. Sample BS12/B1/A. Lai Ping Road landslide. Backscattered secondary electron photomicrograph of a compound slip clay fragment. Folded and disrupted slip clay comprising mid-grey kaolin and bright grey Mn-oxide formed early. Later slip clay and Mn-oxide is undeformed (bottom right of fragment).	22



# **PLATES (continued)**

<b>Plate 7.</b>	<b>Page</b>
7A. Sample BS12/B1/B. Lai Ping Road landslide. Optical photomicrograph showing a pale blue clay gouge with slip clay fragments. The blue-green clay (top left) forms part of a slip plane against a quartz-rich protolith stained dark-brown by ferromanganese minerals (plane-polarized light; field width 9 mm).	23
7B. Sample BS12/B1/B. Lai Ping Road landslide. Optical photomicrograph of quartz-filled tensional veins in the protolith, normal to a slip plane (subvertical, left of field). Two quartz-filled veins have also formed along the slip plane together with dark-brown ferromanganese laminae (plane-polarized light; field width 4.5 mm).	23
<b>Plate 8.</b>	
8A. Sample BS12/B1/B. Lai Ping Road landslide. Optical photomicrograph showing contorted slivers of slip clay consisting of whitish or pale-blue orientated domains of kaolin with dark-brown ferromanganese minerals (plane-polarized light; field width 4.5 mm).	24
8B. Sample BS12/B1/B. Lai Ping Road landslide. Optical photomicrograph of slip clay. Dark blue orientated domains of kaolin minerals alternate with whitish or pale-blue random domains. Brown and yellow staining is from ferromanganese minerals (cross-polarized light; field width 1.1 mm).	24
<b>Plate 9.</b>	
9A. Sample BS12/B1/A. Lai Ping Road landslide. Backscattered secondary electron photomicrograph of Fe-oxyhydroxide forming clusters of radiating platy crystals in slip clay fragments.	25
9B. Sample BS12/B1/A. Lai Ping Road landslide. Backscattered secondary electron photomicrograph of Ce-rich mineral forming granules in slip clay fragment.	25
9C. Sample BS12/B1/B. Lai Ping Road landslide. Backscattered secondary electron photomicrograph showing concentric growth of Mn-oxide.	25
9D. Sample BS12/B1/B. Lai Ping Road landslide. Backscattered secondary electron photomicrograph of well developed concentric growth pattern in Fe-oxyhydroxide.	25
9E. Sample BS12/B1/B. Lai Ping Road landslide. Backscattered secondary electron photomicrograph of kaolinite books heavily replaced and overgrown by fibrous halloysite.	25
9F. Sample BS12/B1/B. Lai Ping Road landslide. Backscattered secondary electron photomicrograph of halloysite fibres replacing books of kaolinite crystals.	25

**British Geological Survey**

**Mineralogy & Petrology Report No. WG/98/25C**

**A MINERALOGICAL AND MICROTTEXTURAL STUDY OF THE  
LAI PING ROAD LANDSLIDE, HONG KONG**

**R J Merriman, S J Kemp, V L Hards & H A Murphy**

**SUMMARY**

Mineralogical and petrological studies of altered tuffs hosting a landslide at Lai Ping Road, Hong Kong, show that halloysite occurs in all the samples investigated, forming 50-82% of clay mineral assemblages. Halloysite appears to form by alteration of kaolinite, replacing both the crystals in kaolinite books and orientated kaolinite in typical slip clays. The alteration may result from post-slip replacement of strained kaolinite crystals associated with fluid movement along slip planes. Fluid movement during static intervals is also responsible for the precipitation of ferromanganese minerals along slip planes. Microtextures suggest that at least three earlier phases of movement have occurred at Lai Ping Road.

**1. INTRODUCTION**

On 2nd July 1997, a series of landslides occurred on cut slope 7NE-C/95, located on the northern side of Lai Ping Road, in Kau To Shan, Sha Tin. The landslide occurred after several days of intense rainfall concentrated mainly within the Sha Tin valley. Slope failure, consisting of five individual landslides (scars 1 to 5 in Figure 1), affected a 135 m section of the cut slope and quasi-natural slope above. A zone of major surface deformation was identified extending up to 50 m above the crest of the cut slope.

A mineralogical and petrological analysis of the altered tuff and rhyolite hosting the Lai Ping Road landslide was commissioned by the Geotechnical Engineering Office, Hong Kong, as part of ongoing geotechnical investigations. Previous mineralogical studies of landslide sites in Hong Kong have shown that volcanic rocks are extensively altered to clay-rich saprolite consisting mainly of kaolin-group minerals, and in some sites slip surfaces appear to have developed preferentially along zones of abundant kaolin-filled veins and fractures (Merriman & Kemp, 1995). Although both kaolinite and halloysite have been identified in the saprolite,



the proportion of halloysite was found to increase in the zones of abundant kaolin-filled joints associated with the landslides at the Fei Tsui Road and Shum Wan Road sites (Merriman *et al.*, 1996). Petrological characterisation of the clay gouges developed at these sites suggests that a history of repeated slip accompanied by static weathering and mineralisation along the slip plane can be identified by analysis of clay microfabrics (Merriman *et al.*, 1996).

The main aims of the work reported here are: (a) to identify halloysite and estimate its proportions relative to kaolinite in saprolite samples from the landslide scars; (b) if possible, relate differences in halloysite:kaolinite proportions to the process of landslide development; (c) if possible, use the microfabrics developed in the saprolite samples to characterise the history of slope failure at the Lai Ping Road site.

## 2. GEOLOGY AND SAMPLE LOCATION

The dominant rock-type at the site is a grey to bluish grey, sparsely lapilli-bearing coarse ash crystal tuff, varying to lapilli-ash tuff and locally ash-lapilli tuff. Lapilli, up to 25 mm in size, include quartz and feldspar crystals and sub-angular fine ash tuff and rhyolite. With increasing decomposition, the tuff becomes white to buff and mottled orange and reddish-brown, yellow and white. Locally the tuff exhibits a discontinuous compactional fabric and alignment of lithic clasts and crystals which together comprise a weak stratification. This dips typically towards the NNE, but also less commonly towards the N or NNW, at angles generally between 25-40°. Less common rock-types include aphyric and quartz-phyric rhyolite, which are bluish-grey, varying to yellowish- and reddish-brown and white when more decomposed.

A zone of intense alteration can be traced from NW to SE across landslide scars 4, 3 and 2 (Figure 1). It is characterised by a deep red to reddish-pink coloration, and the common development of white to buff, kaolin-filled relict joints, up to 30 mm thick, and dark-brown manganiferous mineralization. The zone appears to dip into the hillside, towards the NNE at c. 25°, in the same general direction as the stratification in the tuff. A discontinuous intrusive rhyolite is emplaced along the zone of alteration in the landslide scar 4.

Samples of highly altered tuff were collected from landslide scars 2, 3 and 4, above the surface of the rupture (Figure 1). Samples BS8 and BS12 were taken from within a zone of intense alteration in the tuffs, which is subparallel to a weak fabric.

**Table 1. Sample Descriptions**

Sample No.	Scar	Description
BS5/A5/D	2	Volcaniclastic saprolite: reddish brown, mottled pink, white and grey
BS7/A7/C	3	Volcaniclastic saprolite: reddish brown, mottled white/grey
BS8/A8/B	4	Volcaniclastic saprolite: reddish brown, mottled pink/white, grey streaked
BS12/B1/A	4	Volcaniclastic saprolite: reddish brown, streaked white/grey
BS12/B1/B	4	Volcaniclastic saprolite: reddish brown, streaky white/grey

### **3. MINERALOGICAL ANALYSIS**

#### **3.1. Sample preparation**

In order to identify any clay minerals present in the bulk sample, a fine  $<2\ \mu\text{m}$  fraction was isolated and an oriented mount prepared.

A representative portion of the sample was removed and sloughed in distilled water overnight. The sample was then stirred with a laboratory stirrer for 15 minutes and treated with ultrasound for approximately 5 minutes to disaggregate the material and disperse any clay minerals present. The suspension that successfully passed through a  $63\ \mu\text{m}$  sieve was placed in a measuring cylinder and allowed to stand. In order to prevent flocculation of the clay crystals, 2 ml of 0.1M 'Calgon' (sodium hexametaphosphate) was added to each suspension. After a period calculated using Stokes' Law, a nominal  $<2\ \mu\text{m}$  fraction was removed and dried at  $55^\circ\text{C}$ . An 80 mg portion of the  $<2\ \mu\text{m}$  material was then suspended in a minimum of deionised water and pipetted onto a ceramic tile in a vacuum apparatus to produce an oriented mount.

In order to identify halloysite and estimate its proportion relative to kaolinite in the bulk sample, a further  $<5\ \mu\text{m}$  was removed from the  $<63\ \mu\text{m}$  material and pipetted directly onto a ceramic tile in a vacuum apparatus to produce an oriented mount.

#### **3.2. X-ray diffraction analysis**

XRD analysis was carried out using a Philips PW1700 series diffractometer equipped with a cobalt-target tube and operating at 45kV and 40mA. Diffraction data were analysed using Philips APD1700 software coupled to an ICDD database running on a DEC MicroVax 2000 micro-computer system.



The <2  $\mu\text{m}$  oriented mounts were scanned from 2-32  $^{\circ}2\theta$  at a speed of 0.5  $^{\circ}2\theta/\text{minute}$  after air-drying, glycol-solvating and heating to 550 $^{\circ}\text{C}$  for 2 hours.

The method proposed by Churchman *et al.* (1984), based on the different rate and extent of formamide intercalation, was used to distinguish between the kaolin group minerals halloysite and kaolinite. Concentrated <5  $\mu\text{m}$  oriented mounts were scanned three times from 7.5-16.5  $^{\circ}2\theta$  at a speed of 0.58  $^{\circ}2\theta/\text{minute}$ : (i) wet - having allowed excess water to drain away, (ii) within 30 minutes of formamide application via an aerosol and (iii) after heat treatment of 110 $^{\circ}\text{C}$  for 90 minutes.

Approximate proportions for kaolinite, halloysite and 'mica' in the <5  $\mu\text{m}$  fractions were calculated from normalized peak area measurements taken from the diffraction traces. Kaolinite content was determined from the peak area of the c. 7.1 $\text{\AA}$  spacing after formamide intercalation. 'Mica' content was taken to be represented by the peak area of the c. 10 $\text{\AA}$  spacing after heat treatment. Halloysite content was estimated from the c. 10 $\text{\AA}$  peak area after formamide intercalation after having subtracted the 'mica' component.

### 3.3. Results

XRD traces for the samples are displayed in Figures 1-5 and the results of peak area measurements and estimated clay mineral proportions are summarised in Table 2. Kaolin group minerals were the only clays detected in the gouge of four samples, while the fifth (BS12/B1/B) contained up to 10% of a 10 $\text{\AA}$  phase which is probably a clay mica.

**Table 2. Estimated proportions of clay minerals in the sample fine-fractions from XRD analyses**

Sample No.	% Kaolinite	% Halloysite	% 'Mica'
BS5/A5/D	50	50	0
BS7/A7/C	57	43	0
BS8/A8/B	19	81	0
BS12/B1/A	27	73	0
BS12/B1/B	8	82	10

Considerable differences were found in the proportions of the kaolin group minerals kaolinite and halloysite. The highest proportions of halloysite were found in the samples BS8/A8/B, BS12/B1/A and BS12/B1/B, where it forms 73-83% of the kaolin minerals. These samples

have a significant component of slip clay fragments in the clay matrix (see below). Kaolinite forms the dominant proportion (50-57%) of samples where kaolinite books are a conspicuous component of the clay matrix.

XRD traces of the ferromanganese minerals that are found in compound clay fragments shows that they are essentially amorphous.

#### **4. MICROTTEXTURAL ANALYSIS**

##### **4.1. Sample preparation**

Samples were examined by optical petrographic and scanning electron microscope techniques, using a Cambridge Instruments Stereoscan 250 in both scanning (SEM) and backscattered electron imaging (BSEI) modes. Blocks of clay cut for thin sections were resin-impregnated over a period of 1–2 weeks. This minimized the shrinkage and disturbance of microtextures in the semi-plastic clay and provided a cohesive solid for the thin sections. Blue dye was added to the resin to aid the identification of microfractures, some of which were generated by clay shrinkage during thin section preparation. Stub-mounted samples imaged in the scanning mode were prepared by freeze drying the blocks of clay.

##### **4.2. Microtextural descriptions**

###### **4.2.1. Sample BS5/A5/D**

The sample consists of a kaolinised volcanoclastic protolith cut by a planar fracture with associated deformation of the clay matrix (Plate 1A). Strained and fractured volcanic quartz grains, up to 3 mm across, constitute approximately 15% of the sample. A few polycrystalline quartz grains are also present, and may represent polygonized volcanic grains. Alkali feldspar grains (< 2mm) are heavily altered to kaolin minerals. Igneous rock fragments form approximately 10% of the sample, and include devitrified glassy lava and aggregates of biotite flakes replacing igneous grains (Plate 1B). Primary biotite is invariably altered to chlorite and/or vermiculite, and commonly consists of kinked and bent crystals in the clay matrix. The clay matrix, forming up to 55% of the sample, largely consists of kaolinite and halloysite in essentially random intergrowths. Kaolinite commonly forms books, i.e. tabular



crystals (flakes) stacked on 00l, up to 1.0 mm thick, and in places these have also been deformed (Plate 1C). Deformation of the books has resulted in the bending and fracturing of the planar kaolinite crystals which are replaced by anastomosing intergrowths of a fibrous mineral, possibly halloysite, and granular ferromanganese minerals (Plate 2A). Ferromanganese minerals also occur as clasts and as a replacement of the clay matrix.

#### 4.2.2. Sample BS7/A7/C

A kaolinized volcanoclastic rock containing portions of a slip clay and associated clay gouge. Volcanic quartz grains (<4.0 mm) constitute approximately 25% of the sample, and are commonly fractured and polygonised, and a few have developed a mortar texture of finely comminuted grains between larger grains (Plate 2B). Much of the fine-grained quartz (<0.1 mm) in the matrix appears to have developed by comminution of larger grains. Heavily kaolinised alkali feldspar grains (<3.0 mm) and a few lava fragments together account for 6% of the sample. The clay matrix, forming over 60% of the sample, consists of mostly random intergrowths of kaolinite and halloysite. Kaolinite 'books' are typically equant and up to 1.0 mm thick, but deformed books are also found showing sinuous shapes (Plate 3A). Deformed kaolinite plates are replaced by anastomosing intergrowths of a fibrous mineral which is possibly halloysite (Plate 3B). Many of the kaolin-rich areas in the clay matrix appear to be disrupted or deformed veins (Plate 2C), typically consisting of a kaolin fill with wall linings of ferromanganese minerals.

#### 4.2.3. Sample BS8/A8/B.

The sample is a kaolinized volcanoclastic rock. The clay matrix contains clasts derived from the volcanic protolith and compound clay fragments with contorted fabrics (Plate 3C). Quartz grains (<4.5 mm) form approximately 10% of the sample; they are fractured and strained volcanic phenocrysts typically showing clay-filled cracks (Plate 4A). Highly altered alkali feldspar grains and a few lava fragments from the protolith together form up to 7% of the sample. Elongated fragments of slip clay, up to 3 mm long, constitute approximately 25% of the sample. Typically, these fragments consist of thin domains (10-100  $\mu$ m) of orientated kaolin minerals, interleaved with thin, discontinuous laminae of Mn- oxides (Plate 4B). Some slip clay fragments are bent and disrupted, indicating deformation when they were detached from a slip plane (Plate 3C). Some are compound fragments containing both deformed laminae of oriented kaolin with Mn- oxides, and undeformed laminae of these two

components (Plate 4B). The structure of these compound fragments suggest that the movement responsible of the formation of orientated domains in the slip clay was followed by a static interval when fluids percolated along the slip plane and precipitated thin laminae and clusters of Fe-oxyhydroxides and Mn-oxides (Plate 3D). Thin veins (<0.5 mm) with Mn-oxide fills also cut the sample and commonly give rise to brown or yellow staining in the adjacent clay. In detail the Mn-oxides show patterns of concentric growth with thin platy crystals generally showing a radial arrangement (Plates 3E and 3F). Modification of the orientated kaolin clay (kaolinite?) forming slip clay fragments also appears to have taken place during a static interval, resulting in random fibrous overgrowths on the orientated domains (Plate 6A). These may represent halloysite formed by hydration of kaolinite in response to fluid percolation along a slip plane. Similar fibrous overgrowths are well developed on kaolin books in the matrix of the sample (Plate 6B). In detail some end sections of these fibres appear to be curved (Plate 6C), suggesting that they represent the rolled or tubular morphologies of halloysite, possibly modified by collapse in the SEM vacuum.

The compound fragment shown in Plate 4B preserves evidence that it was generated by three movements on a slip plane. Firstly, formation of an orientated clay by slip plane movement was followed by a static interval when percolating fluids deposited Mn-oxide laminae within the orientated clay. Secondly, renewed movement on the slip plane resulted in detachment and deformation of slivers of the first slip clay with associated Mn-oxide laminae and incorporation into a clay gouge. A new slip clay, Mn-stained but undeformed, was formed adjacent to the sliver of earlier slip clay. Finally, a third movement detached the compound fragment from the slip plane and it was subsequently incorporated into sample BS8/A8/B.

#### 4.2.4. Sample BS12/B1/A.

The thin section contains part of a clay gouge associated with two or more early slip planes developed in a highly altered volcanoclastic protolith. Tension fractures developed in the protolith are enhanced by staining from ferromanganese minerals (Plate 4C). Strained and fractured quartz grains (<5.0 mm) are the largest relicts of the protolith and form up to 10% of the sample (Plate 5A). A few relict grains of alkali feldspar and lava are also preserved but are highly kaolinized. Clay minerals account for approximately 80% of the sample, and mostly form random intergrowths of kaolin books with overgrowths of fibrous halloysite (Plate 6D). Orientated clay microfabrics are found in the slip clays developed along the slip planes and are associated with impersistent laminae of ferromanganese minerals; brown



(green with dye) staining of the clay associated with the ferromanganese minerals tends to enhance the slip plane structures (Plate 5B). A zone of ferromanganese precipitation and staining, 5-8 mm wide, is developed approximately parallel with the main slip plane, and appears to be controlled by tension gashes which have formed normal to the plane (Plate 5C).

Within the gouge, slip clay fragments consisting of kaolin and ferromanganese laminae have been deformed and disrupted (Plate 6E). Some are compound fragments showing internal deformation of the slip clay and associated Mn-oxide (Plate 6F). Fe-oxyhydroxides are also found in the fragments, in clusters of radiating platy crystals (Plate 9A). Granules of a Ce-rich mineral (?carbonate) are associated with some Fe-oxyhydroxide clusters (Plate 9B). The appearance and structure of the clay fragments in the gouge suggest that they are pre-existing slip clays or tension gash fills which were detached and deformed by earlier movements on a slip plane.

#### 4.2.5. Sample BS12/B1/B.

The thin section is a slice through an early slip plane developed in a highly altered volcanoclastic protolith. It contains a clay gouge, 1.5-3.0 mm wide, bounded by slip planes and shows tension gashes developed normal to the slip planes in the enclosing protolith (Plate 7A). The best preserved portion of the protolith consists of large (<8 mm) polygonised quartz grains, many of them fractured and strained, forming approximately 25% of the sample. In the same portion of the sample, a series of tension gashes 0.03-1.0 mm wide, are developed normal to the slip plane. These are quartz-filled but also contain linings and thin lamellae of Fe-oxyhydroxide and Mn-oxide. Quartz-filled veins have also formed along the slip plane (Plate 7B). A zone of brown-stained protolith up to 5 mm wide is developed some 5-6 mm away from the slip plane, and contains tension gashes with a high proportion of Mn-oxide fills.

The clay gouge largely consists of contorted slivers of slip clay, typically comprising domains of well orientated kaolinite (and halloysite) up to 0.15 mm wide, alternating with less well orientated clay lamellae and interleaved discontinuous lamellae of Fe-oxyhydroxide and Mn-oxide (Plate 8A). In detail, the slip clay shows well orientated domains alternating with more random clay fabrics (Plate 8B). This may reflect the partitioning of strain into discrete microdomains of sheared clay, or the selective hydration of orientated kaolinitic clay to form halloysite as a result of water percolation during a static interval. Precipitation of Mn-oxide

appears to be associated with fluid percolation along the static slip plane, and it commonly forms concentric clusters of radial platy crystals (Plate 9C) or subradiating clusters within the slip clays. Some Fe-oxyhydroxide shows pronounced concentric growth patterns (Plate 9D). The clay matrix in the gouge usually shows a random fabric of kaolin books (Plate 9E) which are notably less common than in the samples described above. Many of the books are heavily overgrown and replaced by halloysite (Plate 9F).

## 5. DISCUSSION

XRD analysis indicates that both kaolinite and halloysite are present in the clay-rich saprolite hosting the landslide at Lai Ping Road, with halloysite ranging from 50 to 82% of the clay mineral content. Samples with higher proportions of kaolinite (50-57%) appear to contain better developed books of kaolin crystals, a morphology usually associated with kaolinite. However, where these books have been deformed the planar kaolinite crystals have been overgrown by anastomosing intergrowths of a fibrous mineral, which is probably halloysite (Plates 2A and 3B). Halloysite is more abundant in samples containing clay gouge material, which was probably formed by movements predating the July 1997 landslide. Fragments of pre-formed slip clay are a significant component of these clay gouges. Within these fragments there is evidence that the well-orientated kaolinite domains in the slip clay have been overgrown by halloysite fibres (Plate 6A). Elsewhere, undeformed kaolinite books are also replaced by the same clay fibres (Plates 6B, 9E), which in detail show the curved and rolled morphologies typical of halloysite (Plates 6C, 9F). Similar overgrowths have been observed in the Fei Tsui Road landslip (Merriman *et al.*, 1996), and they resemble the halloysite fibres imaged by Singh & Gilkes (1992).

Microtextural evidence within the portions of clay gouge preserved in the samples from Lai Ping Road landslip suggests that a sequence of movements has occurred, with each movement contributing material detached from both the protolith and pre-formed slip clays. However, the ages of these movements and their relationship to the recent phase of landslide at Lai Ping Road are both uncertain. Static or inactive intervals also contributed to the mineralogy of the gouge and slip clays in the form of Fe-oxyhydroxide and Mn-oxide minerals which appear to have been precipitated by fluid movement along the slip plane. These ferromanganese minerals usually form discontinuous laminae within the slip clay and in detail appear to represent cycles of precipitation and mineral growth from fluid flow punctuated by limited growth and fluid starvation, so giving rise to concentric growth patterns (Plates 3E, 9A, 9C,



9D). The extent to which the growth of the ferromanganese minerals is controlled by seasonal fluid movement is unknown.

Fluid movement along the slip plane may also be responsible for the hydration and replacement of kaolinite by halloysite. This suggests that the generation of halloysite is not directly caused by slip movement, but may be the post-slip response of strained kaolinite crystals to slip plane relaxation accompanied by fluid movement.

Microtextures preserved in the compound slip clay fragment shown in Plate 4B appear to be the result of three movements along an ancient slip plane system at Lai Ping Road. The initial movement which formed the orientated slip clay was followed by a static interval when Mn-oxide laminae were deposited within the slip clay. Renewed movement deformed the earlier slip clay and its associated Mn-oxide laminae as the fragment was detached and incorporated into a clay gouge. A new slip clay, Mn-stained but undeformed, was formed alongside the deformed slip clay. A third movement detached the compound fragment from the slip plane into the gouge. Given the position of the samples, above the surface of rupture of the 1997 landslide, these phases of movement are most likely to be associated with earlier slope failures at Lai Ping Road. If these are associated with the movements of 1978-79 and 1982-89, then they are too recent to be dated by radiocarbon or K-Ar/Ar-Ar methods. However, some of the other direct and indirect landslide dating methods reviewed by Gillespie (1998) may be applicable.

## **6. CONCLUSIONS**

1. Halloysite occurs in all the samples investigated from the Lai Ping Road landslide, ranging from 50 to 82% of the clay mineral assemblages.
2. Halloysite appears to form by alteration of kaolinite, replacing both the crystals in kaolinite books and orientated kaolinite formed in typical slip clays.
3. The generation of halloysite is not directly caused by slip movement, but may represent post-slip replacement of strained kaolinite crystals associated with fluid movement along slip planes.
4. Fluid movement during static intervals is responsible for the precipitation of ferromanganese minerals along slip planes.
5. Ferromanganese minerals show concentric growth patterns which may reflect seasonal fluid movement along ancient slip planes.
6. Microtextures in compound fragments found in clay gouges suggest that at least three earlier phases of movement have occurred at Lai Ping Road.

## 7. REFERENCES

CHURCHMAN, G.J., WHITTON, J.S., CLARIDGE, G.G.C. & THENG, B.K.G. 1984. Intercalation method using formamide for differentiating halloysite from kaolinite. *Clays and Clay Minerals*, **32**, 241-248.

GILLESPIE, M.R. 1998. A literature review: methods for dating landslides. *British Geological Survey Technical Report WG/98/35C*.

MERRIMAN, R.J. & KEMP, S.J. 1995. Mineralogical and microtextural analysis of altered tuffs associated with landslips in Hong Kong. *British Geological Survey Technical Report WG/95/30C*.

MERRIMAN, R.J., KEMP, S.J. & HARDS, V.L. 1996. Halloysite and kaolinite in altered tuffs hosting landslips, Hong Kong. *British Geological Survey Technical Report WG/96/47C*

SINGH, B. & GILKES, R.J. 1992. An electron optical investigation of the alteration of kaolinite to halloysite. *Clays & Clay Minerals*, **40**, 212-229.



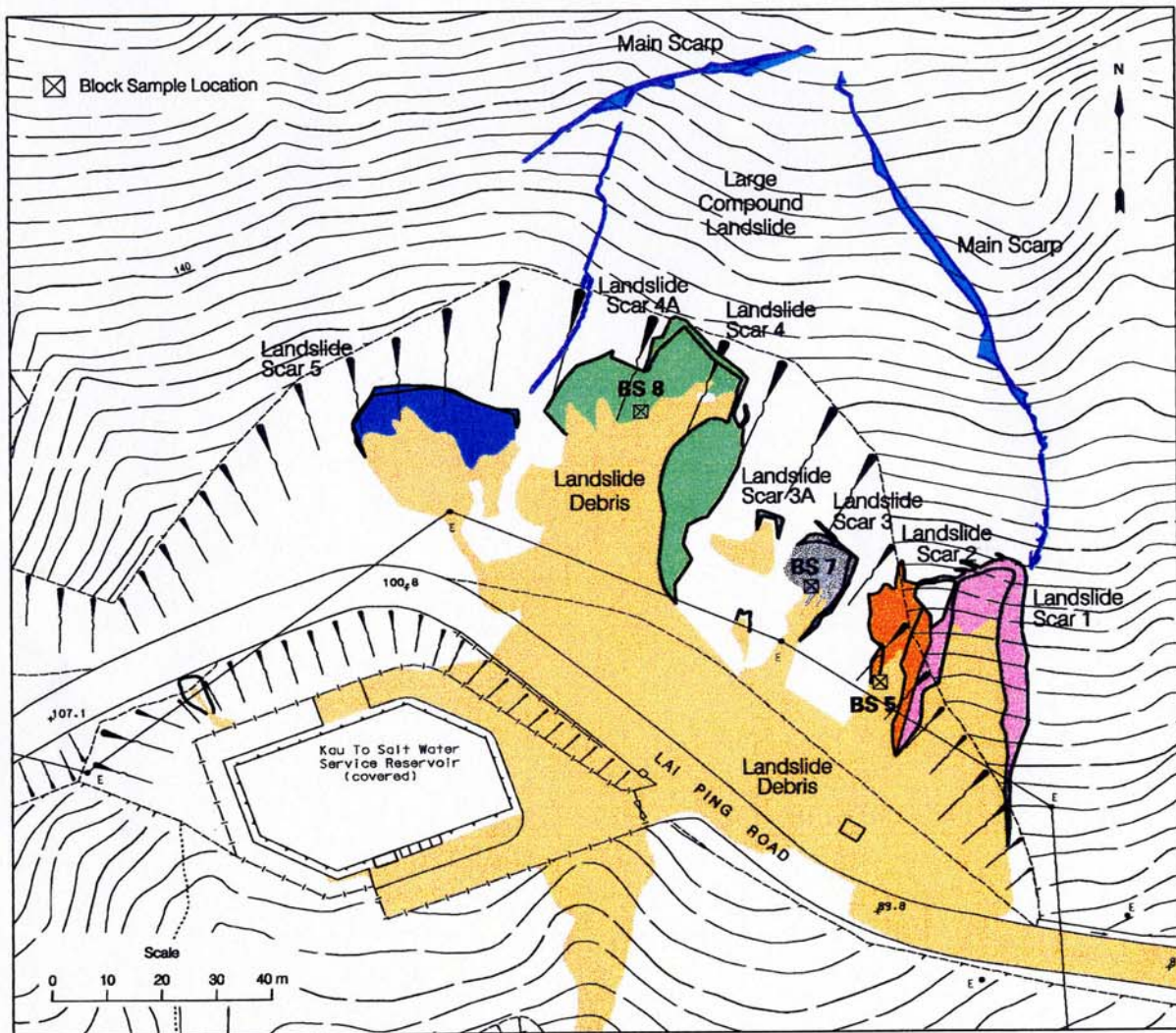


Figure 1. Site plan showing the landslide scars at Lai Ping Road and the location of samples studied for this report.



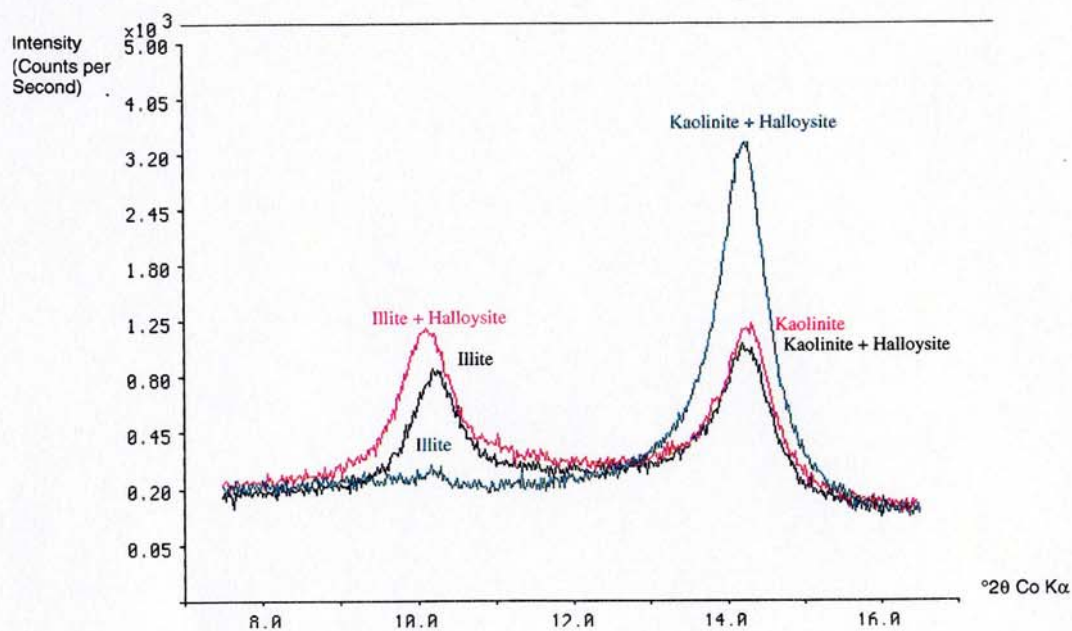


Figure 2. XRD traces illustrating the effects of formamide intercalation on sample BS5/A5/D (black trace = wet run, red trace = formamide intercalation, green trace = heated at 110 °C/90 minutes)

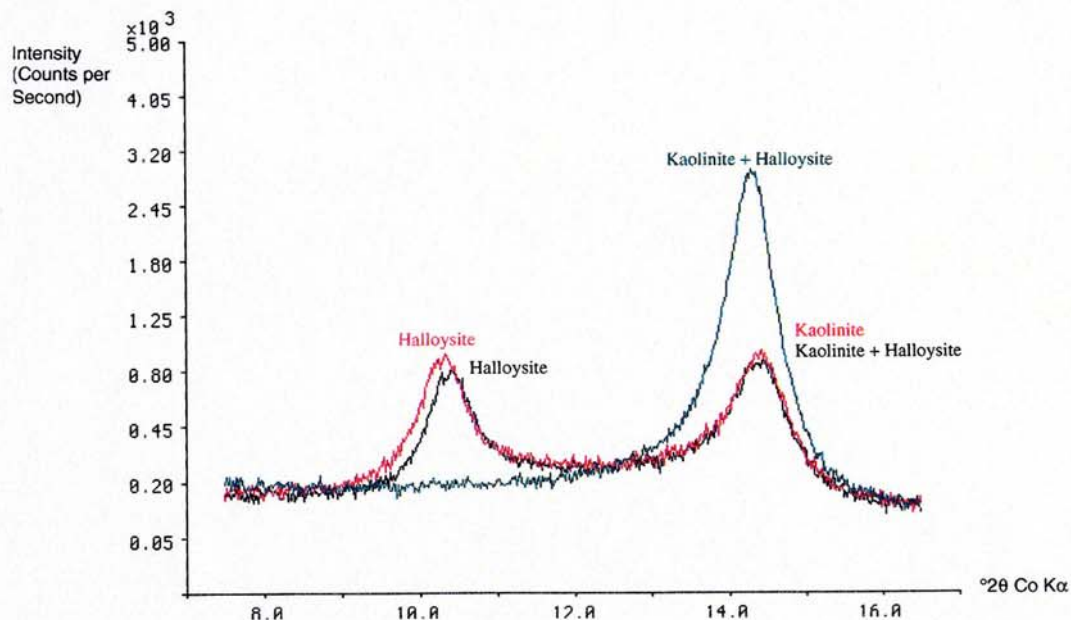


Figure 3. XRD traces illustrating the effects of formamide intercalation on sample BS7/A7/C (black trace = wet run, red trace = formamide intercalation, green trace = heated at 110 °C/90 minutes)

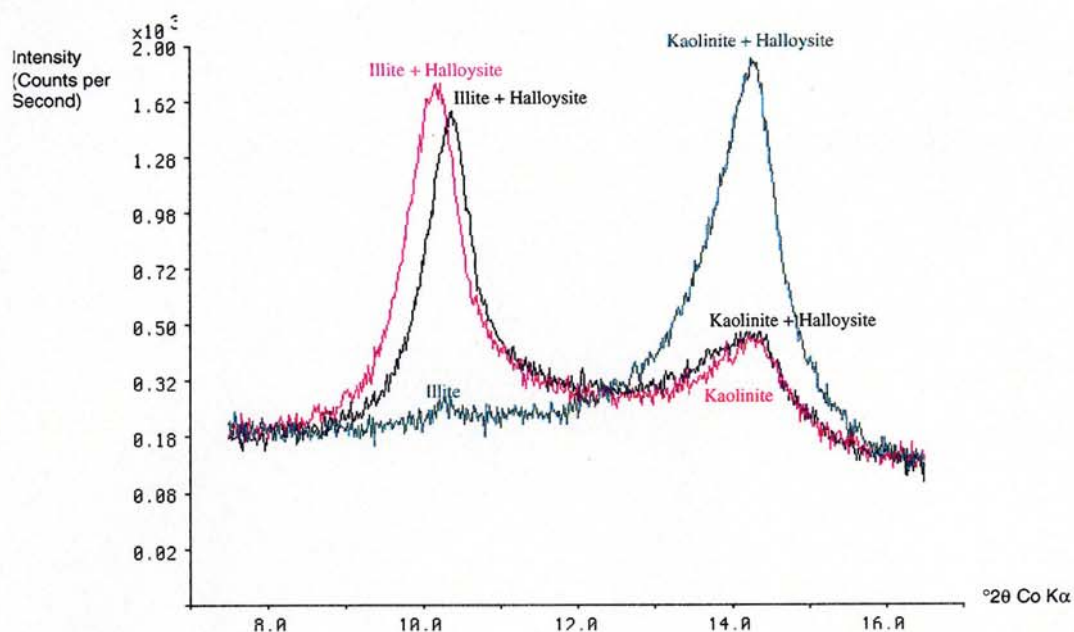


Figure 4. XRD traces illustrating the effects of formamide intercalation on sample BS8/A8/B (black trace = wet run, red trace = formamide intercalation, green trace = heated at 110 °C/90 minutes)

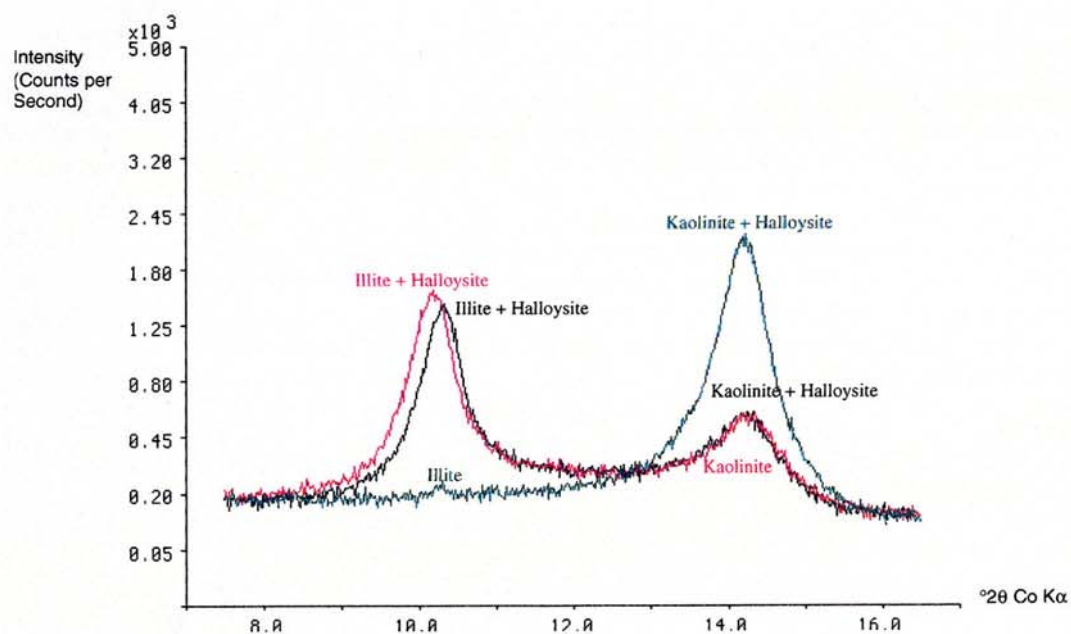


Figure 5. XRD traces illustrating the effects of formamide intercalation on sample BS12/B1/A (black trace = wet run, red trace = formamide intercalation, green trace = heated at 110 °C/90 minutes)

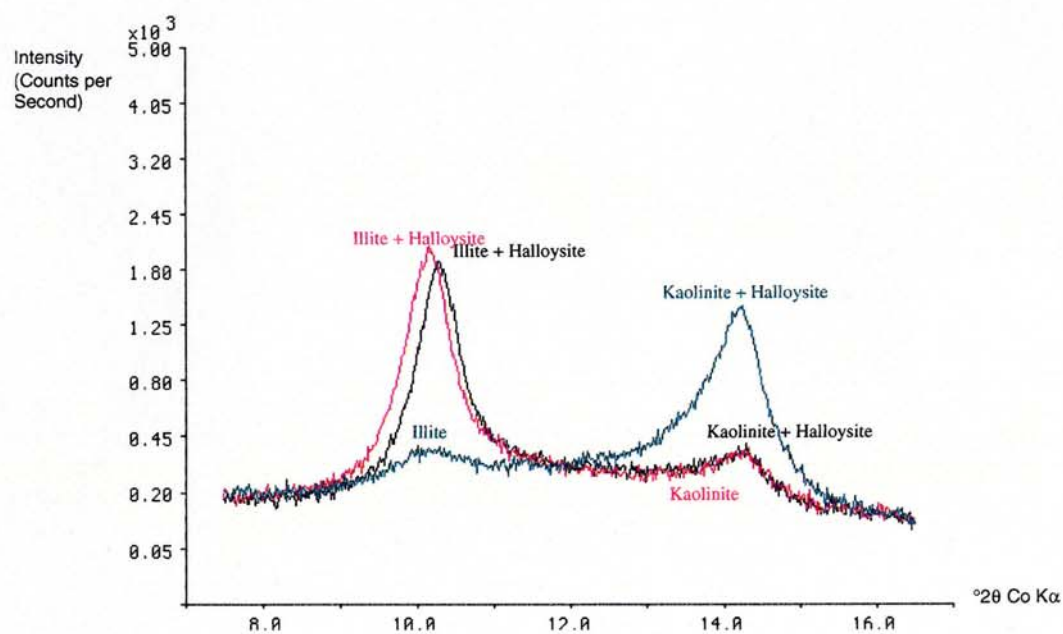
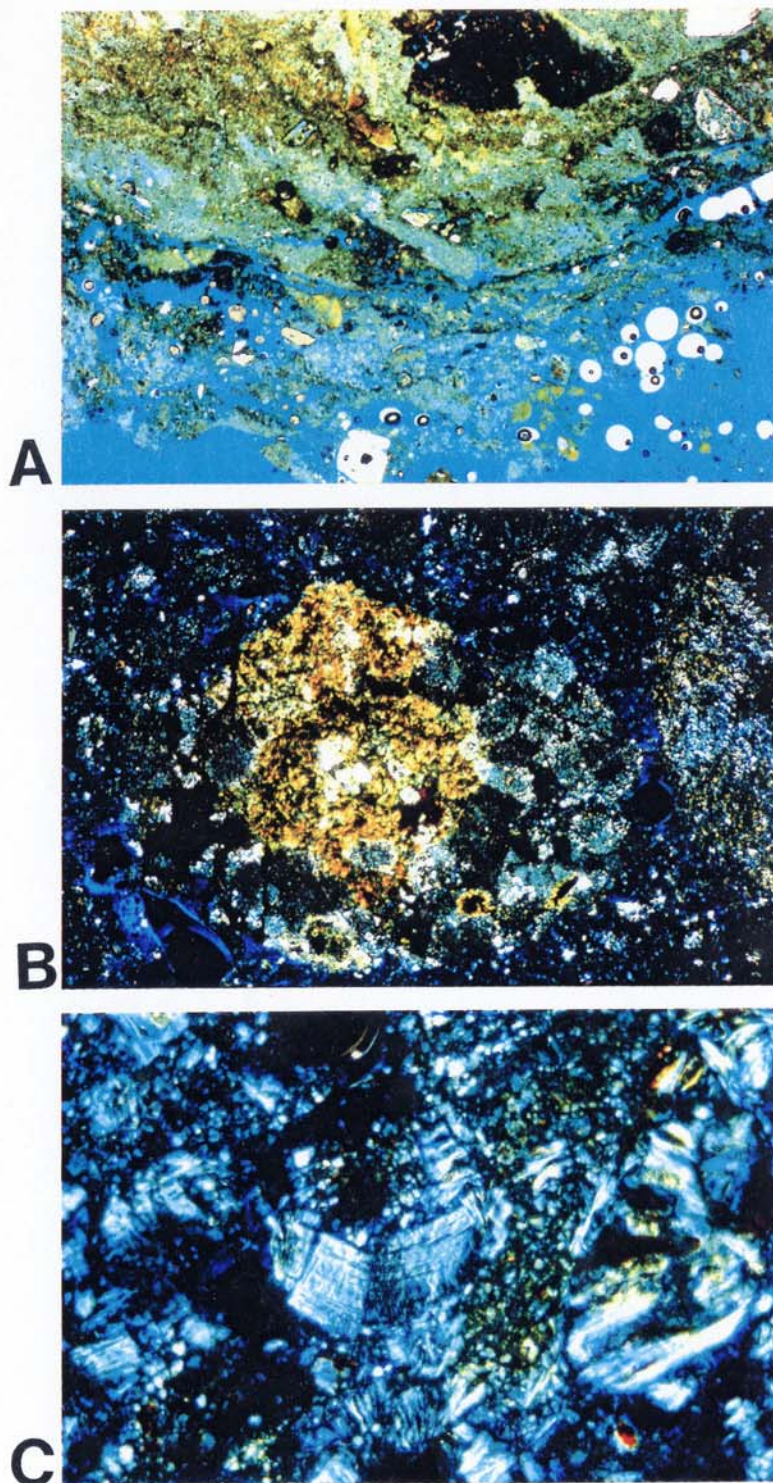


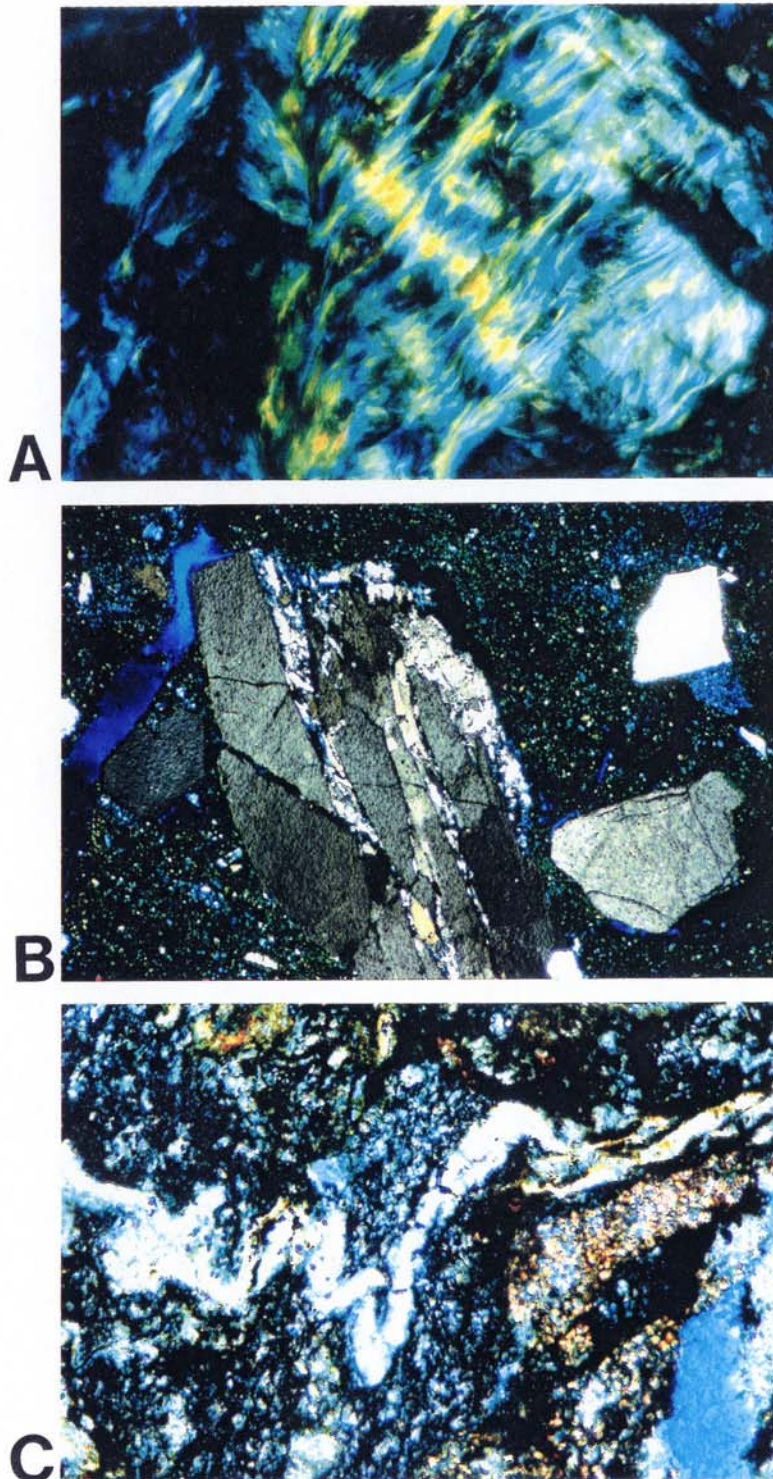
Figure 6. XRD traces illustrating the effects of formamide intercalation on sample BS12/B1/B (black trace = wet run, red trace = formamide intercalation, green trace = heated at 110 °C/90 minutes)





1A. Sample BS5/A5/D. Lai Ping Road landslide. Optical photomicrograph of clay-rich saprolite with dark-brown fragments of ferromanganese minerals. The clay is impregnated with blue-stained resin (plane-polarized light; field width 9 mm).  
1B. Sample BS5/A5/D. Lai Ping Road landslide. Optical photomicrograph of igneous grain partially replaced by intergrowths of yellow-brown biotite (cross-polarized light; field width 4.5 mm).  
1C. Sample BS5/A5/D. Lai Ping Road landslide. Optical photomicrograph of deformed kaolinite 'books' in the clay matrix. (cross-polarized light; field width 1.1 mm).



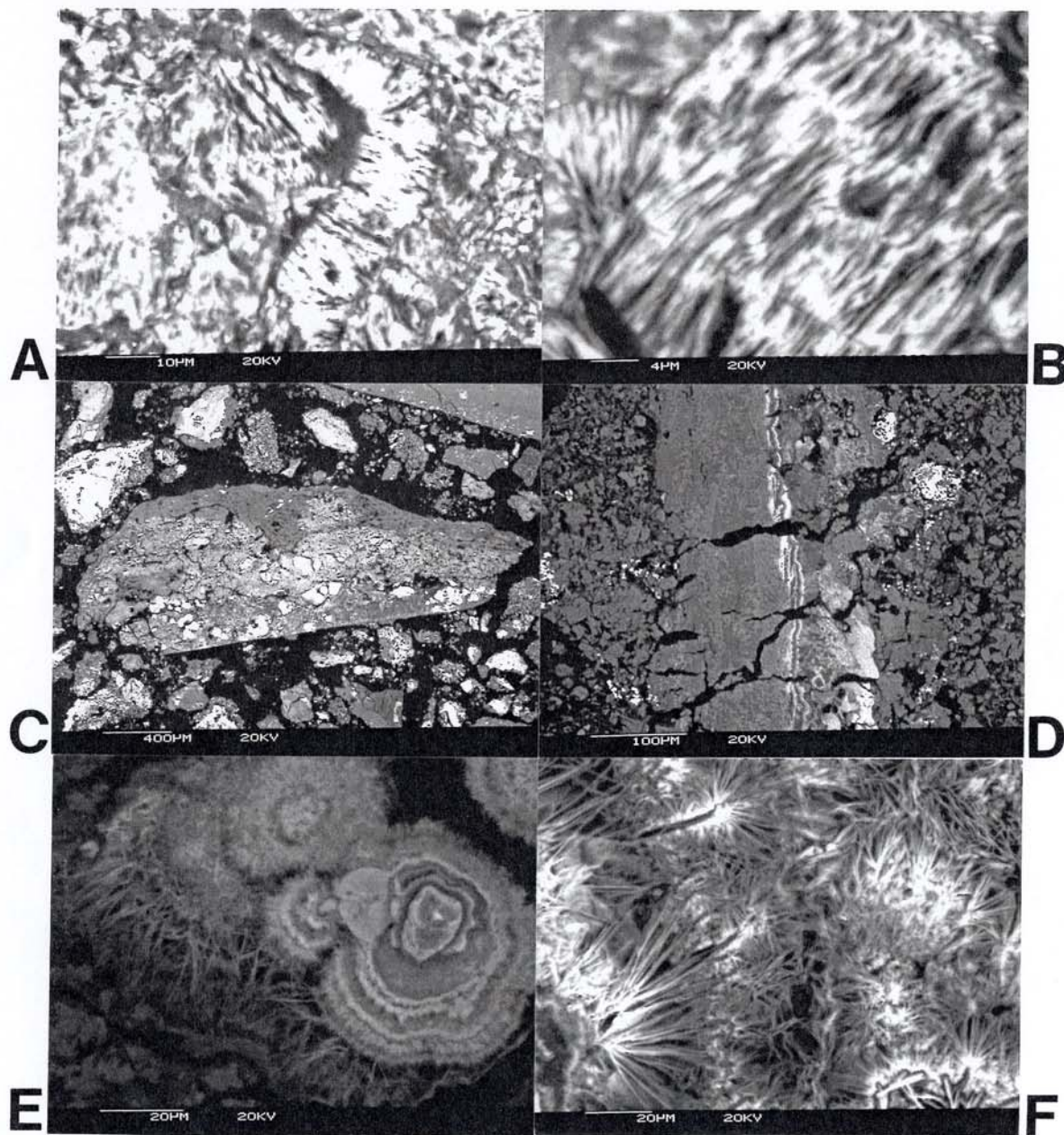


2A. Sample BS5/A5/D. Lai Ping Road landslide. Optical photomicrograph showing replacement of planar kaolinite crystals in a book by fibrous ?halloysite. Clay minerals are stained yellow by ferromanganese mineral (cross-polarized light; field width 0.45 mm).

2B. Sample BS7/A7/C. Lai Ping Road landslide. Optical photomicrograph of deformed quartz grain showing mortar texture (cross-polarized light; field width 4.5 mm).

2C. Sample BS7/A7/C. Lai Ping Road landslide. Optical photomicrograph of deformed kaolin-filled vein (cross-polarized light; field width 1.1 mm).





3A. Sample BS7/A7/C. Lai Ping Road landslide. Backscattered secondary electron photomicrograph of deformed kaolinite book in the clay matrix.

3B. Sample BS7/A7/C. Lai Ping Road landslide. Backscattered secondary electron photomicrograph of deformed book-like kaolinite plates partially replaced by fibrous ?halloysite.

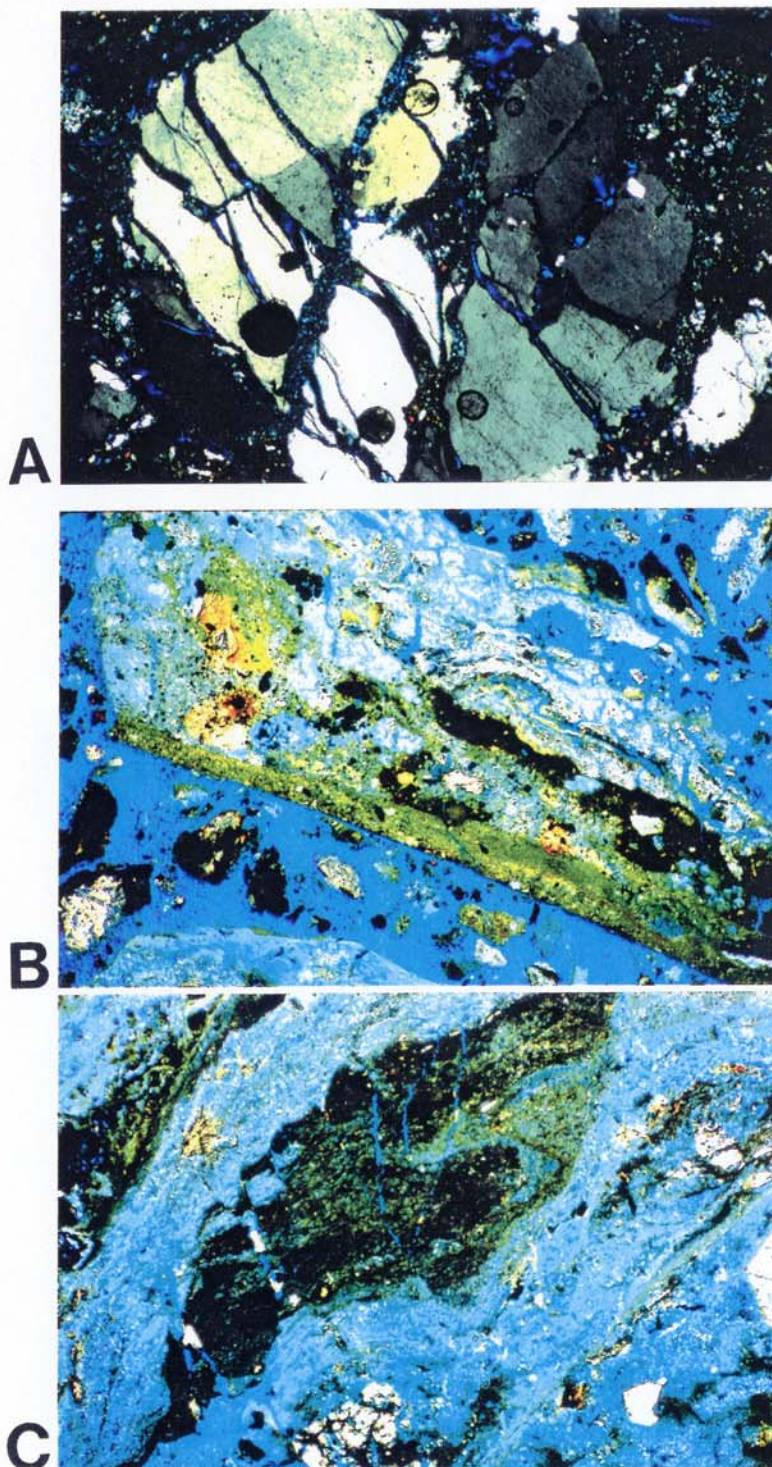
3C. Sample BS8/A8/B. Lai Ping Road landslide. Backscattered secondary electron photomicrograph of slip clay fragment. Dark-grey kaolin-rich clay is highly contorted; associated ferromanganese minerals are bright grey or white.

3D. Sample BS8/A8/B. Lai Ping Road landslide. Backscattered secondary electron photomicrograph of slip clay fragment. Dark-grey kaolin-rich clay generated by slip contains white laminae of Mn-oxide precipitated by fluid movement on a slip plane. The clay matrix consists of numerous kaolinite books.

3E. Sample BS8/A8/B. Lai Ping Road landslide. Backscattered secondary electron photomicrograph of Mn-oxide showing concentric growth of thin platy crystals.

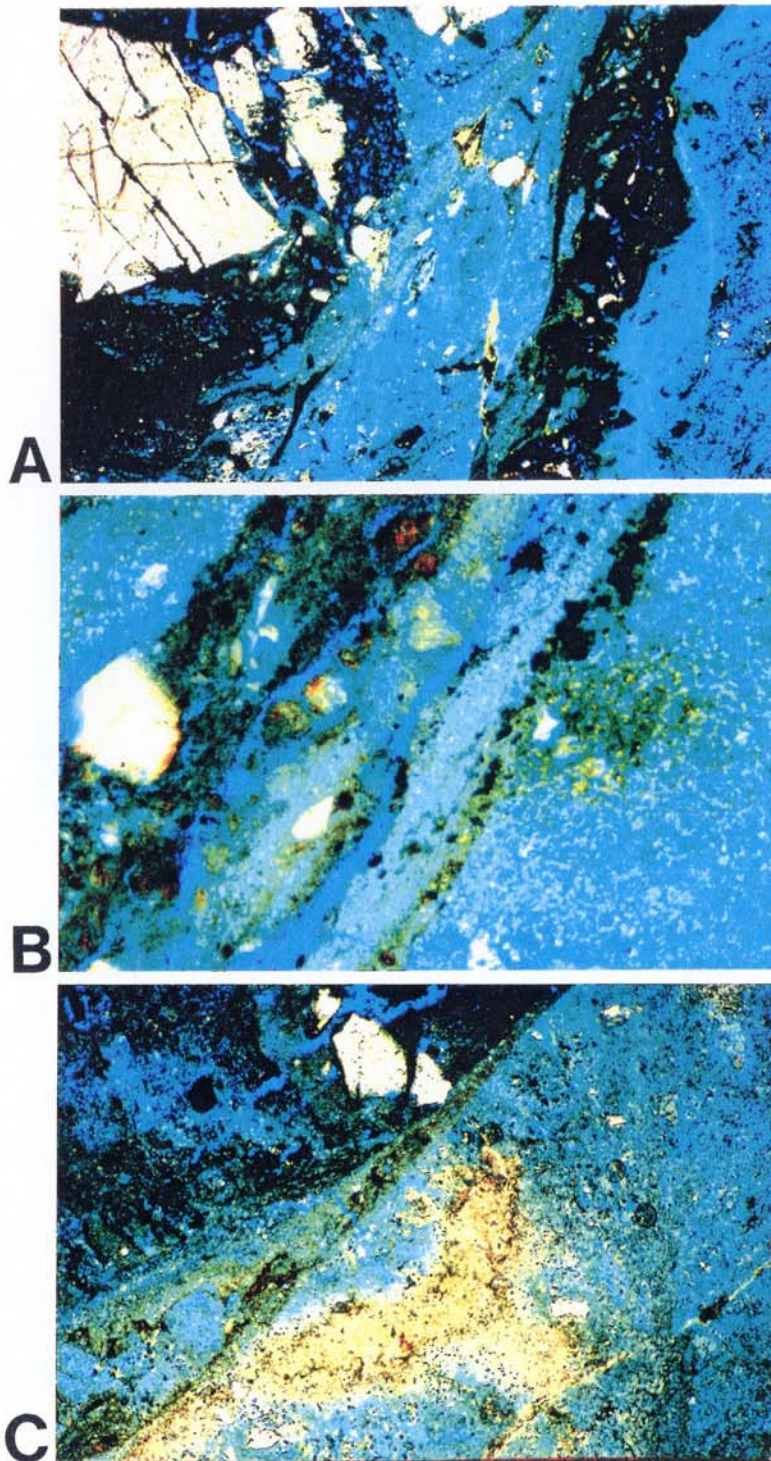
3F. Sample BS8/A8/B. Lai Ping Road landslide. Backscattered secondary electron photomicrograph of Mn-oxide showing radial clusters of thin platy crystals.





- 4A. Sample BS8/A8/B. Lai Ping Road landslide. Optical photomicrograph of highly fractured quartz phenocryst with blue-stained clay filling cracks (cross-polarized light; field width 4.5 mm).
- 4B. Sample BS8/A8/B. Lai Ping Road landslide. Optical photomicrograph of a compound slip clay fragment in the clay matrix. The folded bluish-white kaolin with associated dark-brown Mn-oxide is an early slip clay; the green-stained kaolin is a later slip clay. Resin is deep blue (plane-polarized light; field width 4.5 mm).
- 4C. Sample BS12/B1/A. Lai Ping Road landslide. Optical photomicrograph of an early clay gouge with associated slip planes. Slip clays form green-stained diagonal lines bottom right and top left. Dark-brown ferromanganese minerals stain a detached and disrupted slip clay fragment in the gouge (centre). Thin tensional veins cut the fragment and quartz grains (plane-polarized light; field width 9 mm).



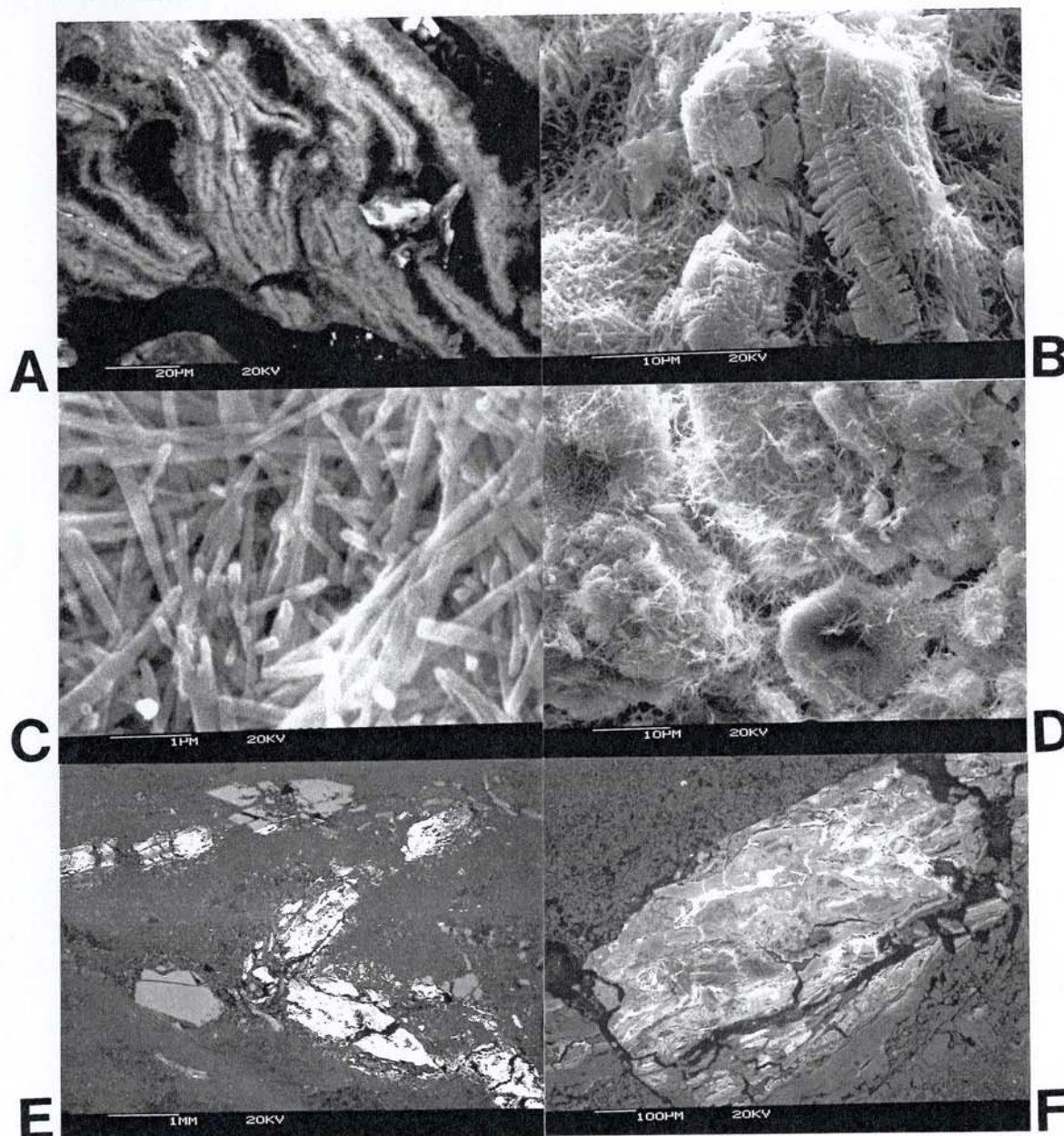


5A. Sample BS12/B1/A. Lai Ping Road landslide. Optical photomicrograph of a fractured quartz grain in a clay gouge. Dark-brown ferromanganese minerals with thin green-stained clays attached are slip clay fragments. Blue-stained kaolin forms the matrix of the gouge. (plane-polarized light; field width 9 mm).

5B. Sample BS12/B1/A. Lai Ping Road landslide. Optical photomicrograph of a slip plane. Slip clays are pale-blue or green-stained in association with dark-brown laminae of ferromanganese minerals. Resin is deep blue. (plane-polarized light; field width 1.1 mm).

5C. Sample BS12/B1/A. Lai Ping Road landslide. Optical photomicrograph of a slip plane. Tensional veins (bottom right) formed normal to the slip plane are filled with ferromanganese minerals (plane-polarized light; field width 4.5 mm).





6A. Sample BS8/A8/B. Lai Ping Road landslide. Backscattered secondary electron photomicrograph of orientated domains of kaolin clay with overgrowths of fibrous halloysite.

6B. Sample BS8/A8/B. Lai Ping Road landslide. Backscattered secondary electron photomicrograph of kaolinite books with overgrowths of fibrous halloysite.

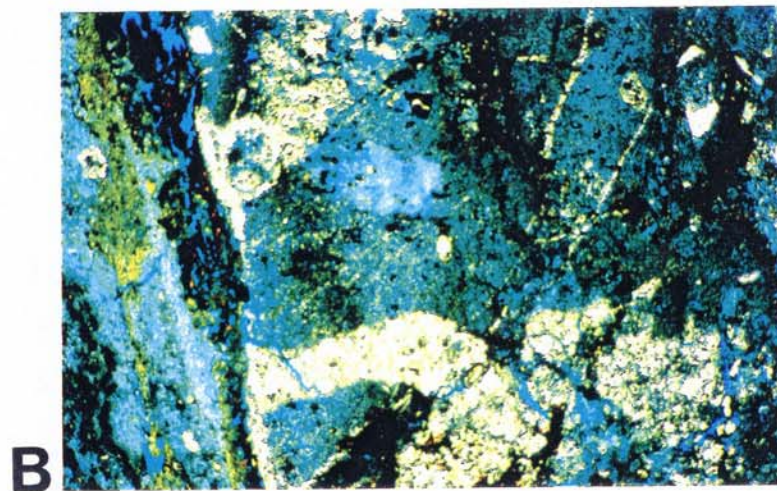
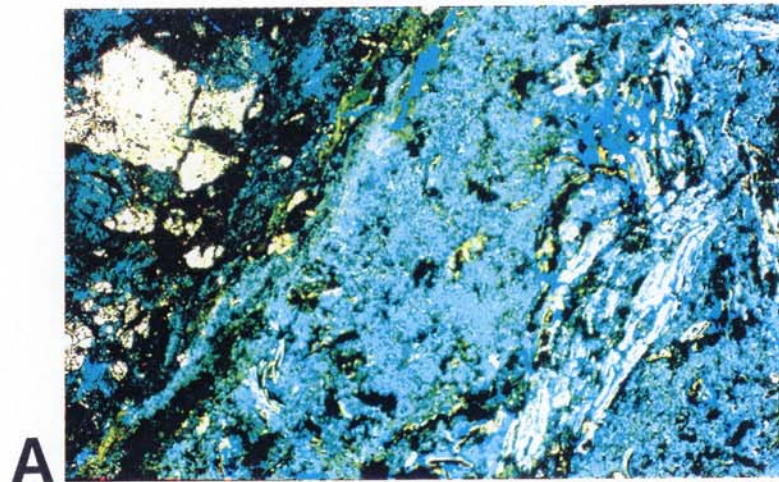
6C. Sample BS8/A8/B. Lai Ping Road landslide. Backscattered secondary electron photomicrograph of the halloysite fibres forming overgrowths on kaolinite. Note the curvature of some end sections of the fibres.

6D. Sample BS12/B1/A. Lai Ping Road landslide. Backscattered secondary electron photomicrograph of kaolinite books with overgrowths of halloysite fibres.

6E. Sample BS12/B1/A. Lai Ping Road landslide. Backscattered secondary electron photomicrograph showing deformed and disrupted ferromanganese laminae (bright grey) and quartz grains (mid-grey).

6F. Sample BS12/B1/A. Lai Ping Road landslide. Backscattered secondary electron photomicrograph of a compound slip clay fragment. Folded and disrupted slip clay comprising mid-grey kaolin and bright grey Mn-oxide formed early. Later slip clay and Mn-oxide is undeformed (bottom right of fragment).

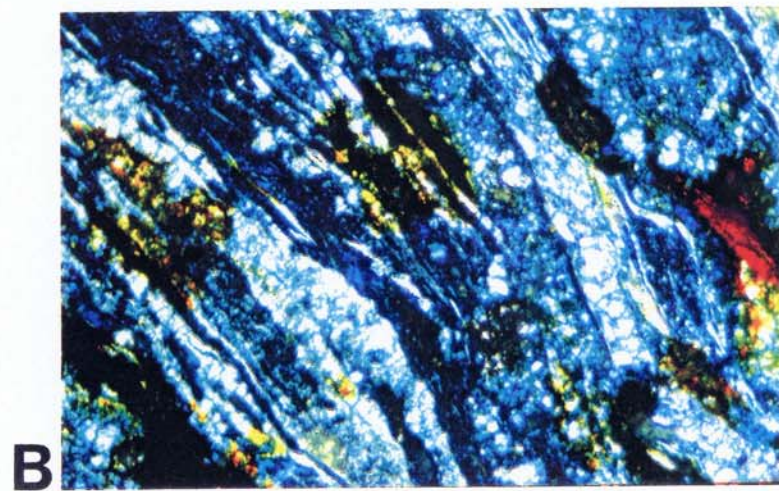
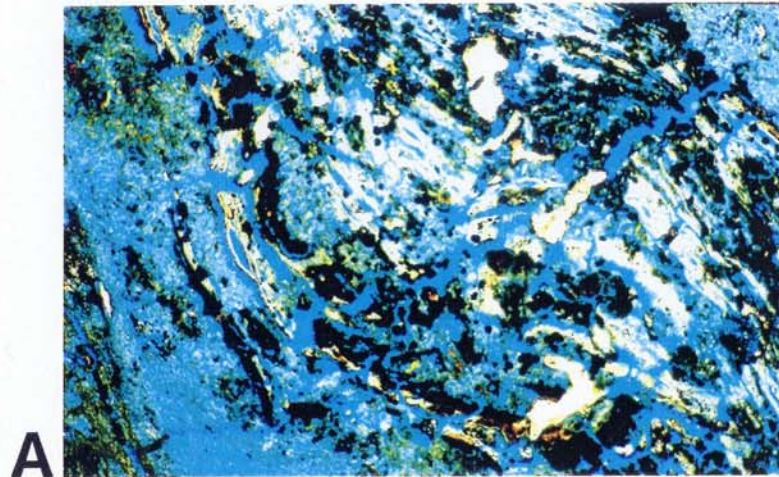




7A. Sample BS12/B1/B. Lai Ping Road landslide. Optical photomicrograph showing a pale blue clay gouge with slip clay fragments. The blue-green clay (top left) forms part of a slip plane against a quartz-rich protolith stained dark-brown by ferromanganese minerals (plane-polarized light; field width 9 mm).

7B. Sample BS12/B1/B. Lai Ping Road landslide. Optical photomicrograph of quartz-filled tensional veins in the protolith, normal to a slip plane (subvertical, left of field). Two quartz-filled veins have also formed along the slip plane together with dark-brown ferromanganese laminae (plane-polarized light; field width 4.5 mm).

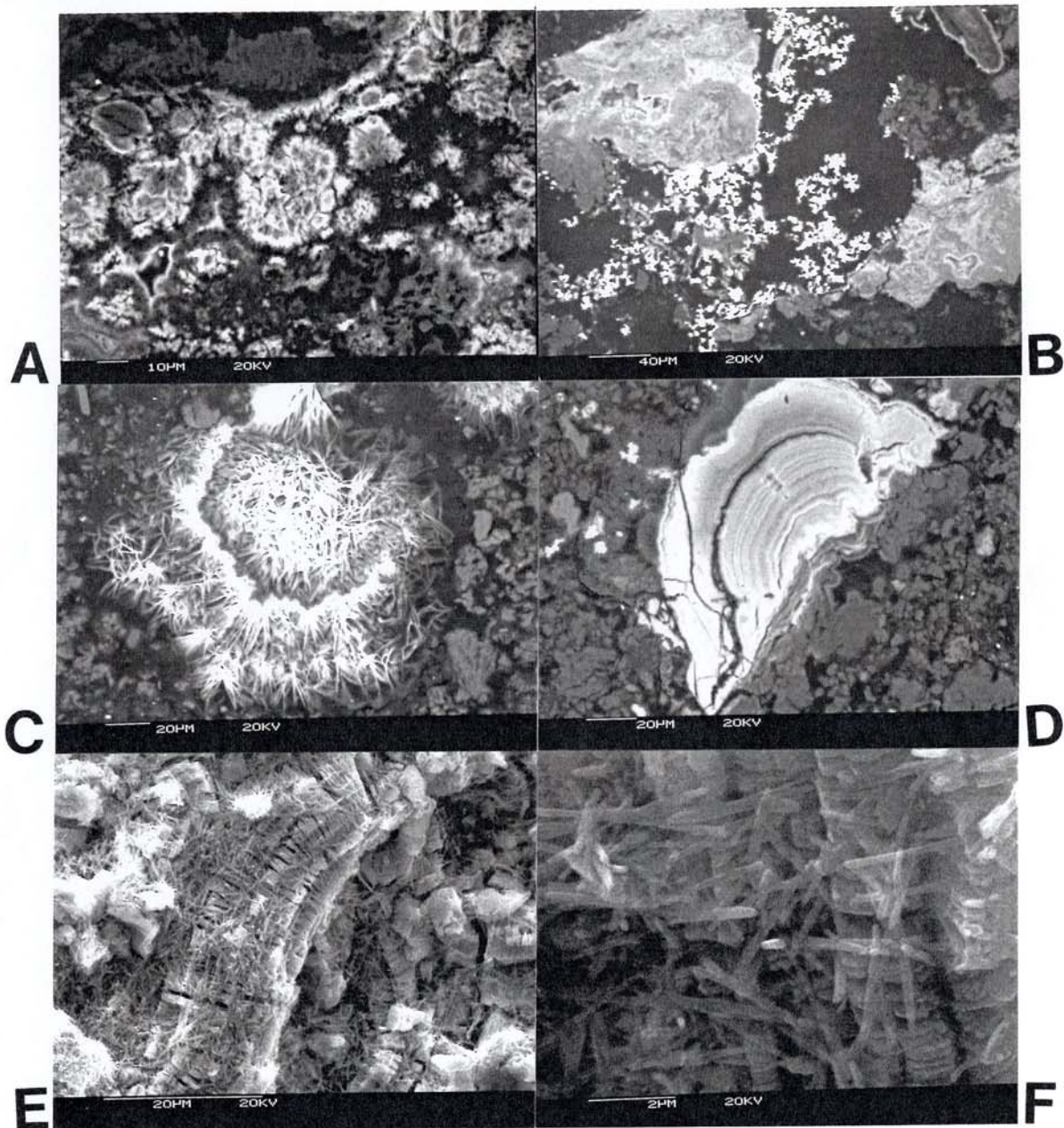




8A. Sample BS12/B1/B. Lai Ping Road landslide. Optical photomicrograph showing contorted slivers of slip clay consisting of whitish or pale-blue orientated domains of kaolin with dark-brown ferromanganese minerals (plane-polarized light; field width 4.5 mm).

8B. Sample BS12/B1/B. Lai Ping Road landslide. Optical photomicrograph of slip clay. Dark blue orientated domains of kaolin minerals alternate with whitish or pale-blue random domains. Brown and yellow staining is from ferromanganese minerals (cross-polarized light; field width 1.1 mm).





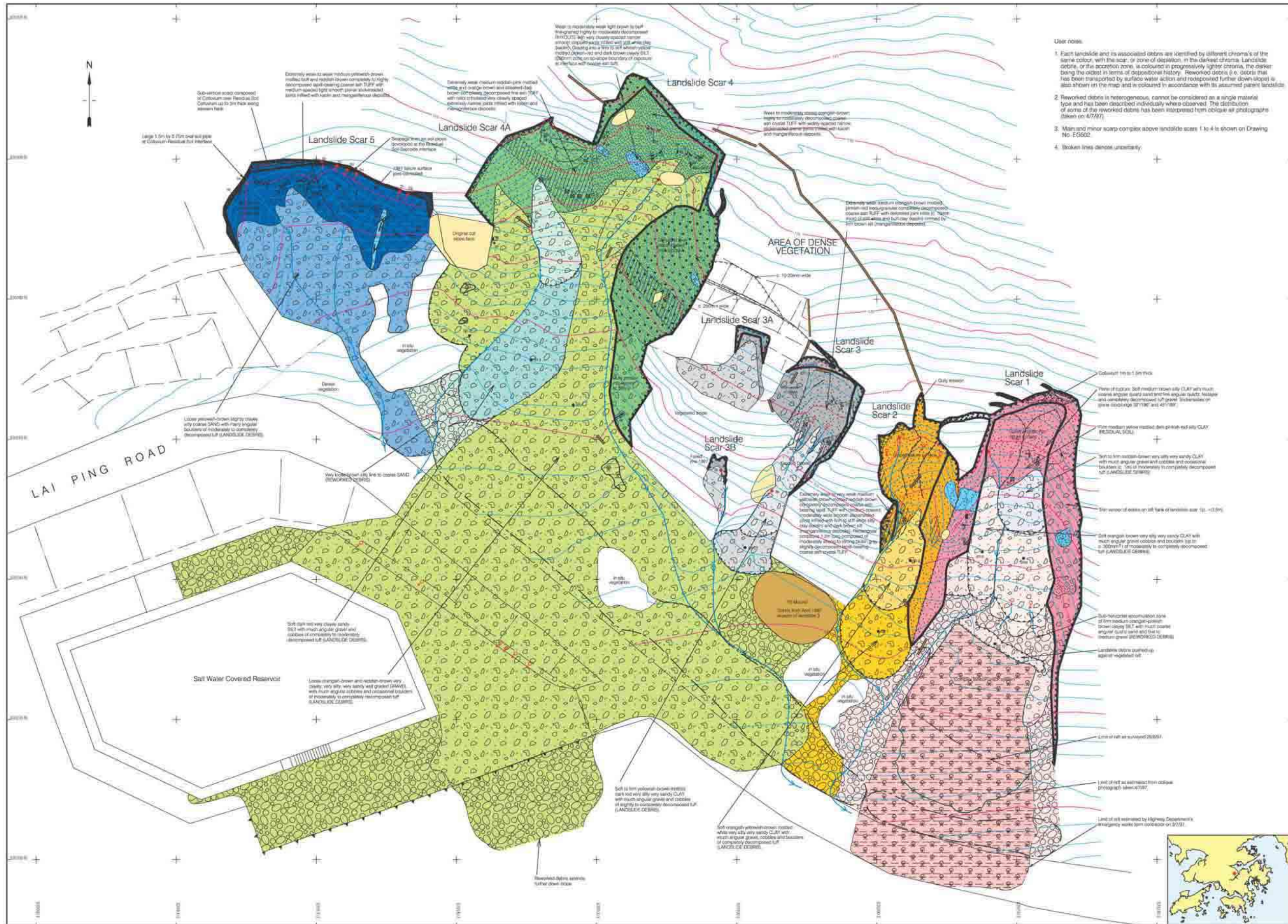
- 9A. Sample BS12/B1/A. Lai Ping Road landslide. Backscattered secondary electron photomicrograph of Fe-oxyhydroxide forming clusters of radiating platy crystals in slip clay fragments.
- 9B. Sample BS12/B1/A. Lai Ping Road landslide. Backscattered secondary electron photomicrograph of Ce-rich mineral forming granules in slip clay fragment.
- 9C. Sample BS12/B1/B. Lai Ping Road landslide. Backscattered secondary electron photomicrograph showing concentric growth of Mn-oxide.
- 9D. Sample BS12/B1/B. Lai Ping Road landslide. Backscattered secondary electron photomicrograph of well developed concentric growth pattern in Fe-oxyhydroxide.
- 9E. Sample BS12/B1/B. Lai Ping Road landslide. Backscattered secondary electron photomicrograph of kaolinite books heavily replaced and overgrown by fibrous halloysite.
- 9F. Sample BS12/B1/B. Lai Ping Road landslide. Backscattered secondary electron photomicrograph of halloysite fibres replacing books of kaolinite crystals.

LIST OF DRAWINGS

Drawing  
No.

EG 499	Geology and Morphology of Landslide Scars 1 to 5 (Scale 1:200)
EG 502	Major and Minor Scarps (Scale 1:200)
EG 503	Features of the Composite Landslide and Ground Investigation Locations (Scale 1:250)
EG 508	Geological Cross-section 6 – 6' (Scale 1:250)
EG 509	Geological Cross-section A – A' (Scale 1:250)





User notes:

1. Each landslide and its associated debris are identified by different chroma's of the same color, with the scar, or zone of depletion, in the darkest chroma, the debris, or the accretion zone, is colored in progressively lighter chroma, the darker being the oldest in terms of depositional history. Reworked debris (i.e. debris that has been transported by surface water action and redeposited further down slope) is also shown on the map and is coloured in accordance with its assumed parent landslide.
2. Reworked debris is heterogeneous, cannot be considered as a single material type and has been described individually where observed. The distribution of some of the reworked debris has been interpreted from oblique air photographs taken on 4/7/97.
3. Main and minor scarp complex above landslide scars 1 to 4 is shown on Drawing No. EG502.
4. Broken lines denote uncertainty.

1. THE SURVEY IS BASED ON THE HONG KONG (1980) GRID SYSTEM.

Base topography taken from:  
CED Survey Division Drawing  
Number GC2527/1A) 2.

Contours in metres above Hong Kong Principal Datum.

2. LEGEND

- Concave break in slope - sharp
- Concave break in slope - rounded
- Ridge line - sharp
- Boundary of fill mound - post 1997 failure
- Failure scar - main
- Failure scar - minor
- Tension crack
- Stream, arrow shows flow direction
- Concrete surface water U-channel
- Retaining structure
- Seepage point with persistent flow (1:6 - seepage point used in Table 3)
- Seepage point with intermittent flow
- Rock sample location
- Sand replacement test location
- Dip and strike of surface of failure
- Dip and strike of joint
- Surface of rupture containing slickensides with trend and plunge direction shown by the arrow
- Dip and strike of joint controlled
- Dip and strike of joint controlled surface of rupture containing slickensides with trend and plunge direction shown by the arrow
- Dip and strike of flow banding
- Marginal zone (M) to planar discontinuity
- Karst in fill to planar discontinuity

- Make ground
- Colluvium
- Residual soils - also including old colluvium
- PW930
- PW9350
- PW9360
- PW93700
- Zone of intense erosion
- Rhyolite dyke
- Landslide debris
- Disrupted vegetation left of landslide debris
- Reworked landslide debris
- Boulder of moderately to highly decomposed coarse silt crystal TUFF or in situ conditions

NO.	DESCRIPTION	REF.
1	1:6 Scale	1:6
2	1:10 Scale	1:10

EG499

1:200

LAI PING ROAD  
LANDSLIDE  
INVESTIGATION

GEOLOGY AND  
MORPHOLOGY OF  
LANDSLIDE SCARS 1 TO 5

PLANNING DIVISION  
GEOTECHNICAL ENGINEERING OFFICE

CIVIL  
ENGINEERING  
DEPARTMENT









**Treatment rate of injury and illness cases**



© 2004 Blackwell Publishing Ltd *Journal of Internal Medicine* 255: 103–110

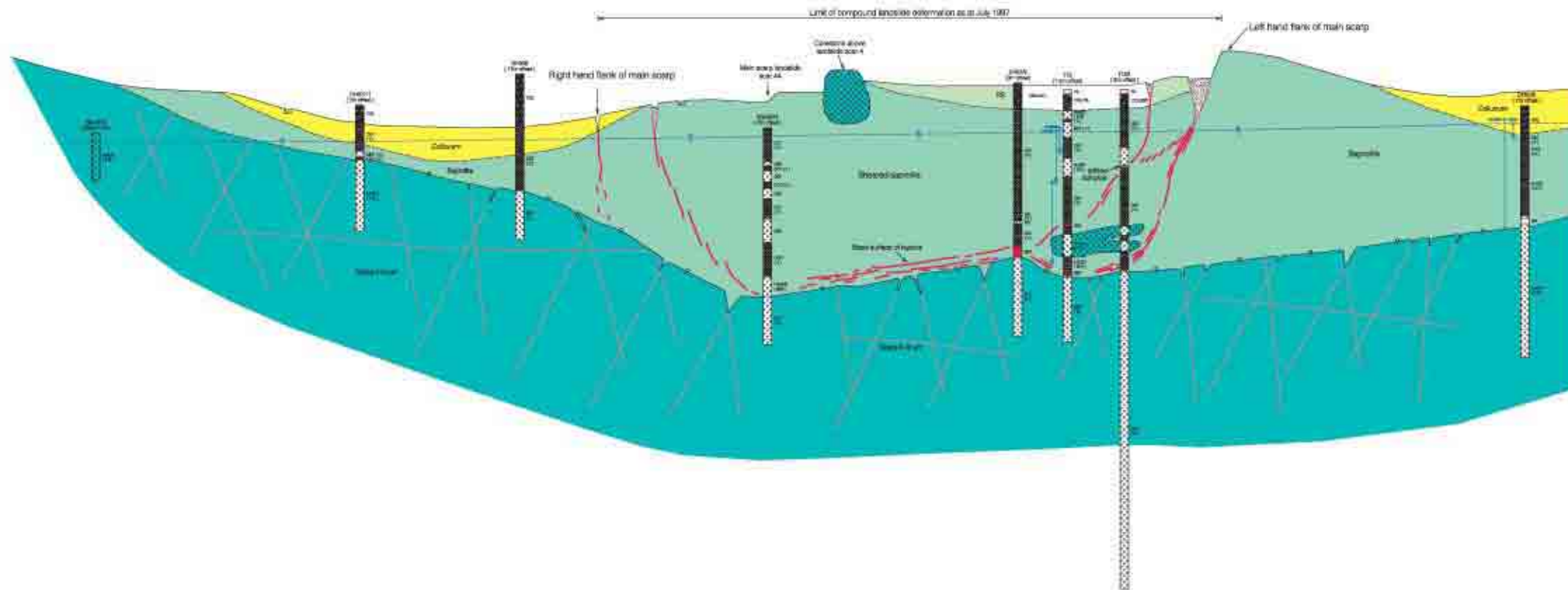
[illegible]





West









East:



- |     |                                 |
|-----|---------------------------------|
| 00  | Normal Set                      |
| 01  | Fast Set                        |
| 226 | Robust                          |
| 231 | Completely Decomposed Full      |
| 401 | Incremental Circuit-based Full  |
| 501 | Integer Decomposed Full         |
| 024 | Highly Decomposed Hybrid        |
| 101 | Completely Decomposed (Integer) |
| 143 | Incremental Decomposed Hybrid   |
| 024 | Decompose                       |
| 027 | Don't Care (Puzzle)             |
| 01  | No Recovery                     |

 Growth with loss will occur  
Fluxions

 Highest axonal growth rates lost neurons of 14 µm/day

-  Odorous
-  Habitat loss
-  Saprophyte
-  Specialist life
-  Consensus of students to require decomposition life
-  Prohibit a company
-  Target state with life
-  Free access to state of a state

Category	Value	Unit
Production	10.0	1000
Consumption	10.0	1000
Inventory	10.0	1000
Production	10.0	1000
Consumption	10.0	1000
Inventory	10.0	1000

GCP2/E2/13-2

LAI PING ROAD LANDSLIDE  
INVESTIGATION

## GEOLOGICAL SECTION A - A'

EG 509

1:250

PLANNING DIVISION  
GEOTECHNICAL ENGINEERING



## GEO PUBLICATIONS AND ORDERING INFORMATION

### 土力工程處刊物及訂購資料

A selected list of major GEO publications is given in the next page. An up-to-date full list of GEO publications can be found at the CEDD Website <http://www.cedd.gov.hk> on the Internet under "Publications". Abstracts for the documents can also be found at the same website. Technical Guidance Notes are published on the CEDD Website from time to time to provide updates to GEO publications prior to their next revision.

**Copies of GEO publications (except maps and other publications which are free of charge) can be purchased either by:**

writing to

Publications Sales Section,  
Information Services Department,  
Room 402, 4th Floor, Murray Building,  
Garden Road, Central, Hong Kong.  
Fax: (852) 2598 7482

or

- Calling the Publications Sales Section of Information Services Department (ISD) at (852) 2537 1910
- Visiting the online Government Bookstore at <http://bookstore.esdlife.com>
- Downloading the order form from the ISD website at <http://www.isd.gov.hk> and submit the order online or by fax to (852) 2523 7195
- Placing order with ISD by e-mail at [puborder@isd.gov.hk](mailto:puborder@isd.gov.hk)

1:100 000, 1:20 000 and 1:5 000 maps can be purchased from:

Map Publications Centre/HK,  
Survey & Mapping Office, Lands Department,  
23th Floor, North Point Government Offices,  
333 Java Road, North Point, Hong Kong.  
Tel: 2231 3187  
Fax: (852) 2116 0774

**Requests for copies of Geological Survey Sheet Reports, publications and maps which are free of charge should be sent to:**

For Geological Survey Sheet Reports and maps which are free of charge:

Chief Geotechnical Engineer/Planning,  
(Attn: Hong Kong Geological Survey Section)  
Geotechnical Engineering Office,  
Civil Engineering and Development Department,  
Civil Engineering and Development Building,  
101 Princess Margaret Road,  
Homantin, Kowloon, Hong Kong.  
Tel: (852) 2762 5380  
Fax: (852) 2714 0247  
E-mail: [jsewell@cedd.gov.hk](mailto:jsewell@cedd.gov.hk)

For other publications which are free of charge:

Chief Geotechnical Engineer/Standards and Testing,  
Geotechnical Engineering Office,  
Civil Engineering and Development Department,  
Civil Engineering and Development Building,  
101 Princess Margaret Road,  
Homantin, Kowloon, Hong Kong.  
Tel: (852) 2762 5345  
Fax: (852) 2714 0275  
E-mail: [ykhui@cedd.gov.hk](mailto:ykhui@cedd.gov.hk)

部份土力工程處的主要刊物目錄刊載於下頁。而詳盡及最新的土力工程處刊物目錄，則登載於土木工程拓展署的互聯網網頁 <http://www.cedd.gov.hk> 的“刊物”版面之內。刊物的摘要及更新刊物內容的工程技術指引，亦可在這個網址找到。

**讀者可採用以下方法購買土力工程處刊物(地質圖及免費刊物除外):**

書面訂購

香港中環花園道  
美利大廈4樓402室  
政府新聞處  
刊物銷售組  
傳真: (852) 2598 7482

或

- 致電政府新聞處刊物銷售小組訂購 (電話: (852) 2537 1910)
- 進入網上「政府書店」選購，網址為 <http://bookstore.esdlife.com>
- 透過政府新聞處的網站 (<http://www.isd.gov.hk>) 於網上遞交訂購表格，或將表格傳真至刊物銷售小組 (傳真: (852) 2523 7195)
- 以電郵方式訂購 (電郵地址: [puborder@isd.gov.hk](mailto:puborder@isd.gov.hk))

讀者可於下列地點購買1:100 000，1:20 000及1:5 000地質圖：

香港北角渣華道333號  
北角政府合署23樓  
地政總署測繪處  
電話: 2231 3187  
傳真: (852) 2116 0774

**如欲索取地質調查報告、其他免費刊物及地質圖，請致函：**

地質調查報告及地質圖:

香港九龍何文田公主道101號  
土木工程拓展署大樓  
土木工程拓展署  
土力工程處  
規劃部總土力工程師  
(請交:香港地質調查組)  
電話: (852) 2762 5380  
傳真: (852) 2714 0247  
電子郵件: [jsewell@cedd.gov.hk](mailto:jsewell@cedd.gov.hk)

其他免費刊物:

香港九龍何文田公主道101號  
土木工程拓展署大樓  
土木工程拓展署  
土力工程處  
標準及測試部總土力工程師  
電話: (852) 2762 5345  
傳真: (852) 2714 0275  
電子郵件: [ykhui@cedd.gov.hk](mailto:ykhui@cedd.gov.hk)



## **MAJOR GEOTECHNICAL ENGINEERING OFFICE PUBLICATIONS**

### **土力工程處之主要刊物**

#### **GEOTECHNICAL MANUALS**

Geotechnical Manual for Slopes, 2nd Edition (1984), 300 p. (English Version), (Reprinted, 2000).

斜坡岩土工程手冊(1998)，308頁(1984年英文版的中文譯本)。

Highway Slope Manual (2000), 114 p.

#### **GEOGUIDES**

Geoguide 1 Guide to Retaining Wall Design, 2nd Edition (1993), 258 p. (Reprinted, 2000).

Geoguide 2 Guide to Site Investigation (1987), 359 p. (Reprinted, 2000).

Geoguide 3 Guide to Rock and Soil Descriptions (1988), 186 p. (Reprinted, 2000).

Geoguide 4 Guide to Cavern Engineering (1992), 148 p. (Reprinted, 1998).

Geoguide 5 Guide to Slope Maintenance, 3rd Edition (2003), 132 p. (English Version).

岩土指南第五冊 斜坡維修指南，第三版(2003)，120頁(中文版)。

Geoguide 6 Guide to Reinforced Fill Structure and Slope Design (2002), 236 p.

#### **GEOSPECS**

Geospec 1 Model Specification for Prestressed Ground Anchors, 2nd Edition (1989), 164 p. (Reprinted, 1997).

Geospec 2 Model Specification for Reinforced Fill Structures (1989), 135 p. (Reprinted, 1997).

Geospec 3 Model Specification for Soil Testing (2001), 340 p.

#### **GEO PUBLICATIONS**

GCO Publication No. 1/90 Review of Design Methods for Excavations (1990), 187 p. (Reprinted, 2002).

GEO Publication No. 1/93 Review of Granular and Geotextile Filters (1993), 141 p.

GEO Publication No. 1/96 Pile Design and Construction (1996), 348 p. (Reprinted, 2003).

GEO Publication No. 1/2000 Technical Guidelines on Landscape Treatment and Bio-engineering for Man-made Slopes and Retaining Walls (2000), 146 p.

#### **GEOLOGICAL PUBLICATIONS**

The Quaternary Geology of Hong Kong, by J.A. Fyfe, R. Shaw, S.D.G. Campbell, K.W. Lai & P.A. Kirk (2000), 210 p. plus 6 maps.

The Pre-Quaternary Geology of Hong Kong, by R.J. Sewell, S.D.G. Campbell, C.J.N. Fletcher, K.W. Lai & P.A. Kirk (2000), 181 p. plus 4 maps.

#### **TECHNICAL GUIDANCE NOTES**

TGN 1 Technical Guidance Documents